NPS69-86-006

NAVAL POSTGRADUATE SCHOOL

Monterey, California

EFFECTS OF AMBIENT TURBULENCE AND STRATIFICATION ON THE DEMISE OF TRAILING VORTICES

T. SARPKAYA

J. J. DALY

11 July 1986

Interim Report for Period July 1985 - July 1986

Approved for public release; distribution unlimited.

Prepared for:

Defense Advanced Research Projects Agency
1400 Wilson Blvd.
Arlington, VA 22209

FedDocs
D 208.14/2
NPS-69-86-006

FedCol
D 208.14/2
NPS-67-86-006

NAVAL POSTGRADUATE SCHOOL
Monterey, California

Rear Admiral R. C. Austin
Superintendent

D. A. Schrady
Provost

The work reported herein was supported by Defense Advanced Research Projects Agency (DARPA) through ARPA Order 3925.

Reproduction of all or part of this report is authorized.

This report was prepared by:

DUDLEY KNOX LIBRARY
NAVAL POSTGRADUATE SCHOOL
MONTEREY CA 93943-5101

REPORT DOCUMENTATION PAGE

1a REPORT SECURITY CLASSIFICATION UNCLASSIFIED	1b. RESTRICTIVE MARKINGS
2a SECURITY CLASSIFICATION AUTHORITY	3 DISTRIBUTION / AVAILABILITY OF REPORT Approved for public release; distribution unlimited.
2b. DECLASSIFICATION / DOWNGRADING SCHEDULE	
4 PERFORMING ORGANIZATION REPORT NUMBER(S) NPS69-86-006	5 MONITORING ORGANIZATION REPORT NUMBER(S)
6a. NAME OF PERFORMING ORGANIZATION Naval Postgraduate School 6b OFFICE SYMBOL (If applicable) 69SL	7a. NAME OF MONITORING ORGANIZATION Defense Advanced Research Projects Agency
6c. ADDRESS (City, State, and ZIP Code) Monterey, CA 93943-5000	7b. ADDRESS (City, State, and ZIP Code) 1400 Wilson Blvd., Arlington, VA 22209
8a NAME OF FUNDING / SPONSORING ORGANIZATION DARPA 8b OFFICE SYMBOL (If applicable)	9. PROCUREMENT INSTRUMENT IDENTIFICATION NUMBER ARPA Order 3925
8c. ADDRESS (City, State, and ZIP Code) 1400 Wilson Blvd. Arlington, VA 22209	10 SOURCE OF FUNDING NUMBERS PROGRAM ELEMENT NO / PROJECT NO / TASK NO / WORK UNIT ACCESSION NO

11. TITLE (Include Security Classification)
Effects of Ambient Turbulence and Stratification on the Demise of Trailing Vortices.

12 PERSONAL AUTHOR(S) TURGUT SARPKAYA & JOHN J. DALY

13a TYPE OF REPORT	13b TIME COVERED	14 DATE OF REPORT (Year, Month, Day)	15 PAGE COUNT
Interim.	FROM Jlu 85 TO July 86	11 July 1986	147

16 SUPPLEMENTARY NOTATION

17 COSATI CODES			18 SUBJECT TERMS (Continue on reverse if necessary and identify by block number)
FIELD	GROUP	SUB-GROUP	Trailing Vortices, Vortex Decay, Ambient Turbulence, Stratification

19 ABSTRACT (Continue on reverse if necessary and identify by block number)

A series of experiments was carried out with two streamlined foils at different speeds in a towing tank. The ambient turbulence (nearly isotropic) was generated by means of a bi-planar grid. The model-grid separation distance was varied systematically in order to subject the trailing vortices to varying degreees of turbulence. The data have been expressed in terms of a normalized turbulence parameter and the relative rise of the vortices. The results have shown that the ultimate height to which the vortices rise prior to their demise is controlled by the two parameter cited, irrespective of the shape and the aspect ratio of the lifting surfaces. A numerical analysis has been initiated to analyze the motion of the trailing vortices and the propagation of internal waves in density stratified medium with the ultimate objective of incorporating the effect of turbulence into the numerical model.

20 DISTRIBUTION / AVAILABILITY OF ABSTRACT ☒ UNCLASSIFIED/UNLIMITED ☐ SAME AS RPT ☐ DTIC USERS	21 ABSTRACT SECURITY CLASSIFICATION Unclassified
22a NAME OF RESPONSIBLE INDIVIDUAL Prof. T. SARPKAYA	22b TELEPHONE (Include Area Code) (408) 646-3425 22c OFFICE SYMBOL 69-SL

DD FORM 1473, 84 MAR 83 APR edition may be used until exhausted
All other editions are obsolete

ABSTRACT

A series of experiments was carried out with two streamlined foils at two different speeds in a towing tank. The ambient turbulence (nearly isotropic) was generated by means of a bi-planar grid. The model-grid separation distance was varied systematically in order to subject the trailing vortices to varying degrees of turbulence. The data have been expressed in terms of a normalized turbulence parameter and the relative rise of the vortices. The results have shown that the ultimate height to which the vortices rise prior to their demise is controlled by the two parameters cited, irrespective of the shape and the aspect ratio of the lifting surfaces. A numerical analysis has been initiated to analyze the motion of the trailing vortices and the propagation of internal waves in density stratified medium with the ultimate objective of incorporating the effect of turbulence into the numerical model.

ACKNOWLEDGEMENTS

The writers wish to acknowledge the generous support of DARPA and the constructive comments and suggestions of Dr. David C. Lewis, Program Manager, Tactical Technology Office, DARPA.

A special note of thanks is extended to Dr. A. Tether for his continued support and encouragement.

Also, the authors wish to thank Mr. Jack Mc Kay for his most skilful and dedicated work in the design, construction and smooth operation of the test facilities.

TABLE OF CONTENTS

I. INTRODUCTION ---------- 11

II. EXPERIMENTAL EQUIPMENT AND PROCEDURES ---------- 15

A. EQUIPMENT ---------- 15

B. MODELS AND GRIDS ---------- 16

C. GRID-GENERATED TURBULENCE ---------- 17

D. TEST PROCEDURES ---------- 20

III. ANALYSIS ---------- 23

A. DIMENSIONAL ANALYSIS ---------- 23

B. NUMERICAL ANALYSIS ---------- 25

IV. DISCUSSION OF RESULTS ---------- 33

A. EFFECTS OF AMBIENT TURBULENCE ---------- 33

B. EFFECTS OF STRATIFICATION ---------- 36

V. CONCLUSIONS ---------- 40

LIST OF REFERENCES ---------- 41

APPENDIX A: FIGURES ---------- 44

APPENDIX B: RP1 TABULATED DATA ---------- 120

APPENDIX C: RP2 TABULATED DATA ---------- 122

APPENDIX D: TOMBACH DATA ---------- 124

APPENDIX E: NUMERICAL ANALYSIS PROGRAM LISTING ---------- 125

INITIAL DISTRIBUTION LIST ---------- 145

LIST OF FIGURES

1. Diagram of Biplanar Grid Construction ---------- 44
2. Comparison of Turbulence Models ---------- 45
3. Vortex Rise for RP1 (U = 0.9 ft/sec, X/M = ∞) --- 46
4. Vortex Rise for RP1 (U = 0.9 ft/sec, X/M = 750) - 47
5. Vortex Rise for RP1 (U = 0.9 ft/sec, X/M = 500) - 48
6. Vortex Rise for RP1 (U = 0.9 ft/sec, X/M = 250) - 49
7. Vortex Rise for RP1 (U = 0.9 ft/sec, X/M = 180) - 50
8. Vortex Rise for RP1 (U = 0.9 ft/sec, X/M = 80) -- 51
9. Vortex Rise for RP1 (U = 1.6 ft/sec, X/M = ∞) --- 52
10. Vortex Rise for RP1 (U = 1.6 ft/sec, X/M = 750) - 53
11. Vortex Rise for RP1 (U = 1.6 ft/sec, X/M = 500) - 54
12. Vortex Rise for RP1 (U = 1.6 ft/sec, X/M = 250) - 55
13. Vortex Rise for RP1 (U = 1.6 ft/sec, X/M = 180) - 56
14. Vortex Rise for RP1 (U = 1.6 ft/sec, X/M = 80) -- 57
15. Vortex Rise for RP2 (U = 0.9 ft/sec, X/M = ∞) --- 58
16. Vortex Rise for RP2 (U = 0.9 ft/sec, X/M = 750) - 59
17. Vortex Rise for RP2 (U = 0.9 ft/sec, X/M = 500) - 60
18. Vortex Rise for RP2 (U = 0.9 ft/sec, X/M = 250) - 61
19. Vortex Rise for RP2 (U = 0.9 ft/sec, X/M = 180) - 62
20. Vortex Rise for RP2 (U = 0.9 ft/sec, X/M = 80) -- 63
21. Vortex Rise for RP2 (U = 0.9 ft/sec, X/M = 50) -- 64
22. Vortex Rise for RP2 (U = 0.9 ft/sec, X/M = 25) -- 65
23. Vortex Rise for RP2 (U = 1.6 ft/sec, X/M = ∞) --- 66

24. Vortex Rise for RP2 (U = 1.6 ft/sec, X/M = 1000) - 67

25. Vortex Rise for RP2 (U = 1.6 ft/sec, X/M = 750) -- 68

26. Vortex Rise for RP2 (U = 1.6 ft/sec, X/M = 500) -- 69

27. Vortex Rise for RP2 (U = 1.6 ft/sec, X/M = 250) -- 70

28. Vortex Rise for RP2 (U = 1.6 ft/sec, X/M = 180) -- 71

29. Vortex Rise for RP2 (U = 1.6 ft/sec, X/M = 80) --- 72

30. Vortex Rise for RP2 (U = 1.6 ft/sec, X/M = 50) --- 73

31. Vortex Rise for RP2 (U = 1.6 ft/sec, X/M = 25) --- 74

32.a Comparison of Vortex Rise for RP1 for Various X/M, U = 0.9 ft/sec, Data Points ---------- 75

32.b Comparison of Vortex Rise for RP1 for Various X/M, U = 0.9 ft/sec, Curves ---------- 76

33.a Comparison of Vortex Rise for RP1 for Various X/M, U = 1.6 ft/sec, Data Points ---------- 77

33.b Comparison of Vortex Rise for RP1 for Various X/M, U = 1.6 ft/sec, Curves ---------- 78

34.a Comparison of Vortex Rise for RP2 for Various X/M, U = 0.9 ft/sec, Data Points ---------- 79

34.b Comparison of Vortex Rise for RP2 for Various X/M, U = 0.9 ft/sec, Curves ---------- 80

35.a Comparison of Vortex Rise for RP2 for Various X/M, U = 1.6 ft/sec, Data Points ---------- 81

35.b Comparison of Vortex Rise for RP2 for Various X/M, U = 1.6 ft/sec, Curves ---------- 82

36. Comparison of H* vs. ε* for RP1, RP2 at U = 0.9 ft/sec and 1.6 ft/sec with Tombach Data ---------- 83

37. Comparison of T* vs. ε* for RP1, RP2 at U = 0.9 ft/sec and 1.6 ft/sec with Tombach Data ---------- 84

38.a Numerical Coordinate Axis and Boundary Conditions ---------- 85

38.b Numerical Nodal Point Arrangement ---------- 86

39.a Velocity Field for T* = 0.0365 ---------- 87
39.b Vorticity Field for T* = 0.0365 ---------- 88
39.c Constant Density Contours for T* = 0.0365 ------- 89
39.d Density Perturbation Contours for T* = 0.0365 --- 90
40.a Velocity Field for T* = 0.728 ---------- 91
40.b Vorticity Field for T* = 0.728 ---------- 92
40.c Constant Density Contours for T* = 0.728 -------- 93
40.d Density Perturbation Contours for T* = 0.728 ---- 94
41.a Velocity Field for T* = 1.46 ---------- 95
41.b Vorticity Field for T* = 1.46 ---------- 96
41.c Constant Density Contours for T* = 1.46 --------- 97
41.d Density Perturbation Contours for T* = 1.46 ----- 98
42.a Velocity Field for T* = 2.18 ---------- 99
42.b Vorticity Field for T* = 2.18 ---------- 100
42.c Constant Density Contours for T* = 2.18 --------- 101
42.d Density Perturbation Contours for T* = 2.18 ----- 102
43.a Velocity Field for T* = 2.9 ---------- 103
43.b Vorticity Field for T* = 2.9 ---------- 104
43.c Constant Density Contours for T* = 2.9 ---------- 105
43.d Density Perturbation Contours for T* = 2.9 ------ 106
44.a Velocity Field for T* = 3.64 ---------- 107
44.b Vorticity Field for T* = 3.64 ---------- 108
44.c Constant Density Contours for T* = 3.64 --------- 109
44.d Density Perturbation Contours for T* = 3.64 ----- 110
45.a Velocity Field for T* = 4.4 ---------- 111
45.b Vorticity Field for T* = 4.4 ---------- 112

45.c Constant Density Contours for T* = 4.4 ---------- 113

45.d Density Perturbation Contours for T* = 4.4 ------ 114

46.a Velocity Field for T* = 5.1 ---------- 115

46.b Vorticity Field for T* = 5.1 ---------- 116

46.c Constant Density Contours for T* = 5.1 ---------- 117

46.d Density Perturbation Contours for T* = 5.1 ------ 118

47. Comparison of Numerical and Experimental Results for SP = 0.75, $\dot{F}_v$ = 0.018 ---------- 119

LIST OF TABLES

I. NORMALIZED INTEGRAL SCALE OF TURBULENCE (L_{11}/b_o) FOR VARIOUS X/M VALUES ---------- 33

TABLE OF SYMBOLS AND ABBREVIATIONS

AR	Aspect Ratio of the Wing
B	Wing Span
b_o	Initial Vortex Core Spacing
d_o	Initial Depth of the Vortex Pair
F_v	Froude Number
g	Gravitational Acceleration
H	Vortex Rise Height
H*	Normalized Migration Height, H/b_o
L_{11}	Integral Scale of Turbulence Field
N_c	$(g/b_o)^{1/2}$
N_o	Brunt-Vaisala Frequency
n	N_o/N_c
Re	Reynolds Number
r	Radial Distance
r_e	Effective Core Radius
T*	Normalized Time, $V_o t/b_o$
t	Time
U	Model Velocity
u	x-Component of Velocity
v	y-Component of Velocity
V_o	Initial Mutual Induction Velocity
x	Horizontal Component of the Coordinate Axis (Parallel to the Line Joining the Vortex Cores)
y	Vertical Component of the Coordinate Axis

α	Model Angle of Attack
Γ	Circulation of the Vortex
Γ_o	Initial Circulation of the Vortex
Δ	d_o/b_o
ε	Rate of Decay of Turbulence Energy
ε^*	Turbulence Parameter
ν	Kinematic Viscosity of Water
ν_t	Eddy Viscosity
ρ	Density of Water
ρ_o	Reference Density of Water in Stratified Medium
ρ'	Density Fluctuations
$\bar{\rho}(y)$	Density of y at t = 0

I. INTRODUCTION

Vortices and vortex wakes have become a major theme of aerodynamics research since the advent of the large aircraft and the understanding of their evolution required an examination of many fundamental problems in fluid mechanics. Much of the progress made during the past two decades was discussed at the Symposium on Aircraft Wake Turbulence and Its Detection [Ref. 1] and at the Aircraft Wake Vortices Conference [Ref. 2]. Comprehensive reviews of the entire subject have been given by Donaldson and Bilanin [Ref. 3], Widnall [Ref. 4] and Hallock and Eberle [Ref. 5].

These studies, as well as numerous others carried out since 1977, have uncovered a number of complex problems which must be resolved in order to achieve a better understanding of the important features of trailing vortices in homogeneous and stratified media. The principal ones are as follows [Ref. 6]:

(a) Roll-up process: The velocity and turbulence distributions at any station behind the wing depend on the wing section, wing-tip shape, Reynolds number, wing incidence, and the distance of the station from the wing [Ref. 7]. The distributions of the initial velocity and turbulence, which influence the roll-up and the decay process, cannot be changed independently. For example, a change in tip shape changes the core size, as well as the velocity and turbulence distributions. High levels of turbulence result in an increased diffusion of vorticity, which in turn increases the core size.

(b) Probe sensitivity of the vortices: Flow visualization studies suggest that trailing vortices are extremely sensitive to disturbances created by even very small probes or bubbles. This forces one to use non-intrusive

means of measurements such as an LDV. Even then, 'vortex wandering' [Ref. 8], which makes the vortices appear larger than normal in time-averaged velocity measurements (for vortices generated by a wing in a wind tunnel), or the unsteady nature of the flow (for vortices generated by a wing in a tow basin) makes the mean velocity profiles in the vortices difficult to determine.

(c) Large-scale instabilities: The vortices are seldom observed to decay away owing to viscous and turbulent dissipation, but are almost always destroyed by either mutual induction instability (Crow instability [Ref. 9]) and/or vortex breakdown. The Crow instability grows exponentially, and results either in a linking of the vortex pair into a series of crude vortex rings or in a highly disorganized intermingling of the vortices. Vortex breakdown, whose mathematical details have not yet been adequately treated, rearranges the vortex structure and increases the core size, turbulence, and energy dissipation. Thus, it is very difficult to measure accurately the trajectories of the three-dimensional vortices from their creation to their ultimate demise.

(d) Reynolds number: Even the highest Reynolds numbers, based on wing chord, reached in wind tunnels or towing basins, are an order of magnitude lower than what is possible for an aircraft. Thus, the scale effects are not easy to assess.

(e) Ambient conditions such as turbulence and stratification play major roles in the evolution of vortices. The quantification of these effects requires numerical analysis and extremely careful experiments.

(f) Ground or free-surface effects: The vortex pair may move towards a rigid boundary at which the no-slip condition must be satisfied or towards a free surface at which the zero-shear condition must be satisfied. In either case, the vortices come under the influence of their images and move accordingly.

The phenomenon is further complicated by several additional facts. When the vortices are propelled towards a rigid surface, vorticity of opposite sign is generated on the no-slip boundary and swept towards the vortex pair. The total vorticity diminishes very quickly as vorticity from the two regions

diffuses, the wall region serving as a strong sink for the vorticity associated with the original vortex [Ref. 10]. The development of a boundary layer along the rigid wall may give rise to flow separation for sufficiently high Reynolds numbers. With or without such a separation, however, the center of the vortex pair eventually moves away, or 'rebounds,' from the wall [Refs. 10-12].

For the case of a zero-stress boundary, the free surface still acts as a vorticity sink, but this is relatively weak due to the absence of intense oppositely-signed vorticity. Thus, in the absence of other impeding phenomena, one expects a mild interaction between the vortices and the free surface and a small rebound of the vortex center from the free surface. However, the ability of the free surface to deform under the influence of strain fields leads to a strong interaction between the vortices and the free surface.

It is evident from the foregoing that the motion and the life-span of trailing vortices are governed by a number of nonlinearly-dependent complex phenomena. A number of experimental and analytical studies have been carried out at the Naval Postgraduate School by Sarpkaya and his students [Refs. 6, 13-16] in order to investigate the effects of these parameters on the rise and demise of the trailing vortices in homogeneous and density stratified media. These studies have clearly identified the various demise mechanisms in both media and established basic relationships between the rise of vortices and the governing parameters in a finite as well as effectively

infinite medium [Ref. 17], free from ambient turbulence. The present investigation is a continuation of the foregoing studies and is confined to the determination of the effect of ambient turbulence on the rise and demise of trailing vortices.

II. EXPERIMENTAL EQUIPMENT AND PROCEDURES

A. EQUIPMENT

The equipment used to generate the trailing vortices has been extensively used at this facility over the past three years [Refs. 6, 14-17]. Only the salient features, most recent modifications and the adaptation for this work are briefly described in the following.

The system consists essentially of a towing basin. The auxiliary components of the basin are the plumbing for water and for water and brine mixture (to establish a density stratification), turbulence management system, top and bottom carriages, velocity measuring system, lighting system, and the models [Refs. 14-17].

A mirror, inclined 45 degrees from the horizontal, is attached to the top of the tank at the test section to allow viewing of the vortex pair and the surface disturbances from the top of the basin.

The drains are provided at the bottom at each end of the basin. Two parallel rails are mounted along the bottom of the tank. A carriage rides smoothly on these rails and provides the test body with a constant velocity through the use of an endless cable and a DC motor. The velocity of the model is measured and continuously monitored through the use of a magnetic linear displacement transducer. It yields a signal

proportional to the velocity of the model with an error less than 1 percent.

The two rails, the carriage and the filling pipes are located on or near the bottom of the basin and under a turbulence management system. The system consists of one inch thick polyurethane foam sandwiched between two perforated aluminum plates.

B. MODELS AND GRIDS

Two rectangular foils (NACA 0012) were used in the present study (RP1 with B = 6.8 in., b_o = 5.34 in., and c = 3.50 in., and RP2 with B = 4.50 in., b_o = 3.53 in., and c = 2.32 in.). The interior of these models was hollowed and used as a dye reservoir to seed the vortex cores. The models are mounted on their bases by means of a thin streamlined aluminum bar with a cross section of a NACA 0006 foil and set at the desired angle of attack. As noted earlier, all models are pulled by means of a DC motor, pulley, and cable system at the desired speed (ranging from 0.8 to 4.0 feet/second). Additional details of the model construction and mounting are given in Ref. 13.

Two grids were constructed but only one was used in the experiments. The test grid consisted of square plexiglass bars (3/8 in. x 3/8 in.). One layer was placed orthogonally on top of another layer so as to form a biplanar grid. The mesh size of the grid was M = 2.5 in. (see Fig. 1). The solidity of the mesh, defined as $(2Md-d^2)/M^2$ was 0.2775. The grid was attached to the top carriage and towed at desired speeds and x/M distances ahead of the model. It was made sure,

through repeated experiments, that both the model and the grid ran smoothly, with very little or no velocity fluctuations.

C. GRID-GENERATED TURBULENCE

A large number of grid-turbulence experiments have been conducted in wind tunnels and in water flumes [Refs. 18-23]. The measurements have shown that the grid-generated turbulence is only approximately isotropic with $u_2^2 = u_3^2 = 0.83\, u_1^2$ for a uniform duct where u_1, u_2, u_3 are the longitudinal, lateral and vertical velocity components, respectively. In general, the mean-square velocity components of the turbulence decrease with the downstream distance according to the power law [Ref. 21]:

$$u_i^2/U^2 = A_i(x/M)^{-n} \qquad (i = 1 \text{ to } 3) \qquad (1)$$

where A_i are constants, M is the mesh size of the grid, U is the mean velocity of the ambient flow, and the power n ranges from 1.25 to 1.5. A careful examination of the data presented in Refs. 18-23 has shown (see Fig. 2) that the most suitable values of A_1 and n for the grid used in the present investigation are $A_1 = 0.05$ and $n = 1.3$. Thus, one has

$$u_1^2/U^2 = 0.05(x/M)^{-1.3} \qquad (2)$$

Consequently, the twice the turbulent kinetic energy per unit mass becomes,

$$q^2 = (u_1^2 + u_2^2 + u_3^2) = ((0.05 + 2 \times 0.83)U^2(x/M)^{-1.3} \quad (3)$$

The dissipation rate ε of the grid-generated turbulence per unit mass is defined as

$$\varepsilon = -(1/2)dq^2/dt \quad (4)$$

and decreases with increasing x/M. Using Eq. (1) and the definitions of ε and q, one has

$$\frac{\varepsilon M}{q^2 U} = (n/2)(x/M)^{-1} \quad (5)$$

Friehe and Schwarz [Ref. 20] were able to collapse all of their grid turbulence data onto a single curve through the use of Eq. (4). For n = 1.3, one has

$$\frac{\varepsilon M}{q^2 U} = 0.65(x/M)^{-1} \quad (6)$$

and

$$\frac{\varepsilon M}{U^3} = 0.0865(x/M)^{-2.3} \quad (7)$$

The turbulence parameter ε^*, defined by Crow [Ref. 24] as,

$$\varepsilon^* = (\varepsilon b_o)^{1/3}/V_o \quad (8)$$

may be combined with Eq. (7) to yield

$$\varepsilon^* = \frac{1}{(V_o/U)} \frac{0.4423}{(M/b_o)^{1/3}} (x/M)^{-0.767} \qquad (9)$$

in which M/b_o represents the ratio of the mesh size to the initial vortex separation. The values of V_o/U and M/b_o are known for a given grid, model, and model velocity. It must also be noted that the exact value of A_1 (0.05 in Eq. (2)) is not very critical. It is easy to show that a change even as large as 20 percent in A_1 (say from 0.05 to 0.06) causes only a 6 percent change in ε^*.

The integral scale L_{11} of the grid-generated-turbulence field has been measured by a number of investigators (see e.g., Refs. 18-23). The results have shown that L_{11} increases with x/M. Huot et al. [Ref. 23] found experimentally that L_{11}/M may be represented by

$$L_{11}/M = 0.14(x/M - x_o/M)^{0.4} \qquad (10)$$

in which x_o/M represents the distance to a fictitious origin. For the grid size used in the present experiments, x_o/M is about 2.5. However, it is not necessary to retain x_o/M in Eq. (10) simply because in the present experiments x/M ranged from a minimum value of 50 to about 1000. Thus, one has

$$L_{11}/b_o = 0.14(M/b_o)(x/M)^{0.4} \qquad (11)$$

Equation (11) shows that L_{11}/b_o is about 1.57 for the smaller model (RP-2 with $M/b_o = 0.707$) and about 1.0 for the larger model (RP-1 with $M/b_o = 0.47$). Thus, it is seen that the integral scale of the turbulence generated by the grid used in the present experiments varies from one half to 1.5 times the initial vortex separation. In other words, it is within the distances cited that the integral scale of the background increases and becomes comparable to the size of the individual vortices.

D. TEST PROCEDURES

A model is placed in the basin and the basin is filled gradually with fresh water to the desired level. In the cases where dye was used to seed the vortex pair, the models were filled with dye prior to filling the tank. After removal of trapped air and after a sufficient period of waiting for the escape of dissolved air in the water and the elimination of any internal currents in the basin, the grid was set in motion at the desired speed. When the grid has moved a prescribed distance of x/M, the model was set in motion. As noted earlier, the grid and the model moved at identical speeds, i.e., the horizontal distance between them was kept constant at a given value of x/M. Most of the experiments were repeated at least three times.

The motion of the trailing vortices are recorded on high-speed Polaroid film at the test section (one of the plexiglass panels near the middle of the basin). Each picture included

two clocks accurate to 0.1 seconds, the vertical and horizontal scales on the plexiglass window and, of course, the side view of the trailing vortices as they rose from the model after formation. The time interval between successive pictures is determined from the two clocks. The first picture always captured the instant the grid arrived at the test section. The second picture captured the instant the model passed through the test section. The subsequent pictures (taken at about 0.75 second intervals) captured the rise and demise of the vortices. The vertical rise of the vortices is determined from the vertical scale. Attention has been paid to the fact that the vortices are farther away from the scale on the window and that the scale placed vertically in the middle of the test section does not exactly correspond to the scale marked on the window due to refraction and parallax. The necessary correction was made by photographing a scale placed in water in the middle of the test section together with the scale marked on the window. This resulted in a simple conversion table which enabled the determination of the actual position of the vortex from the scale reading on the photograph.

The results are normalized and plotted in various forms and compared with those obtained in the previous runs. Each experiment was repeated three times for most of the data presented herein. All trailing vortices were recorded on film until the time they have completely dissipated either due to aging (diffusion of vorticity due to viscosity, turbulence, entrainment, and detrainment), or due to Crow instability

(sinusoidal instability and linking of vortices), and/or due to vortex breakdown (core bursting). It was thus possible to determine the life span of vortex cores from their formation to their final demise.

III. ANALYSIS

A. DIMENSIONAL ANALYSIS

The dependent parameter of major importance is the instantaneous position of the vortex pair (x,y). It may be expressed as a function of the following parameters [Ref. 17]:

$$x = f(t,U,d_o,\rho_o,d\rho/dy,\nu,B,Ar,\alpha,g,r_e,\varepsilon,L_{11}) \quad (12)$$

and

$$y = f(t,U,d_o,\rho_o,d\rho/dy,\nu,B,AR,\alpha,g,r_e,\varepsilon,L_{11}) \quad (13)$$

in which t represents the time, U the velocity of the model, d_o the initial depth of the vortex pair, ρ_o the reference density of water, $d\rho/dy$ the linear density gradient, ν the kinematic viscosity of water, B the base width of the model, AR the aspect ratio of the model, α the angle of attack of the model, g the gravitational acceleration, σ the surface tension of water, r_e an effective core radius, characterizing the effect of the wing-tip shape in addition to other wing parameters, ε the rate of decay of the turbulent energy per unit mass, and L_{11} the integral scale of the turbulent field.

The height and width of the test section and the height of the model within it were not included in the foregoing because

a detailed analysis, based on ideal vortices, has shown that the velocities induced by the bottom were negligible. Effects of surface tension on the instantaneous position of the vortex pair is deemed negligible. It is for this reason that σ is not included in Eqs. (12) and (13).

A dimensional analysis of Eqs. (12) and (13) yields

$$x/B = f(Ut/B, d_o/B, NB/U, U^2/gB, UB/\nu, AR, \alpha, r_e/B, \varepsilon^*, L_{11}/b_o)$$
$$y/B = f(Ut/B, d_o/B, NB/U, U^2/gB, UB/\nu, AR, \alpha, r_e/B, \varepsilon^*, L_{11}/b_o) \quad (14)$$

in which

$$N = (-g/\rho_o \, d\rho/dy)^{1/2} \quad (15)$$

and is known as the Brunt-Vaisala frequency. The other variables have been defined previously.

Equation (14) may be recast in terms of the initial separation b_o of the vortex pair, and the initial mutual induction velocity V_o of the vortices by noting that B/b_o and V_o/U are uniquely determined by AR and α for a given wing shape. Thus, one has

$$x/b_o = f(V_o t/b_o, d_o/b_o, Nb_o/V_o, V_o^2/gb_o, V_o b_o/\nu, r_e/b_o, \varepsilon^*, L_{11}/b_o)$$
$$y/b_o = f(V_o t/b_o, d_o/b_o, Nb_o/V_o, V_o^2/gb_o, V_o b_o/\nu, r_e/b_o, \varepsilon^*, L_{11}/b_o) \quad (16)$$

Experiments have shown that [Ref. 6] the ratio of the initial vortex-core spacing to wing span, b_o/B, is 0.70 for the sharp-edged Delta wing, 0.73 for the round-edged Delta wing, and nearly equal to $\pi/4$ for the rectangular wings (NACA 0012). Whereas all the parameters in Eq. (16) may be changed independently, r_e/b_o is taken as nature provides it. The primary reason for this is that a century of theoretical and experimental aerodynamics research has been incapable of describing the details of the structure of the tip vortex to be used as initial conditions in a viscous solution. It is surprising, but true, that until recently the importance of the wing-tip shape and its influence upon both the initial tangential velocity profile and the initial turbulence in the vortex has not been fully appreciated. Here the said influence has been characterized in terms of an effective core radius with full awareness of its shortcomings.

B. NUMERICAL ANALYSIS OF THE VORTEX MOTIONS

The generation of the internal waves and the rise and demise of the vortices in a stratified medium may be analyzed through the use of the equations of motion for an incompressible fluid for both laminar and turbulent motions provided that a suitable turbulence closure model is adopted and the usual Boussinesq approximation (gravitational acceleration is much larger than the fluid accelerations) is made. For the type of motions considered herein the Boussinesq approximation is quite valid and

has been used in the investigation of all types of internal waves in stratified fluids.

For a two-dimensional flow, with y vertical and x horizontal, the equations of motion are

$$\frac{\partial u}{\partial t} + u \frac{\partial u}{\partial x} + v \frac{\partial u}{\partial y} = - \frac{1}{\rho} \frac{\partial p}{\partial x} + \nu \nabla^2 u \tag{17}$$

and

$$\frac{\partial v}{\partial t} + u \frac{\partial v}{\partial x} + v \frac{\partial v}{\partial y} = - g - \frac{1}{\rho} \frac{\partial p}{\partial y} + \nu \nabla^2 v \tag{18}$$

and the equation of continuity

$$\frac{\partial u}{\partial x} + \frac{\partial v}{\partial y} = 0 \tag{19}$$

Defining vorticity as usual by

$$\zeta = \frac{\partial u}{\partial y} - \frac{\partial v}{\partial x} \tag{20}$$

and eliminating pressure between Eq. (17) and Eq. (18), one has

$$\frac{\partial \zeta}{\partial t} + \frac{\partial u\zeta}{\partial x} + \frac{\partial v\zeta}{\partial y} = \nu \nabla^2 \zeta + \frac{g}{\rho_o} \frac{\partial \rho'}{\partial x} \tag{21}$$

in which ρ' is the fluctuating part of the density ρ given by

$$\rho = \rho_o + \bar{\rho}(y) + \rho'(x,y,t) \tag{22}$$

where ρ_o is the reference density, and $\bar{\rho}(y)$ the initial density at elevation y at t = 0.

The diffusion of density is given by

$$(\frac{\partial}{\partial t} + u \frac{\partial}{\partial x} + v \frac{\partial}{\partial y} - \nu\nabla^2)\rho = 0 \qquad (23)$$

Combining Eqs. (19), (22) and (23), and simplifying, one has

$$\frac{\partial \rho'}{\partial t} + \frac{\partial u\rho'}{\partial x} + \frac{\partial v\rho'}{\partial y} = - v \frac{\partial \bar{\rho}}{\partial y} + \nu\nabla^2\rho' + \nu \frac{\partial^2 \bar{\rho}}{\partial y^2} \qquad (24)$$

It is convenient to cast the foregoing equations into nondimensional forms, scaling each variable by a quantity characteristic of its expected magnitude. Two possible time scales exist. There is the dynamic time scale, which is the time a characteristic length would be traversed by a fluid particle traveling at the characteristic velocity, and there is the buoyant time scale based on the natural buoyancy frequency of the stratified flow, i.e., the Brunt-Vaisala frequency N, defined by Eq. (15). Each of the scales gives a slightly different form of the normalized governing equations.

Dynamic Scale:

Introducing U_c and L_c as the characteristic velocity and length, one has

$$\zeta_m = \zeta L_c/U_c, \quad t_m = U_c t/L_c, \quad Re = U_c L_c/\nu, \qquad (25)$$

$$F_v = U_c/(gL_c)^{1/2}$$

Normalizing Eqs. (21) and (24), one has

$$\frac{\partial \zeta_m}{\partial t_m} + F_v\left(\frac{\partial u_m \zeta_m}{\partial x_m} + \frac{\partial v_m \zeta_m}{\partial y_m}\right) = \frac{1}{Re} \nabla^2 \zeta_m + \frac{1}{F_v^2} \frac{\partial \rho_m'}{\partial x_m} \tag{26}$$

and

$$\frac{\partial \rho_m'}{\partial t_m} + F_v\left(\frac{\partial u_m \rho_m'}{\partial x_m} + \frac{\partial v_m \rho_m'}{\partial y_m}\right) = n^2 V_m + \frac{1}{Re}\left(\nabla^2 \rho_m' + \frac{\partial^2 \overline{\rho_m}}{\partial y_m}\right) \tag{27}$$

in which

$$F_v = \frac{U_c^2}{g L_c}, \qquad Re = \frac{U_c L_c}{\nu}, \qquad n = \frac{N_o}{N_c},$$

$$N_c^2 = \frac{g}{L_c}, \qquad N_o^2 = -\frac{g}{\rho_o}\frac{\partial \bar{\rho}(y)}{\partial y} = -\frac{g}{L_c}\frac{\partial \bar{\rho}_m}{\partial y_m} = \frac{g n^2}{L_c}$$

Equations (25) and (26) are valid when $F_v >> 1$, i.e., when the buoyancy has very little influence on the nonlinear dynamics of the motion. In this case, the density perturbation acts as a passive scalar advected by the velocity field.

Buoyant Scale:

Introducing the following dimensionless parameters:

$$\bar{\rho}_m = \frac{\bar{\rho}}{\rho_o}, \qquad u_m = \frac{u}{U_c}, \qquad v_m = \frac{v}{U_c}, \qquad x_m = \frac{x}{L_c}$$

$$y_m = \frac{y}{L_c}, \qquad t_m = t N_c, \qquad \zeta_m = \frac{\zeta}{N_c}, \qquad N_c^2 = \frac{g}{L_c} \tag{28}$$

and normalizing Eqs. (21) and (24), one has

$$\frac{\partial \zeta_m}{\partial t_m} + F_v\left(\frac{\partial u_m \zeta_m}{\partial x_m} + \frac{\partial v_m \zeta_m}{\partial y_m}\right) = \frac{F_v}{Re} \nabla^2 \zeta_m + \frac{\partial \rho'_m}{\partial x_m} \tag{29}$$

and

$$\frac{\partial \rho'_m}{\partial t_m} + F_v\left(\frac{\partial u_m \rho_m}{\partial x_m} + \frac{\partial v_m \rho_m}{\partial y_m}\right) = F_v\, n^2\, v_m \tag{30}$$

in which F_v, Re and n^2 are as defined in Eq. (27).

Equations (29) and (30) are valid when $F_v << 1$ and buoyancy dominates the flow. When F_v approaches zero, the equations that result from Eqs. (29) and (30) describe the propagation of linear internal waves. The $F_v << 1$ regime is of interest in the present investigation because for submerged bodies of naval interest F_v (the Froude number) is about 0.01. The analysis will consider the full nonlinear equations given by Eqs. (29) and (30) rather than their linearized form (i.e., the case of $F_v = 0$). However, the flow will be assumed to be inviscid, i.e., the viscous diffusion will be ignored to a first order approximation. Subsequent analysis will incorporate the effects of viscous and turbulent diffusion into the numberical calculations. The velocities u and v are given by the Biot-Savart law as

$$u(x,y) = \int \frac{(y'-y)\zeta(x',y')dx'dy'}{2\pi r^2} \tag{31}$$

and

$$v(x,y) = \int \frac{(x-x')\zeta(x',y')dx'dy'}{2\pi r^2} \tag{32}$$

in which x,y is the point at which the velocity is calculated and x',y' is an arbitrary point at which the vorticity is $\zeta(x',y')$.

The radial distance r is given by:

$$r^2 = (x-x')^2 + (y-y')^2 \tag{33}$$

Normalizing Eqs. (31-33) through the use of the characteristic dimensions given in Eq. (28), one has:

$$F_v u_m = \int \frac{(y'_m - y_m)\zeta_m(x'_m,y'_m)dx'_m dy'_m}{2\pi r_m^2} \tag{34}$$

$$F_v v_m = \int \frac{(x_m - x'_m)\zeta_m(x'_m,y'_m)dx'_m dy'_m}{2\pi r_m^2} \tag{35}$$

and

$$r_m^2 = (x_m - x'_m)^2 + (y_m - y'_m)^2 \tag{36}$$

It is appropriate to take v_o, the initial mutual induction velocity of the vortex pair, as the characteristic velocity

and the b_o, the initial separation of the vortices, as the characteristic length. Thus, one has:

$$L_c = b_o, \quad u_c = v_o = \frac{\Gamma_o}{2\pi b_o}, \quad F_v = \frac{v_o}{N_c b_o} = \frac{v_o}{\sqrt{g b_o}} \tag{37}$$

In dimensionless forms, one has:

$$\Gamma_m = \frac{\Gamma_o}{N_c b_o^2} = 2\pi F_v, \quad n = F_v \frac{N_o b_o}{v_o}$$

$$t_m = tN_c = \frac{v_o t/b_o}{F_v} \tag{38}$$

in which $N_o b_o/v_o$ is called the stratification parameter SP. The value of SP normally varies from zero to about 100. The larger the SP, the stronger the stratification. For example, for a model running at a speed of 5 ft/sec at an angle of attack of 10 degrees, SP smaller than about 1.0 represents weak stratification, SP between about 1 and 5 represents medium stratification, and SP larger than 5 corresponds to strong stratification.

The numerical solution of Eqs. (29) and (30) through the use of Eqs. (34)-(36) and the appropriate boundary conditions will be discussed later.

IV. DISCUSSION OF RESULTS

A. EFFECTS OF AMBIENT TURBULENCE ON VORTEX MIGRATION

Figures 3-8 show the trajectories of the vortex cores for the model RP1, moving at U = 0.9 ft/sec, for various values of X/M. In each figure $H^* = H/b_o$ and $T^* = V_o t/b_o$. The solid line represents $H^* = T^*$ which is the theoretical result [Ref. 6] for the migration of a pair of vortices in a smooth, inviscid, homogeneous medium. Figures 9-14 show similar results for the same model at a speed of U = 1.6 ft/sec. Figures 15-22 show the vortex trajectories for the model RP2, moving at U = 0.9 ft/sec. Finally, Figures 23-31 show similar data for RP2 at a model speed of U = 1.6 ft/sec.

Figures 3-31 show that there is some scatter in the data. The maximum migration of vortices, at which time they are completely destroyed by instability events, decreases with increasing ambient turbulence. The scatter is partly due to the random nature of the ambient turbulence, and partly due to the fact that the vortex pair does not deform or demise in a similar manner either in one test or from one test to another. The three-dimensional nature of the ambient turbulence, the rotation of the pair along a horizontal axis (under certain circumstances), sinusoidal instability, and the occurrence of vortex breakdown (in only one of the vortex pair) change the relative positions of the vortices at the test section and give rise to scatter in the data. It is remarkable that the scatter is not any larger.

Figures 32-35 are composite plots of Figures 3-8, 9-14, 15-22 and 23-31, respectively. This same data are presented in tabular form in Appendices B-D in terms of T*, H* and ε*.

For the grid used in the tests, the normalized integral scale of the turbulence, L_{11}/b_o, is given in Table I for the X/M values encountered in the tests.

TABLE I

NORMALIZED INTEGRAL SCALE OF TURBULENCE (L_{11}/b_o) FOR VARIOUS X/M VALUES

x/M	L_{11}/b_o (for RP1)	L_{11}/b_o (for RP2)
∞	-----	-----
1000	1.04	1.57
750	0.93	1.40
500	0.79	1.19
250	0.60	0.90
180	0.52	0.79
80	0.38	0.57
50	0.31	0.47
25	0.24	0.36

The integral scale of the turbulence field for RP1 is comparable to the separation distance of the vortices for x/M larger than about 500. The same is true for RP2 for x/M larger than about 180. Figures 32-34 show that the path of the vortices in the turbulent field does not significantly deviate from the path of

the vortices in the non-turbulent medium until the vortex pair rises at least one initial separation distance. Subsequently, the vortices slow down considerably before the onset of instability and eventual dissipation. It is during this deceleration period that the integral scale becomes important in bringing about the instability which breaks up the vortices. In other words, strong turbulence with small integral scale (small x/M) leads to the eventual deposition of the circulation in larger and larger regions of the vortex without the more dramatic and destructive effects of larger scale motions. On the other hand, weaker turbulence with larger integral scale (for large x/M) leads to strong instabilities, breaks up the vortices and leaves them in a state to be devoured by small intensity turbulence. Subsequently, the vorticity is diffused outward and finally destroyed completely. It is clear from the foregoing that the lifespan of the vortices depends significantly both on the scale and the intensity of the ambient turbulence. The quantification of the separate roles of these two parameters needs additional experiments with other grids.

Figures 32-34 also show that the smaller x/M, the smaller is the ultimate rise of vortices. Leaving aside for the time being the rise history of the vortices and the separate effects of the integral scale and turbulence intensity, the attention will be focused now on the maximum height attained by the vortices. The said height is of extreme importance in practical situations. Figure 36 shows the maximum height data obtained with both models as a function of ε^*. Also shown in this figure

is the flight data obtained by Tombach [Ref. 25]. There is reasonable agreement between the laboratory and flight data in spite of the considerable scatter due to the difficulty of determining the maximum height attained by the vortices. As noted earlier, the uncertainties stem partly from the randomness in the occurrence of the instabilities leading to the destruction of the vortices and partly from the experimental difficulties and uncertainties (diffusion of dye, subjectivity in deciding the exact position of the vortex core, etc.). Evidently, the turbulence parameter is the primary governing parameter in the determination of the maximum height. The role of the integral scale is not clearly discernible and is partly obscured by the scatter in the data.

Figure 37 shows the dimensionless time t^* ($= V_o t/b_o$) as a function of the turbulence parameter. The data points shown on the T^* axis correspond to the no-turbulence case. It is assumed that the effect of turbulence is negligible for ε^* smaller than about 0.1 in order to show the entire data in the figure. Clearly, the effect of turbulence is to reduce both the lifespan and the maximum height attained by the vortices. The data have also shown that the vortices in the non-turbulent medium break up primarily due to linking [Ref. 6] and mostly due to vortex breakdown in the turbulent medium. Thus, it is concluded from Figures 36-37 and the numerous observations that turbulence enhances the instabilities leading to the vortex breakdown and, at the same time, diffuses vorticity rapidly,

eventually leading to the total destruction of the vortices. This mechanism is far more powerful than the sinusoidal instability leading to the linking of the vortices. It remains to be determined as to what the individual effects of the turbulence intensity and scale are in bringing about the destruction of the vortices due to the vortex breakdown.

B. EFFECTS OF STRATIFICATION ON VORTEX MIGRATION

Equations (29) and (30) were integrated through the use of an efficient upwind differencing scheme [Ref. 26] for the inviscid flow case, i.e., Re = ∞. A copy of the complete computer code is given in Appendix E.

The initial vorticity distribution was assumed to be Gaussian, i.e.,:

$$\zeta_m = \frac{F_v}{r_{om}^2} \exp[-(r_m^2/2r_{om}^2)] \tag{39}$$

The calculations had to be carried out in a finite mesh, as in all other numerical analysis. The approximate boundary conditions are shown on the boundaries of the quadrant in which the calculations have been performed, as well as a schematic of the computational nodal points (see Figs. 38a and 38b). It should be noted that the boundary conditions $u(0,y) = v(x,0) = 0$ on the axes are automatically satisfied by evaluating the Biot-Savart equations in all four quadrants. The fields of velocity, vorticity, density ($\bar{\rho}(y)$), and the fluctuating components of the density (ρ') are calculated at each time step and plotted at regular intervals.

Among the several calculations carried out only one utilizing the initial parameters corresponding to those of an experiment will be reported here. The computer code is quite general and can be applied to any stratified and unstratified flow situation. As the velocity field is computed from analytic expressions (i.e., the Biot-Savart equations) vice an algorithm involving an iterative convergence scheme, stability of the program is enhanced at a slight expense of execution time.

The plots of the velocity field, constant vorticity, density and density fluctuation are shown in Figures 39a-39d through Figures 46a-46d for various values of the normalized time T*. In the calculations, the initial depth of the vortices from the free surface was taken $d_o/b_o = 8$, the initial value of $r_o/b_o = 0.09$, the stratification parameter $Nb_o/V_o = 0.75$ and $F_v = 0.018$. These values correspond to those of experiments with which the numerical calculations are to be compared to.

Figures 39-46 show that at small times the vortices rise vertically and the circulation in the flow field is primarily due to the initial vortices. As time increases (see e.g., Figure 43a), the regions of circulation with countersigned vorticity develop in the upper right and lower left regions of the vortex. It is easy to show that this counter vorticity not only reduces the rise velocity of the original vortex pair, but pushes the pair against each other. Consequently,

the vorticity is lost in the overlapping regions of the vortex pair, and the rise velocity is further reduced. As time increases, the countersigned vorticity begins to dominate the flow (see e.g., Figure 44a) and the vortex migration stops. With further increases in time the vortex begins to migrate downward.

The density contours reveal the same phenomenon in a different context. As the vortices rise, fluid of greater density is pushed upwards (see e.g., Figure 43c) into regions of lesser density. Since such a migration cannot go on indefinitely, the vortices rise to a maximum height and then begin to sink downwards. The calculations do not take into account the sinusoidal instability and the vortex breakdown. Consequently, the vortices in the numerical calculations continue to exist unimpeded by the instability mechanisms. In reality, the vortices begin to break up as they near the end of their maximum migration and eventually disappear.

The experimental and calculated values are compared in Figure 47. The correspondence between the measured and calculated values is surprisingly good up to the time of maximum rise. This is partly because of the experimental fact that the rise of vortices in a highly stratified medium ($Nb_o/V_o = 0.75$, $F = 0.018$) is not strongly dominated by sinusoidal instability or vortex breakdown. The migration of vortices is inhibited primarily due to the reduction of vorticity of the initial vortices and the creation of countersigned vorticity.

Additional calculations are underway to examine the effects of viscous diffusion and ambient turbulence for various degrees of initial stratification. The results presented herein and the initial comparisons are extremely encouraging and are expected to lead to a better understanding of this extremely complex and challenging phenomenon.

V. CONCLUSIONS

The investigation reported herein warranted the following conclusions:

1. The effect of ambient turbulence in homogeneous medium is to inhibit the rise of the vortices;

2. The larger the intensity of the ambient turbulence, the smaller is the ultimate rise of vortices;

3. The phenomenon seems to be governed primarily by the turbulence parameter ε^*. The effect of the integral scale of the turbulence field seems to be secondary, at least for integral scales on the order of initial vortex separation;

4. The demise mechanism appears to be the precipitation of the instabilities (primarily vortex breakdown) by turbulence, the breaking up of the vortex filaments, and the eventual destruction of the remaining vorticity by turbulent diffusion;

5. Numerical calculations regarding the migration of vortices in a non-turbulent stratified medium have shown that the effect of stratification is to reduce the rate of rise of vortices and the maximum height attained by them;

6. The reduction in maximum height is brought about partly by the development of countersign vorticity and partly by the destruction of vorticity in the overlapping regions of the vortex pair;

7. The predictions of the numerical model are in good agreement with the experimental data. The theoretical model could be made more realistic through the inclusion of at least the effects of turbulence and possibly those of the demise mechanisms.

LIST OF REFERENCES

1. Olsen, J.H., Goldburg, A., and Rogers, M. (eds.), Aircraft Wake Turbulence and Its Detection, Plenum Press, New York, 1971.

2. Hallock, J.N. (ed.), Proceedings of the Aircraft Wake Vortices Conference, 1977, National Technical Information Services, Springfield, VA 22161.

3. Donaldson, C. duP. and Bilanin, A.J., Vortex Wakes of Conventional Aircraft, AGARDograph AGARD-AG-204, 1975.

4. Widnall, S.E., "The Structure and Dynamics of Vortex Filaments," Annual Reviews of Fluid Mechanics, Vol. 7, 1975, pp. 141-165.

5. Hallock, J.N. and Eberle, W.R. (eds.), Aircraft Wake Vortices: A State-of-the-Art Review of the United States R&D Program, Transportation Systems Center, Cambridge, MA, Report No. FAA-RD-77-23, 1977.

6. Sarpkaya, T., "Trailing Vortices in Homogeneous and Density-Stratified Media," Journal of Fluid Mechanics, Vol. 136, 1983, pp. 85-109.

7. Panton, R.L., Oberkampf, W.L., and Soskic, N., "Flight Measurements of a Wing Tip Vortex," Journal of Aircraft, Vol. 17, 1980, pp. 250-259.

8. Baker, G.R., Barker, S.J., Bofah, K.K. and Saffman, P.G., "Laser Anemometer Measurements of Trailing Vortices in Water," Journal of Fluid Mechanics, Vol. 65, pp. 325-336.

9. Crow, S.C., "Stability Theory for a Pair of Trailing Vortices," AIAA Journal, Vol. 8, 1970, pp. 2172-2179.

10. Peace, A.J. and Riley, N., "A Viscous Vortex Pair in Ground Effect," Journal of Fluid Mechanics, Vol. 129, 1983, pp. 409-426.

11. Barker, S.J. and Crow, S.C., "The Motion of a Two-Dimensional Vortex Pair in Ground Effect," Journal of Fluid Mechanics, Vol. 82, 1977, pp. 659-671.

12. Tombach, I.H., "Transport of a Vortex Wake in a Stably Stratified Atmosphere," Aircraft Wake Turbulence and Its Detection, Edited by J.H. Olsen et al., Plenum Press, New York, 1971, pp. 41-57.

13. Maxworthy, T., "Solitary Waves on Density Interfaces," Waves on Fluid Interfaces, Edited by R.E. Meyer, Academic Press, New York, 1983, pp. 201-220.

14. Naval Postgraduate School, Monterey, California, NPS-69-82-003, Trailing Vortices in Stratified Fluids, by T. Sarpkaya and S.K. Johnson, June 1982.

15. Johnson, S.K., Trailing Vortices in Stratified Fluids, M.S. Thesis, Naval Postgraduate School, Monterey, California, June 1982.

16. Turkmen, C., Trailing Vortices in Stratified and Unstratified Fluids, M.S. Thesis, Naval Postgraduate School, Monterey, California, December 1982.

17. Sarpkaya, T. and Henderson, D.O., Free Surface Scars and Striations due to Trailing Vortices Generated by a Submerged Lifting Surface, AIAA Paper No. AIAA-85-0445, January 1985.

18. Compte-Bellot, G. and Corrsin, S., "The Use of a Contraction to Improve the Isotropy of Grid-Generated Turbulence," Journal of Fluid Mechanics, Vol. 25, 1966, pp. 657-682.

19. Compte-Bellot, G. and Corrsin, S., "Simple Eulerian Time Correlation of Full- and Narrow-Band Velocity Signals in Grid-Generated 'Isotropic' Turbulence," Journal of Fluid Mechanics, Vol. 48, 1971, pp. 273-337.

20. Friehe, C.A. and Schwarz, W.H., "Grid-Generated Turbulence in Dilute Polymer Solutions," Journal of Fluid Mechanics, Vol. 44, 1970, pp. 173-193.

21. Gad-el-Hak, M., Experiments on the Nearly Isotropic Turbulence Behind a Jet Grid, Ph.D. Dissertation, The Johns Hopkins University, 1972.

22. Schedvin, J.C., Stegen, G.R. and Gibson, C.H., "Universal Similarity at High Grid Reynolds Numbers," Journal of Fluid Mechanics, Vol. 65, 1974, pp. 561-579.

23. Huot, J.P., Rey, C. and Arbey, H., "Experimental Analysis of the Pressure Field Induced on a Square Cylinder by a Turbulent Flow," Journal of Fluid Mechanics, Vol. 162, 1986, pp. 283-298.

24. Crow, S.C. and Bate, E.R. Jr., "Lifespan of Trailing Vortices in a Turbulent Atmosphere," Journal of Aircraft, Vol. 13, 1976, pp. 476-482.

25. Tombach, I., "Observations of Atmospheric Effects on Vortex Wake Behaviors," Journal of Aircraft, Vol. 10, 1973, pp. 641-647.

26. Chow, C.Y., An Introduction to Computational Fluid Mechanics, John Wiley & Sons, New York, 1979.

APPENDIX A

FIGURES

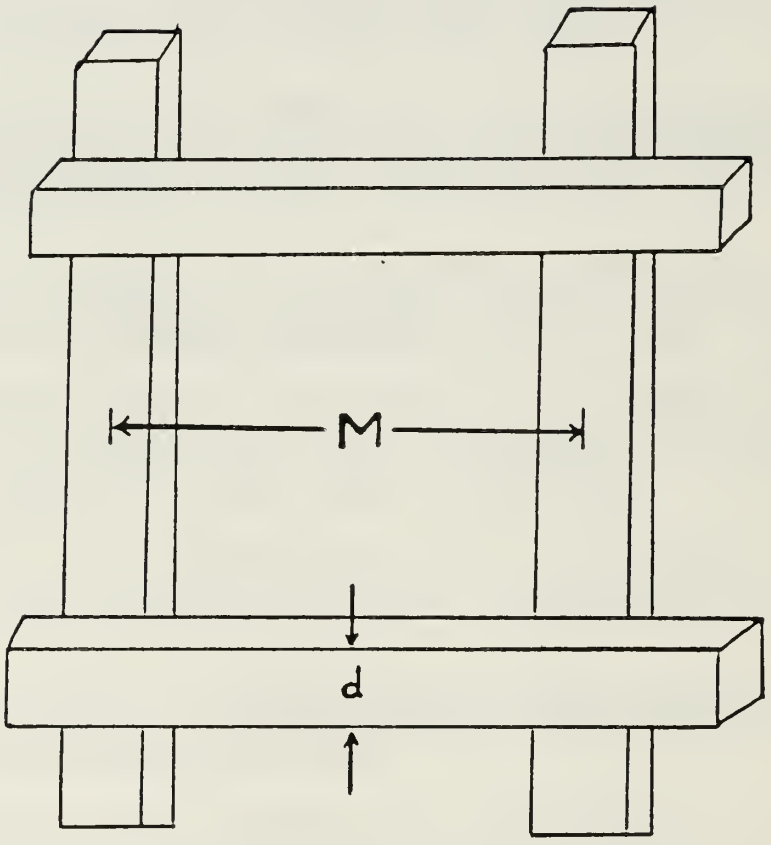

Figure 1. Diagram of Biplanar Grid Construction

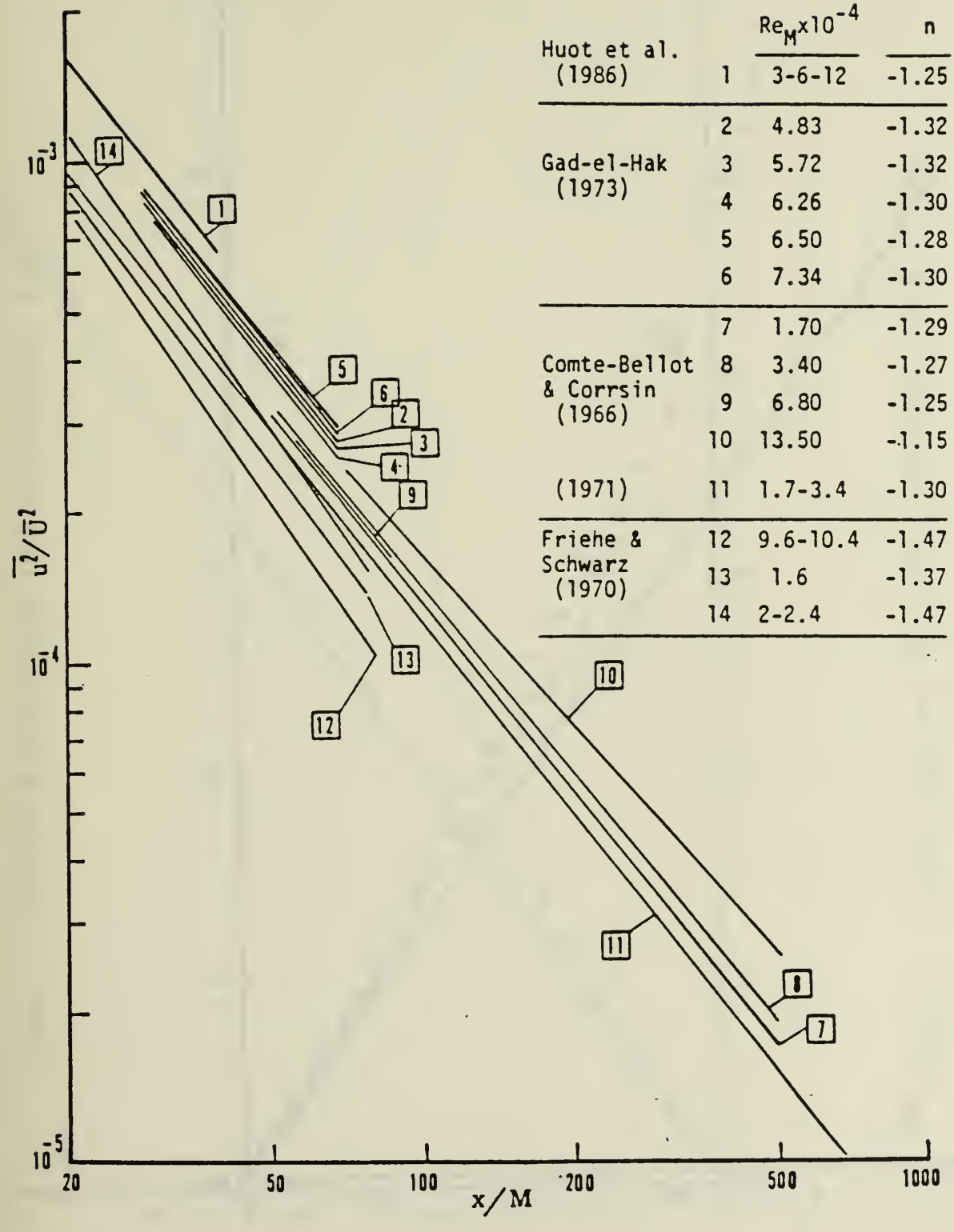

		$Re_M x10^{-4}$	n
Huot et al. (1986)	1	3-6-12	-1.25
Gad-el-Hak (1973)	2	4.83	-1.32
	3	5.72	-1.32
	4	6.26	-1.30
	5	6.50	-1.28
	6	7.34	-1.30
Comte-Bellot & Corrsin (1966)	7	1.70	-1.29
	8	3.40	-1.27
	9	6.80	-1.25
	10	13.50	-1.15
(1971)	11	1.7-3.4	-1.30
Friehe & Schwarz (1970)	12	9.6-10.4	-1.47
	13	1.6	-1.37
	14	2-2.4	-1.47

Figure 2. Comparison of Turbulence Models

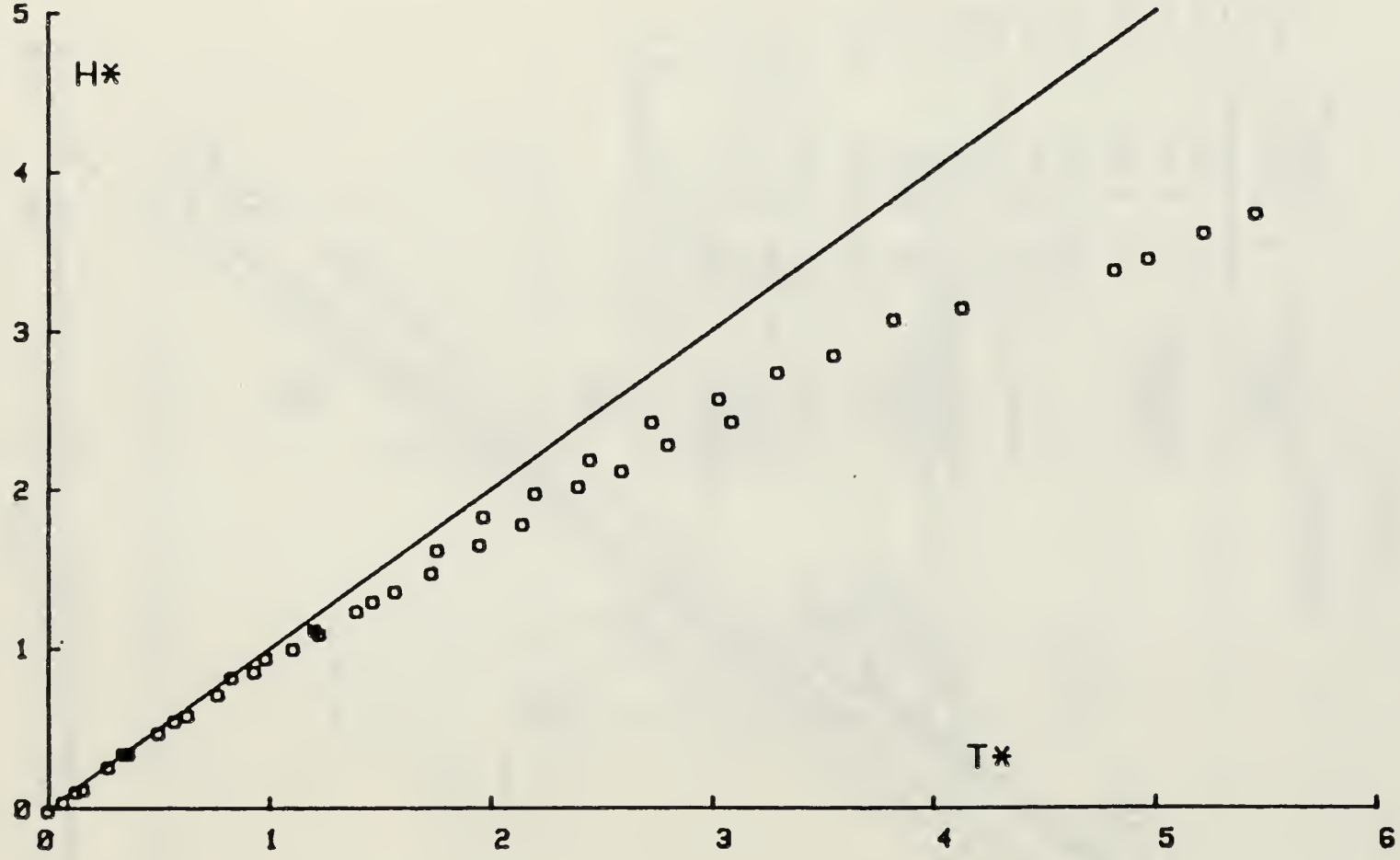

Figure 3. Vortex Rise for RP1 (U = 0.9 ft/sec, X/M = ∞)

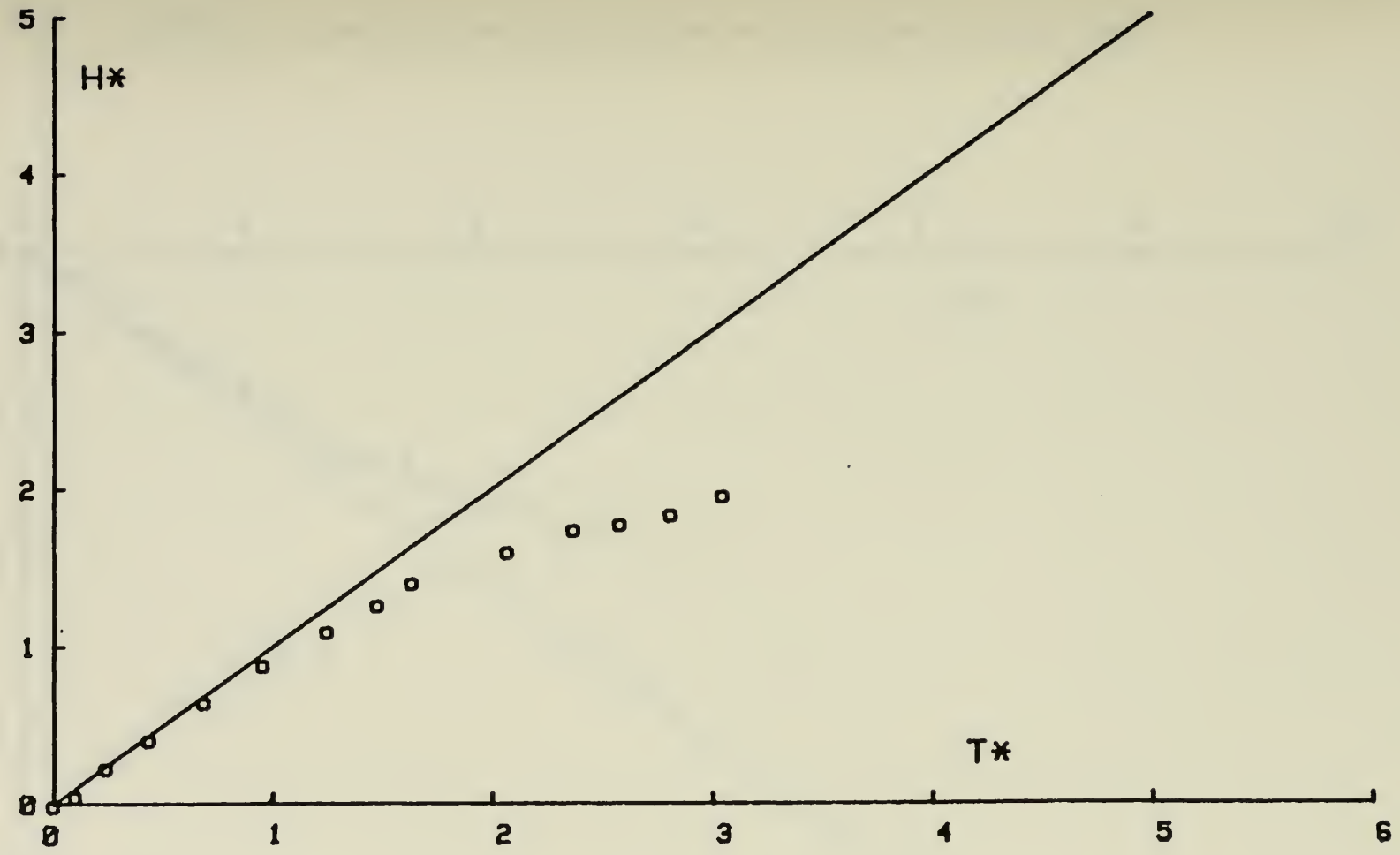

Figure 4. Vortex Rise for RP1 (U = 0.9 ft/sec, X/M = 750)

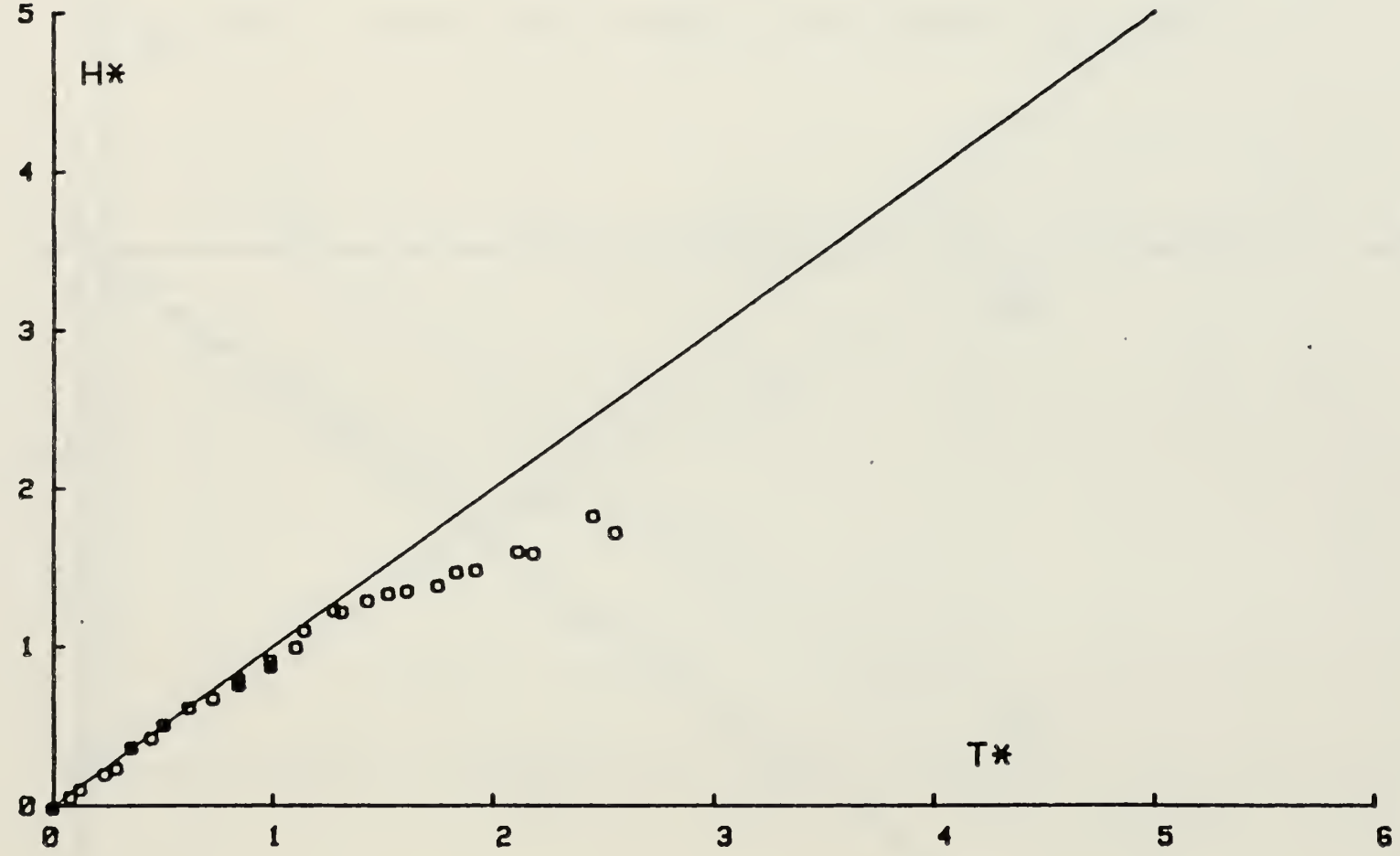

Figure 5. Vortex Rise for RP1 (U = 0.9 ft/sec, X/M = 500)

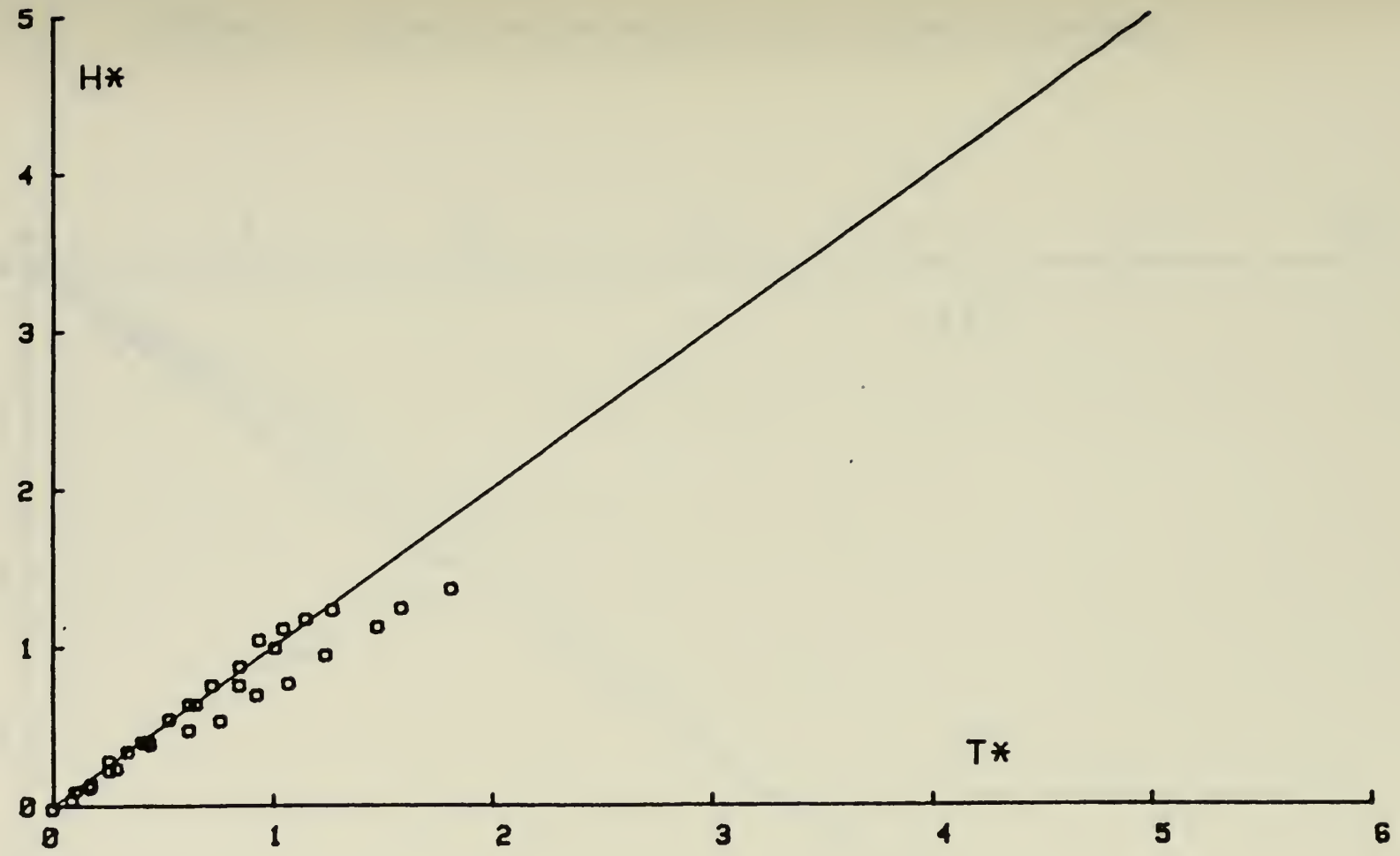

Figure 6. Vortex Rise for RP1 (U = 0.9 ft/sec, X/M = 250)

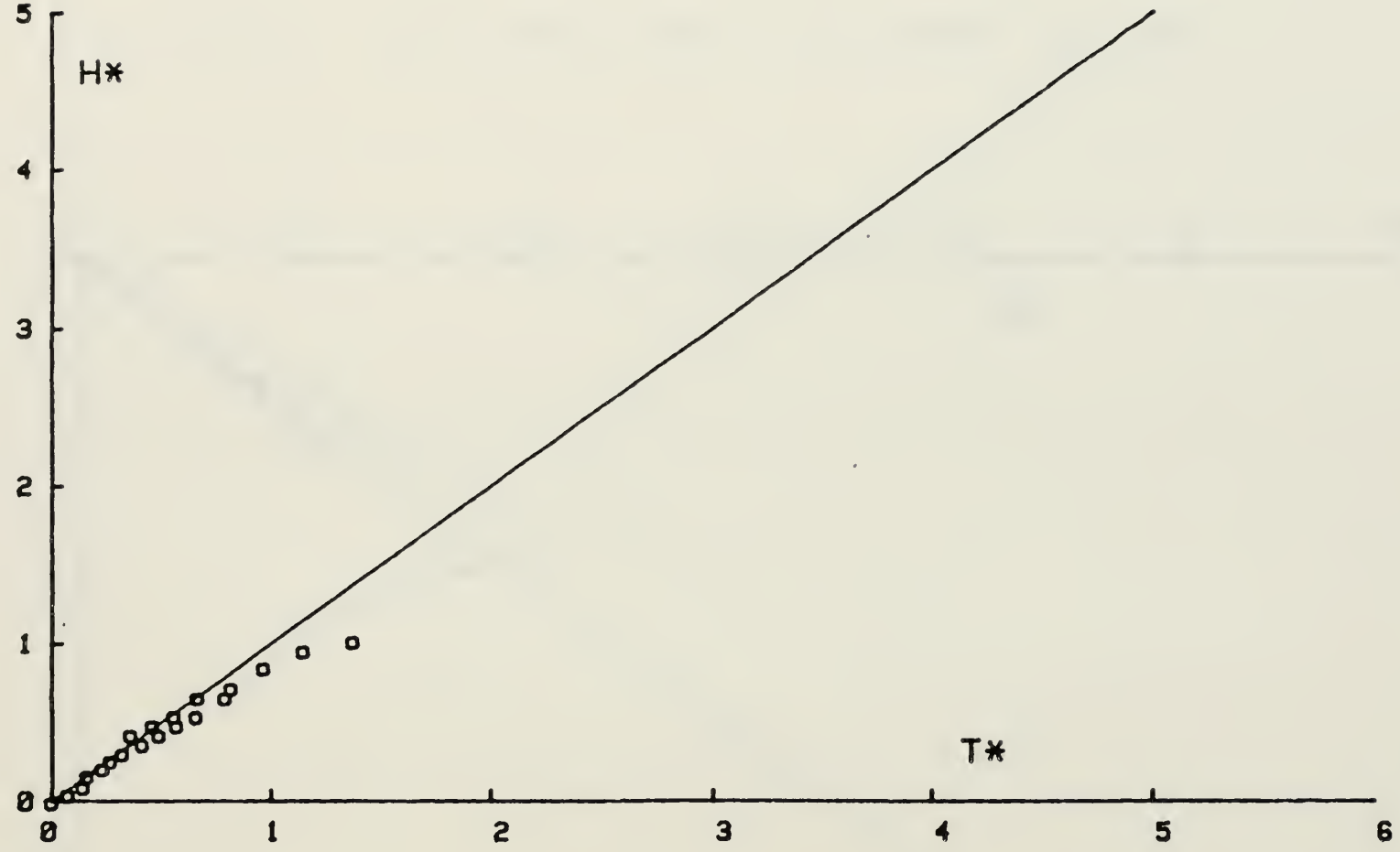

Figure 7. Vortex Rise for RP1 (U = 0.9 ft/sec, X/M = 180)

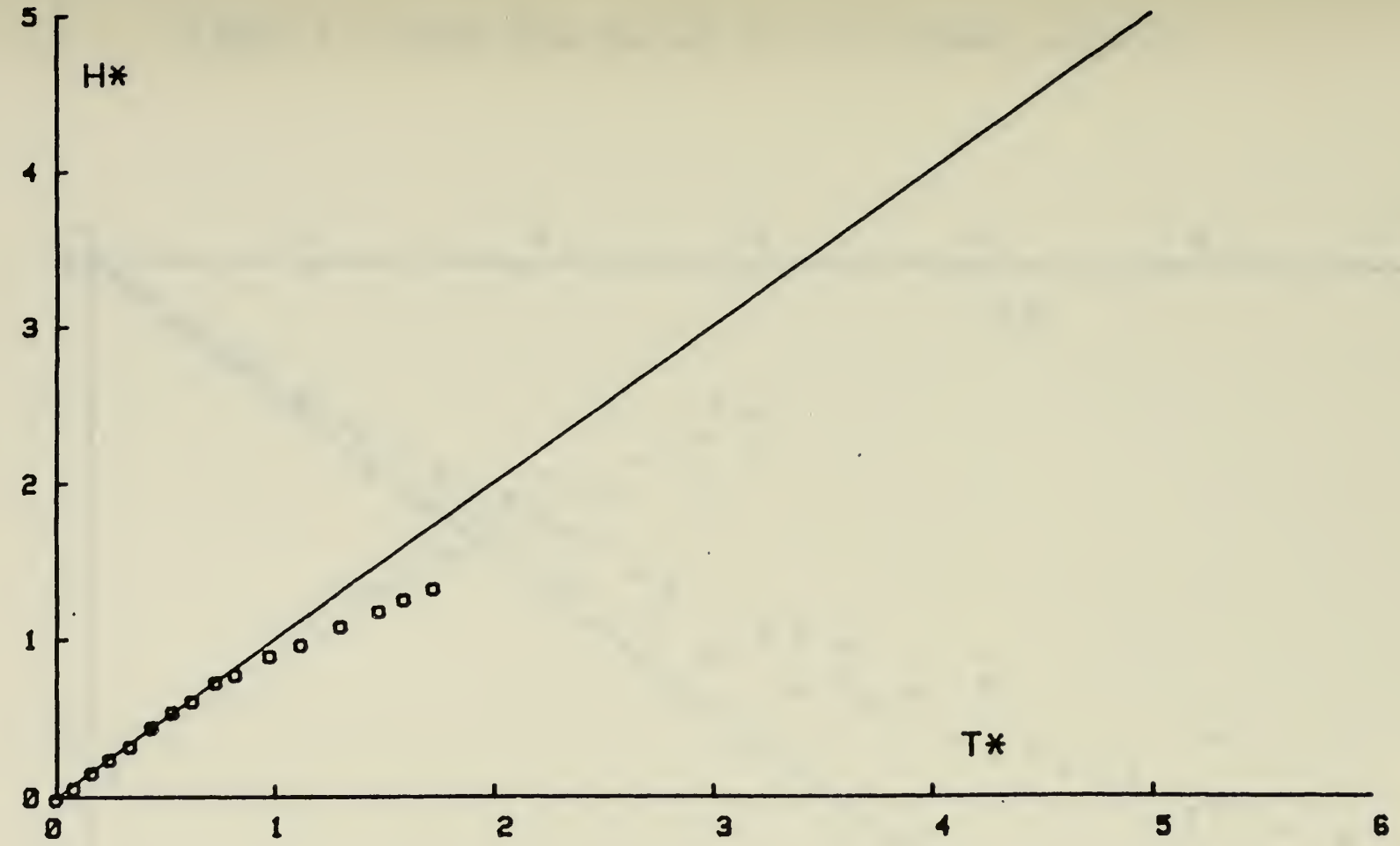

Figure 8. Vortex Rise for RP1 (U = 0.9 ft/sec, X/M = 80)

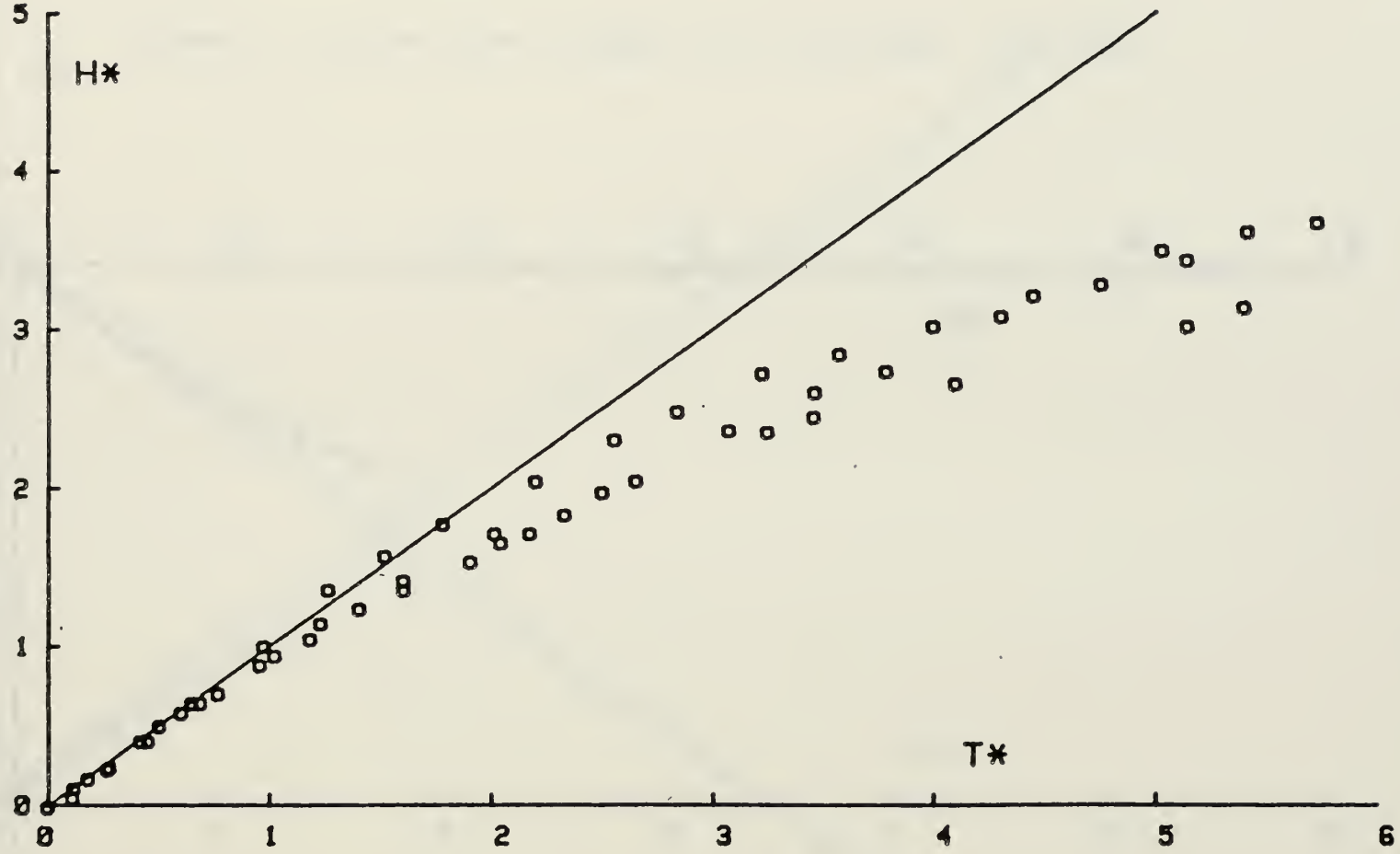

Figure 9. Vortex Rise for RP1 (U = 1.6 ft/sec, X/M = ∞)

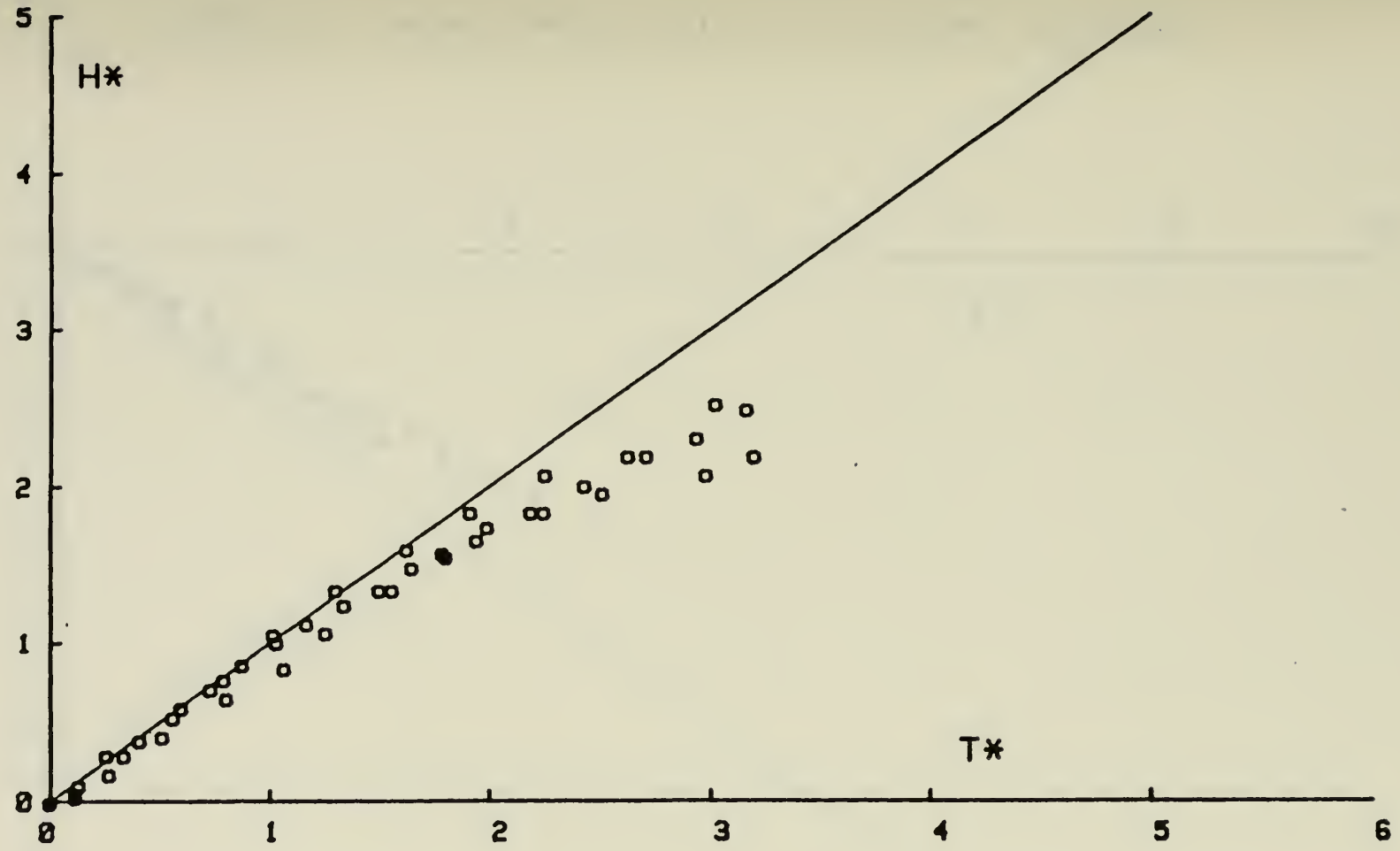

Figure 10. Vortex Rise for RP1 (U = 1.6 ft/sec, X/M = 750)

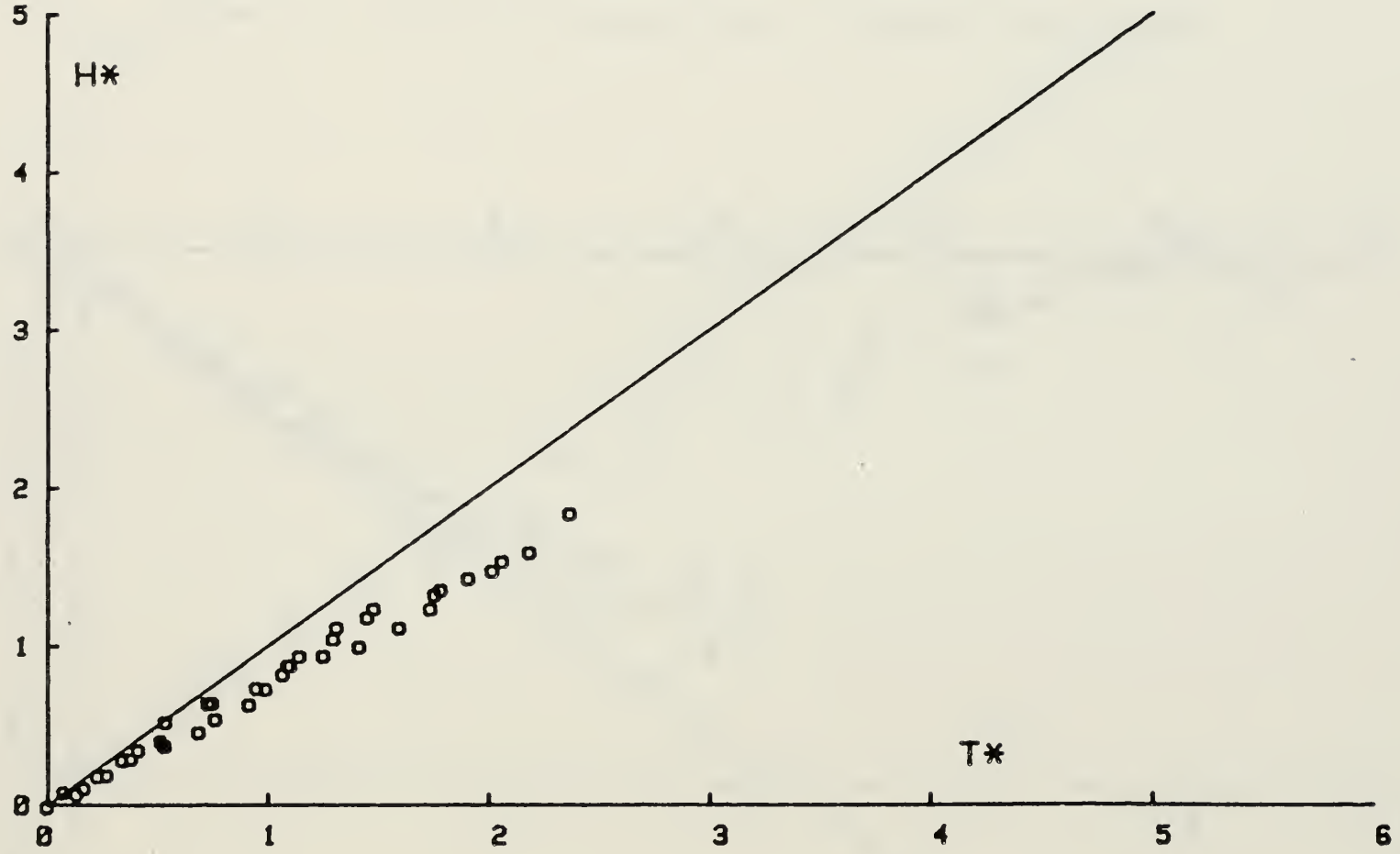

Figure 11. Vortex Rise for RP1 (U = 1.6 ft/sec, X/M = 500)

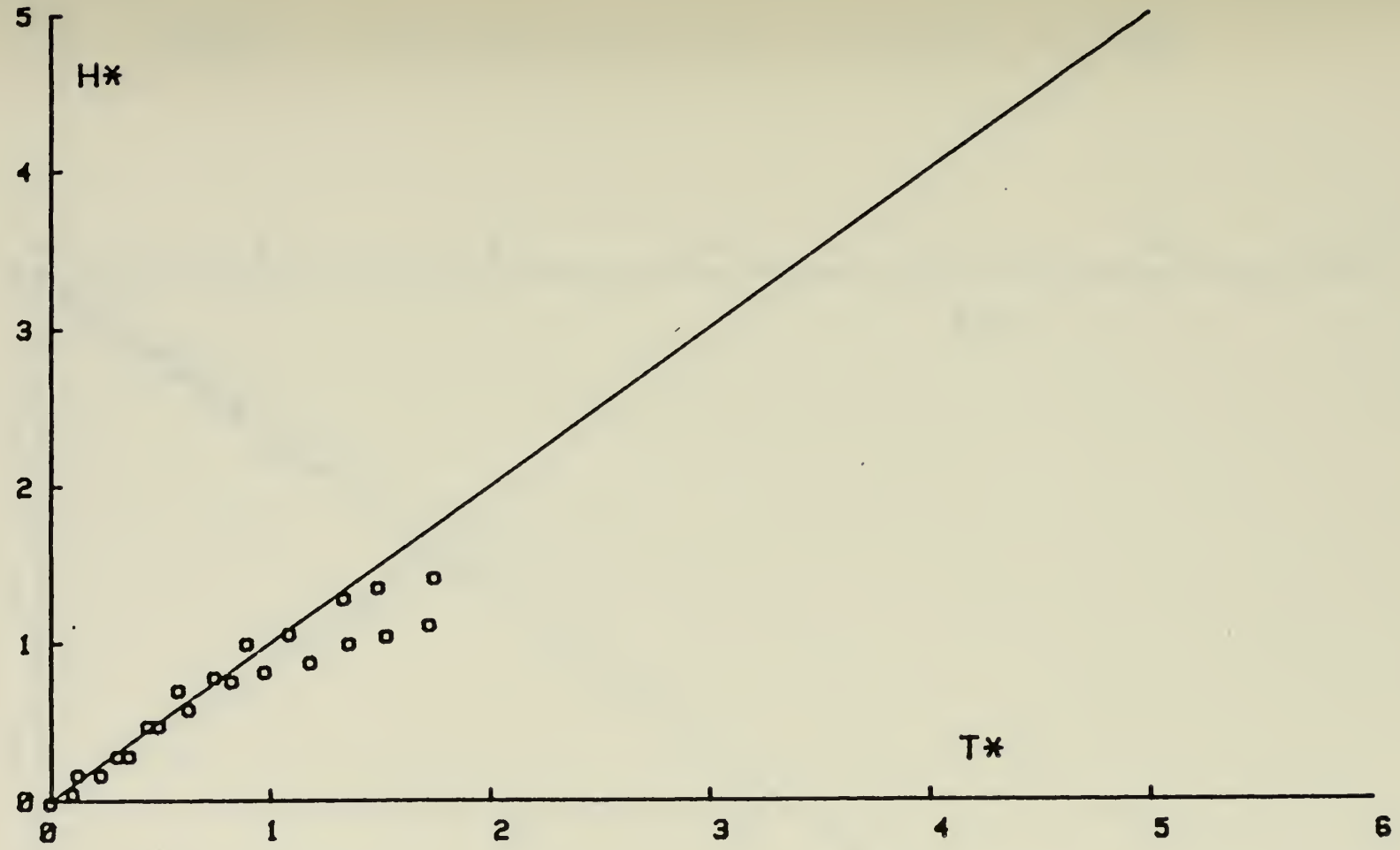

Figure 12. Vortex Rise for RP1 (U = 1.6 ft/sec, X/M = 250)

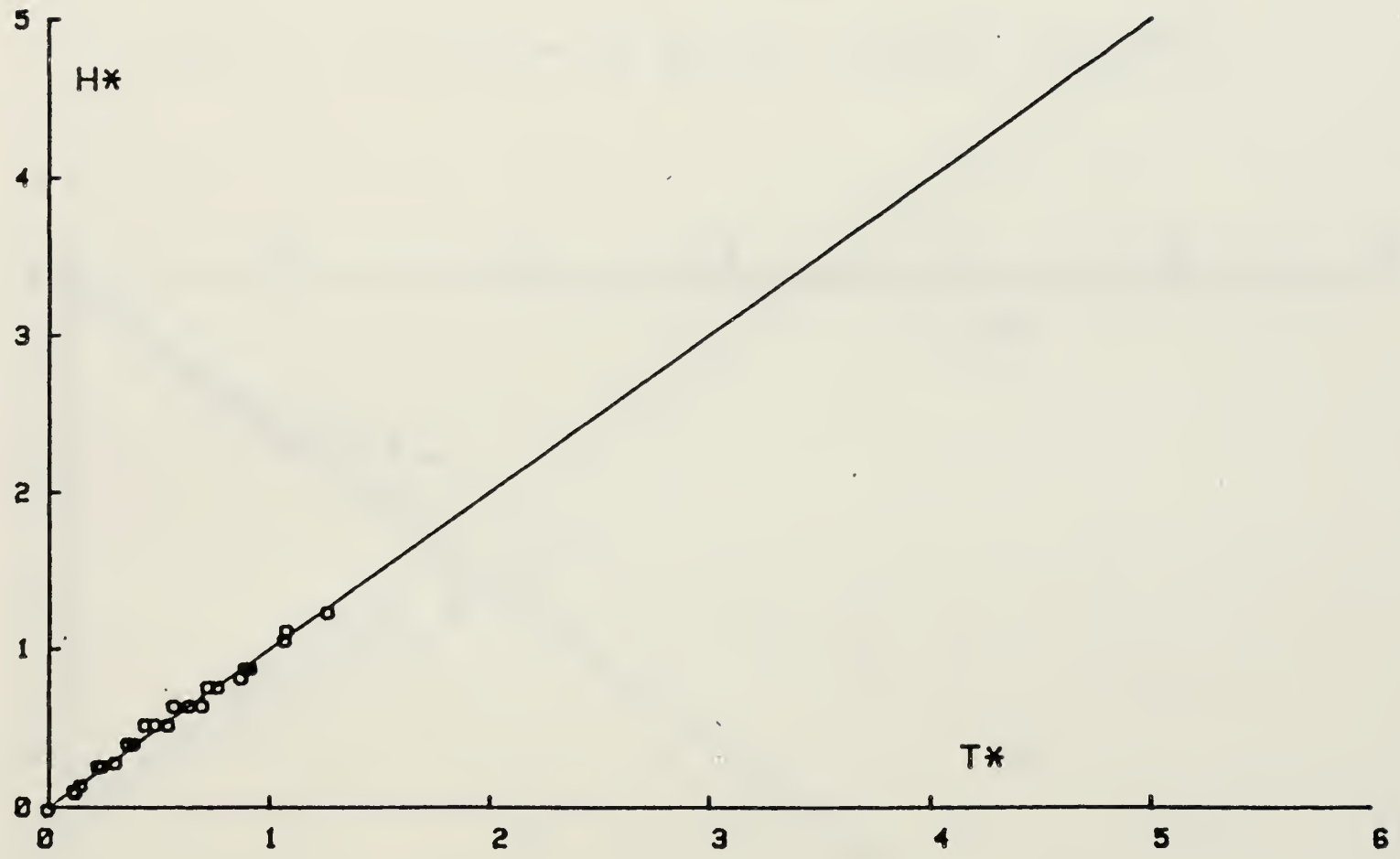

Figure 13. Vortex Rise for RP1 (U = 1.6 ft/sec, X/M = 180)

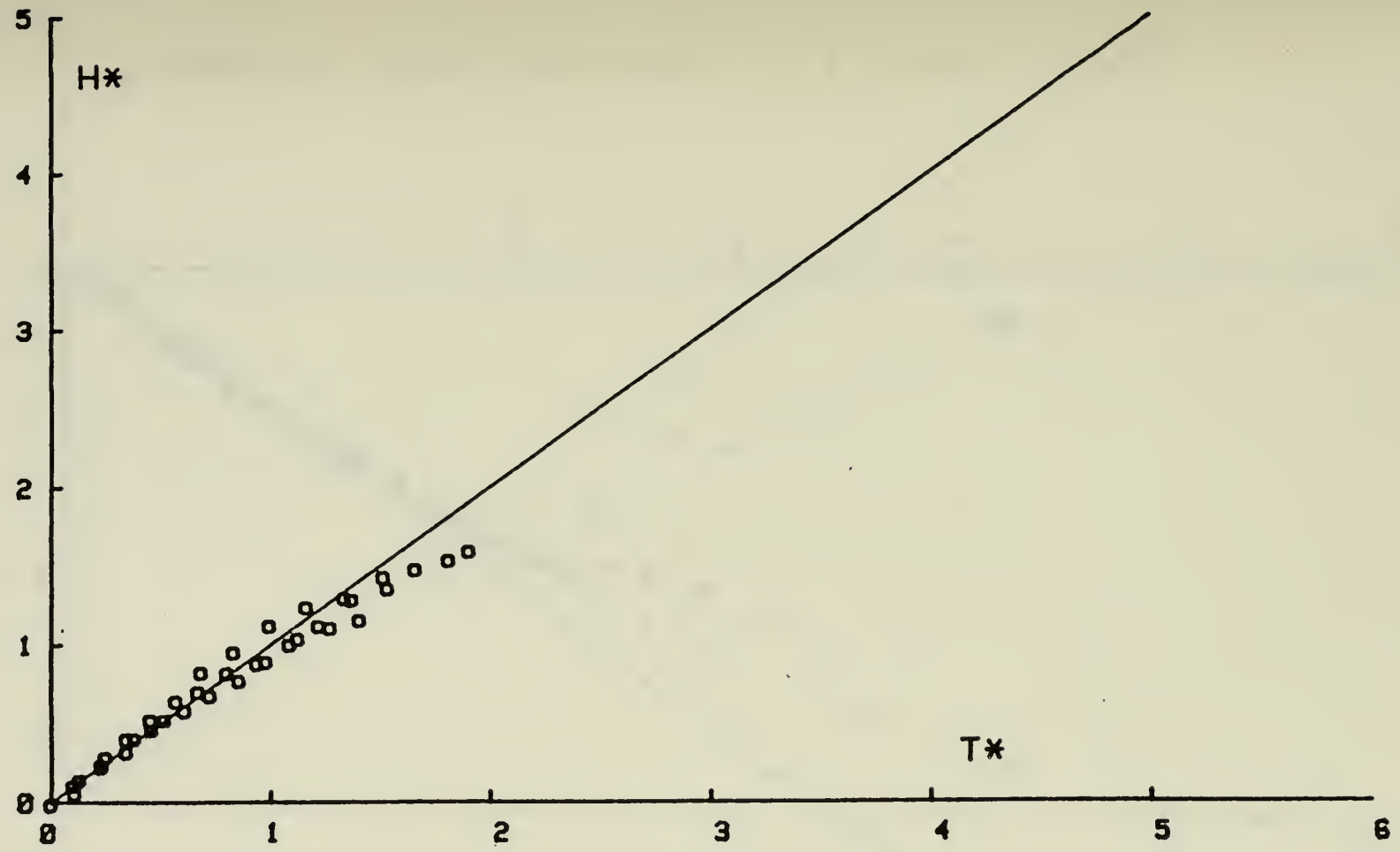

Figure 14. Vortex Rise for RP1 (U = 1.6 ft/sec, X/M = 80)

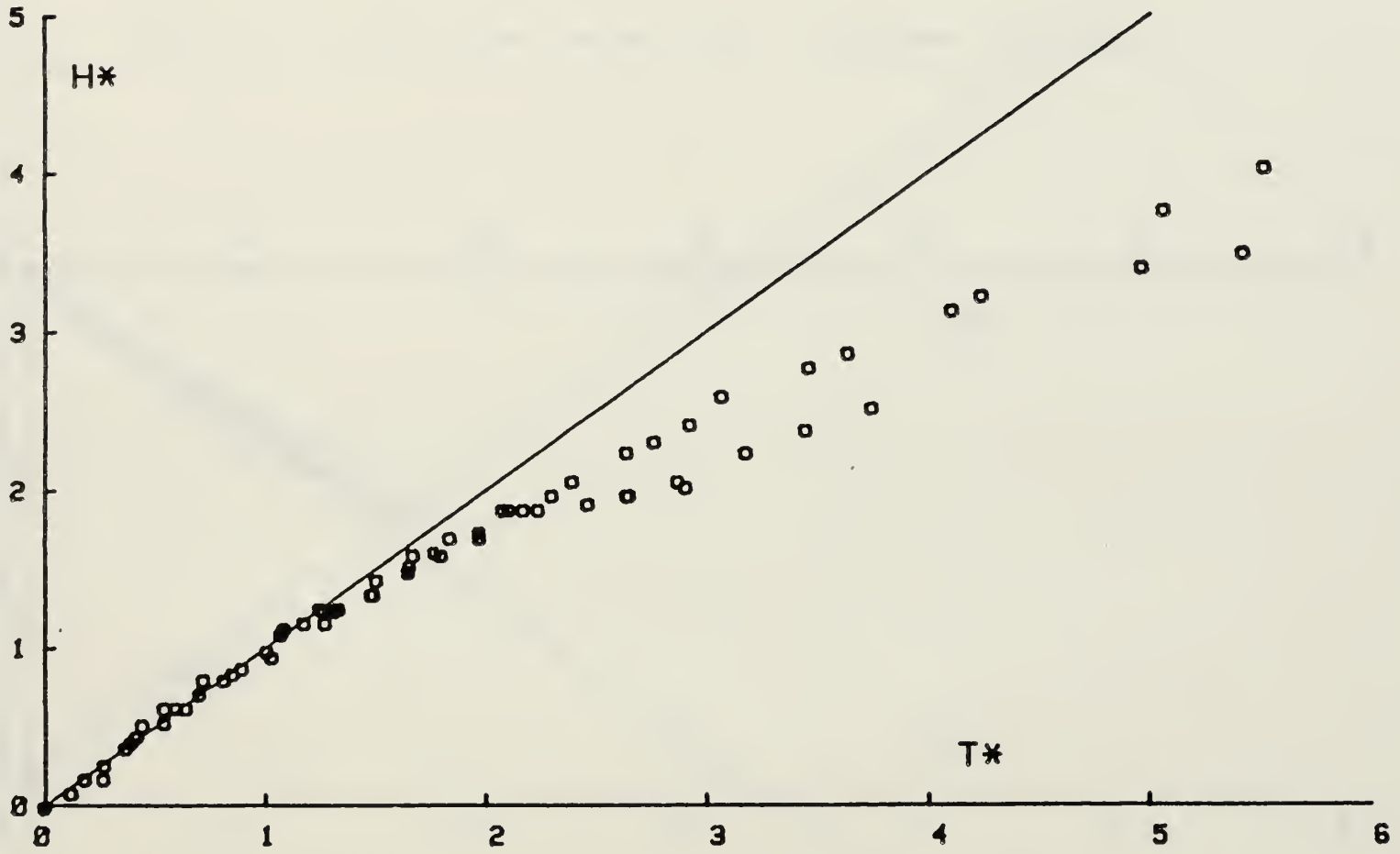

Figure 15. Vortex Rise for RP2 (U = 0.9 ft/sec, X/M = ∞)

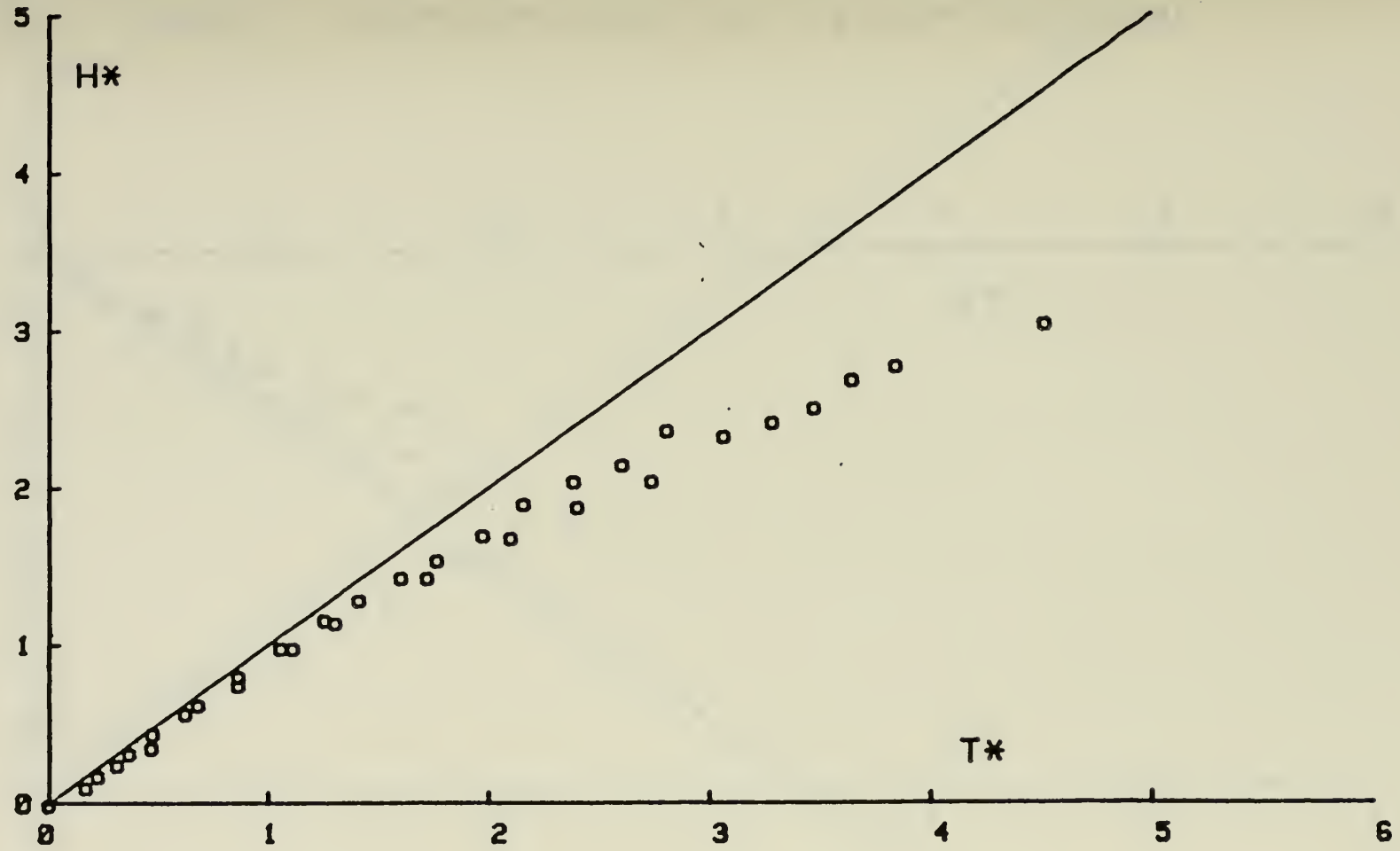

Figure 16. Vortex Rise for RP2 (U = 0.9 ft/sec, X/M = 750)

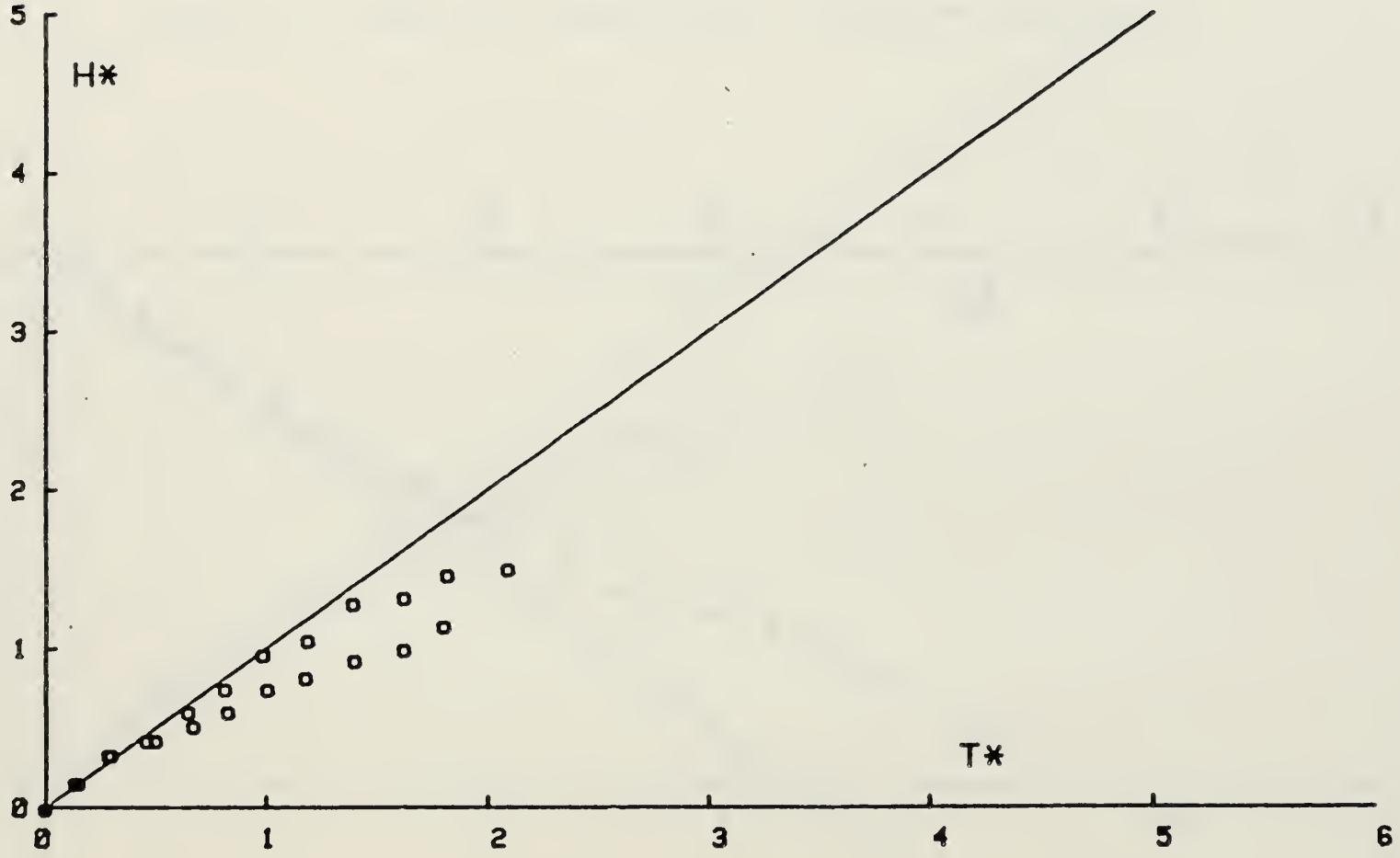

Figure 17. Vortex Rise for RP2 (U = 0.9 ft/sec, X/M = 500)

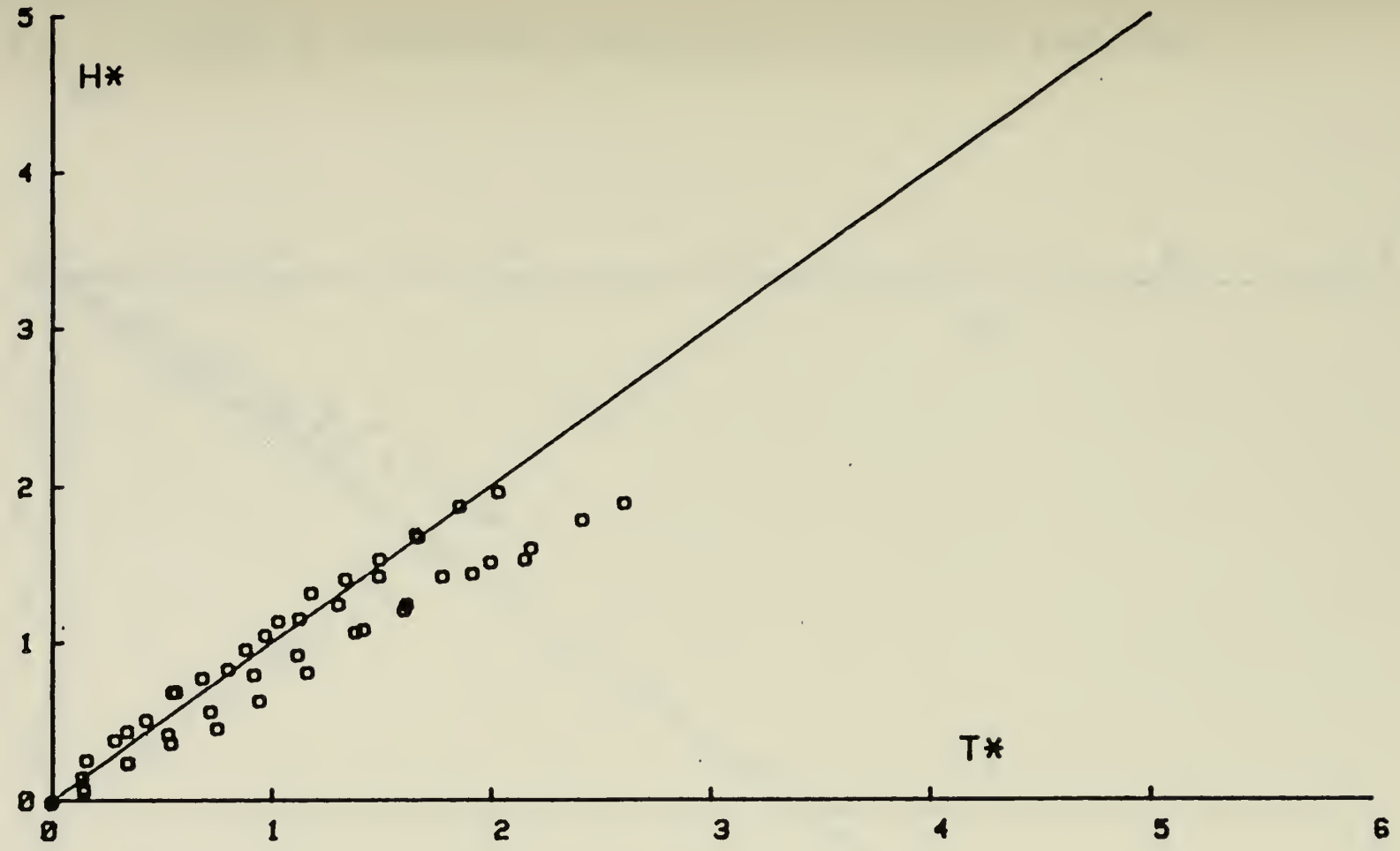

Figure 18. Vortex Rise for RP2 (U = 0.9 ft/sec, X/M = 250)

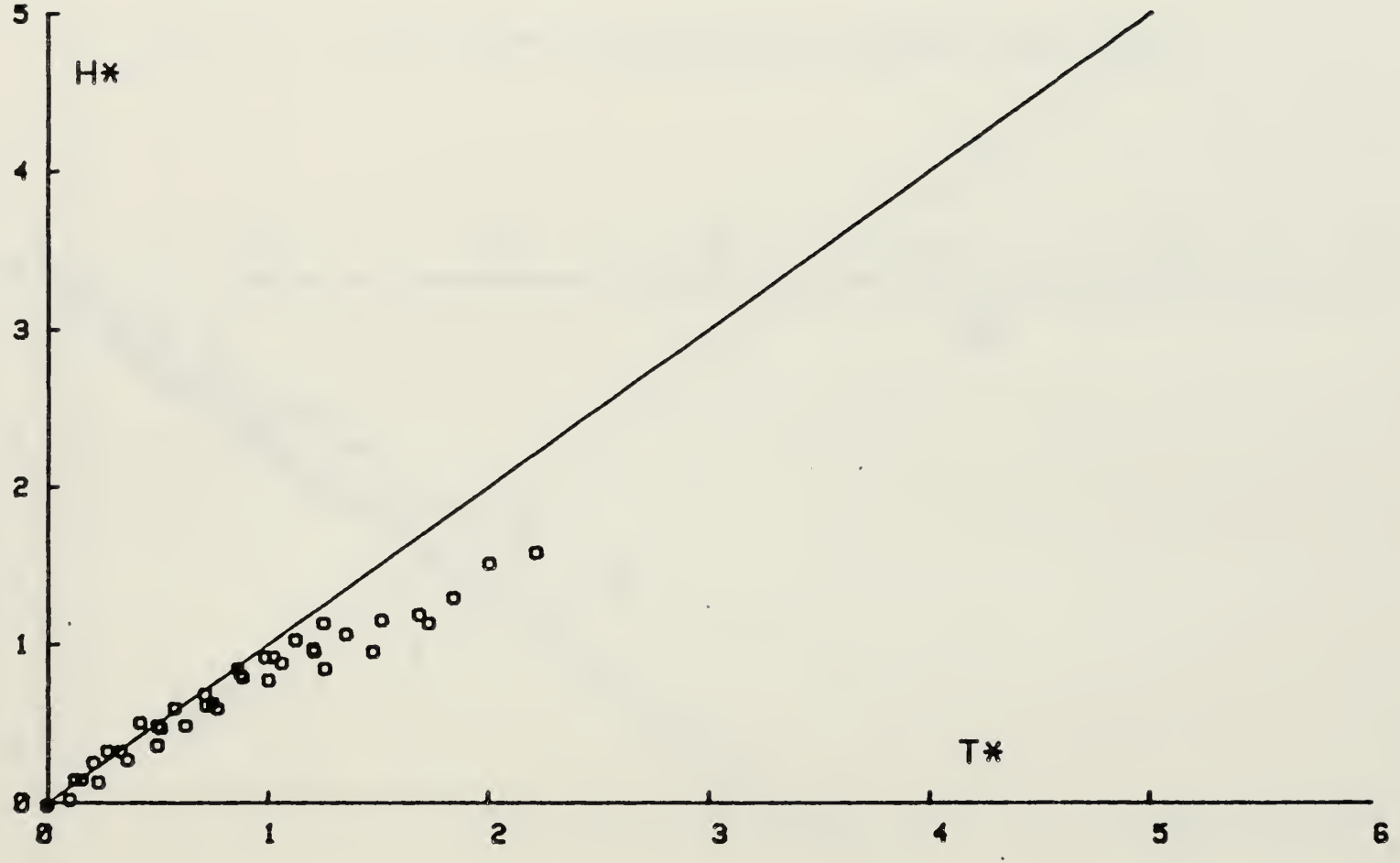

Figure 19. Vortex Rise for RP2 (U = 0.9 ft/sec, X/M = 180)

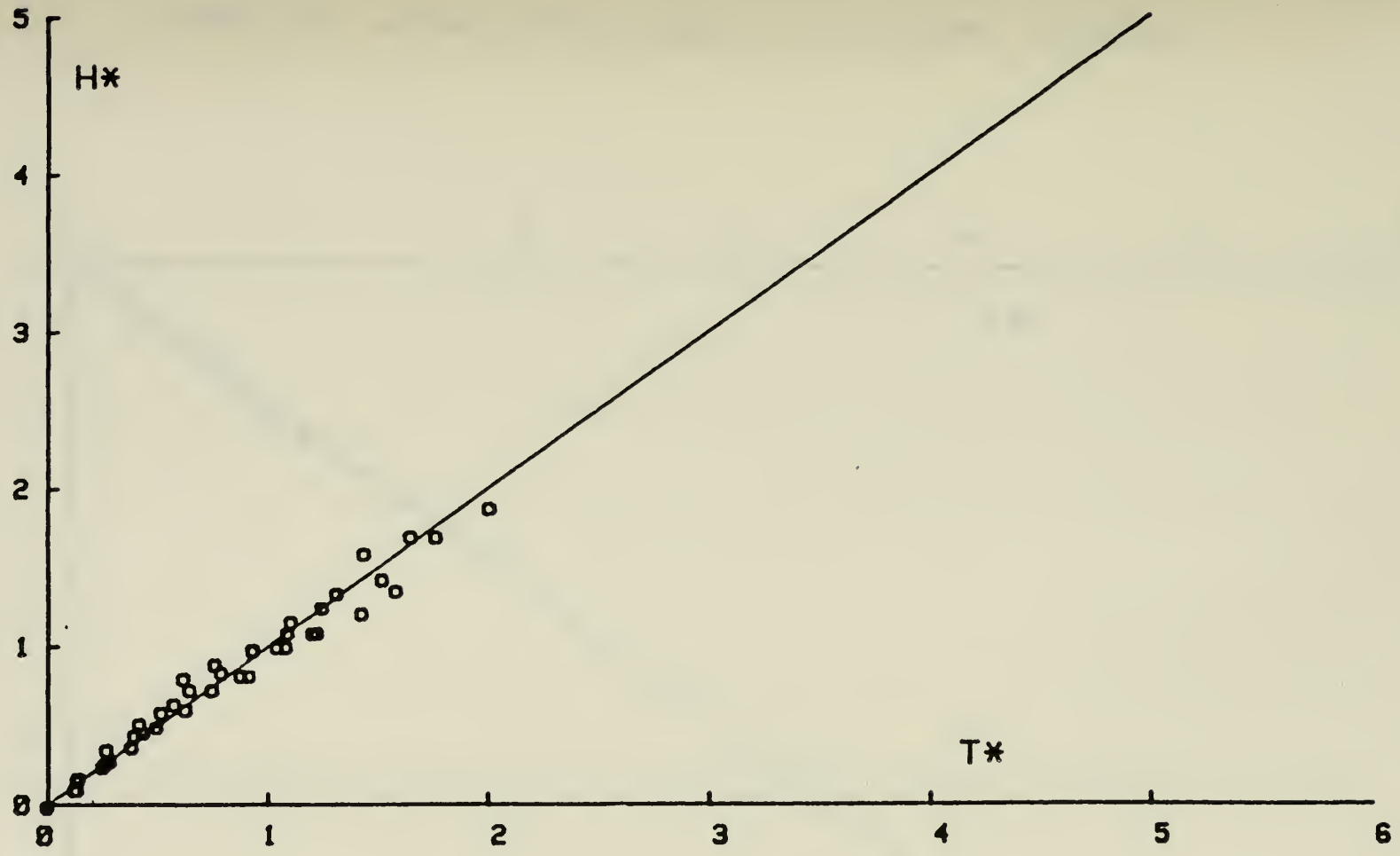

Figure 20. Vortex Rise for RP2 (U = 0.9 ft/sec, X/M = 80)

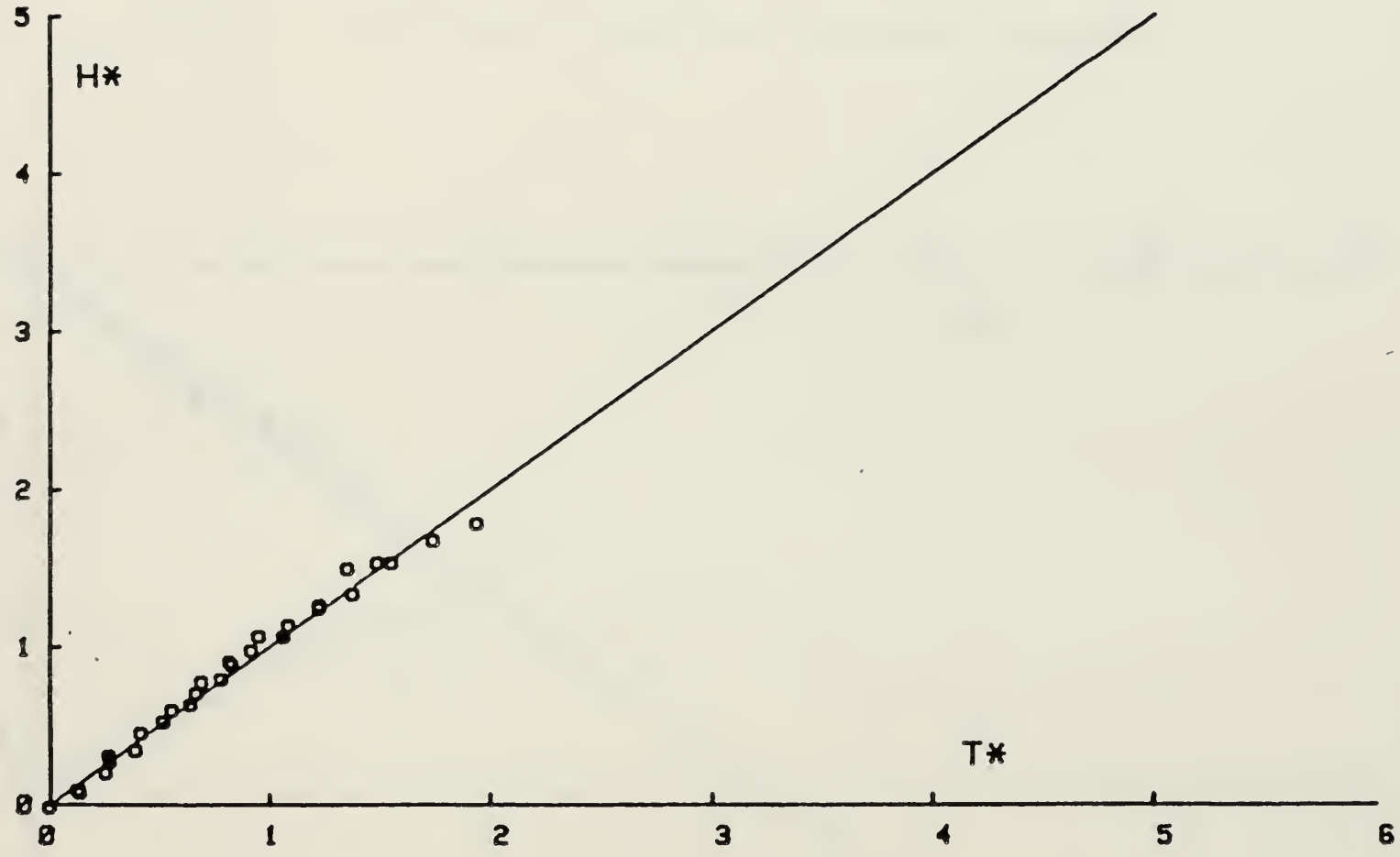

Figure 21. Vortex Rise for RP2 (U = 0.9 ft/sec, X/M = 50)

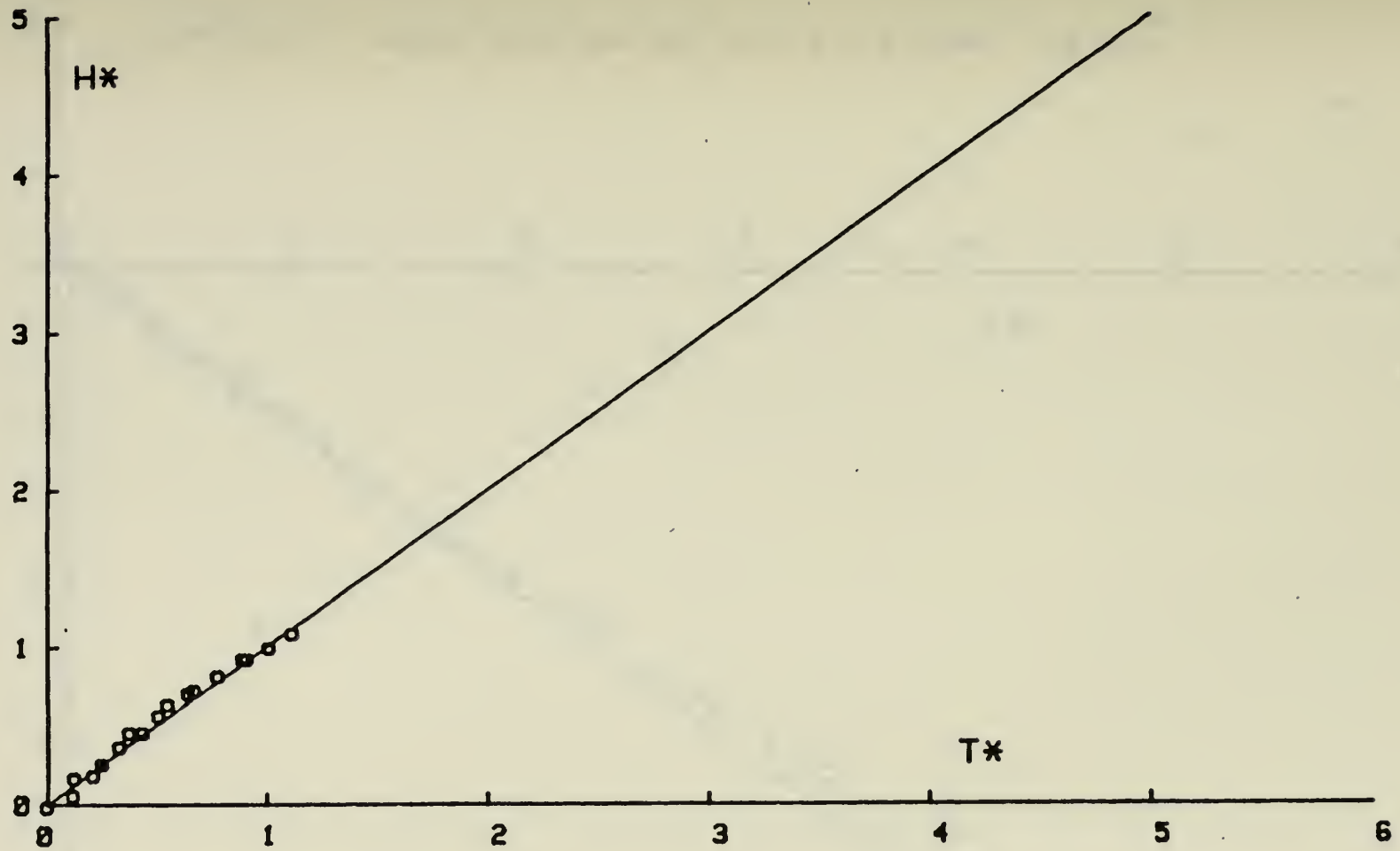

Figure 22. Vortex Rise for RP2 (U = 0.9 ft/sec, X/M = 25)

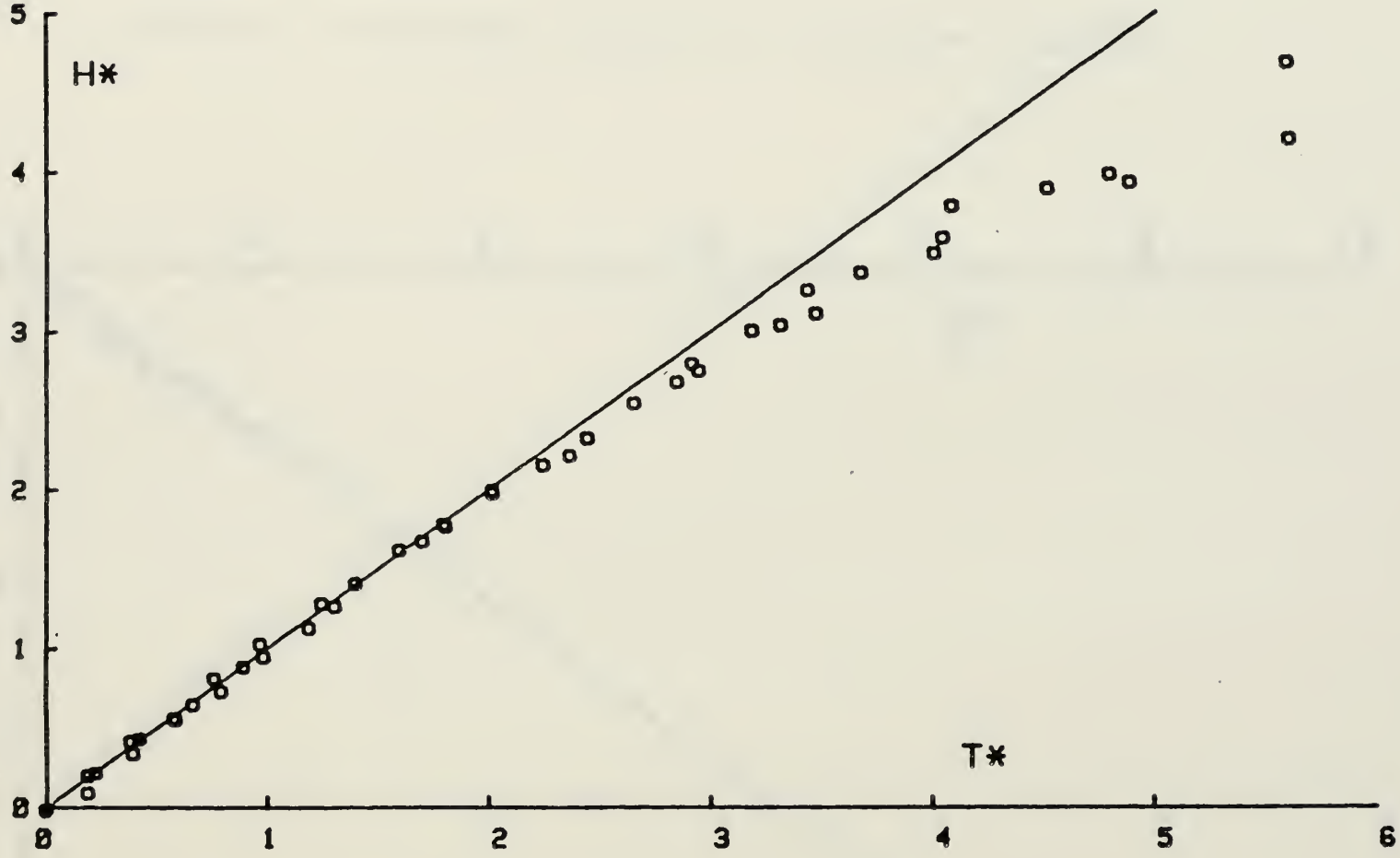

Figure 23. Vortex Rise for RP2 (U = 1.6 ft/sec, X/M = ∞)

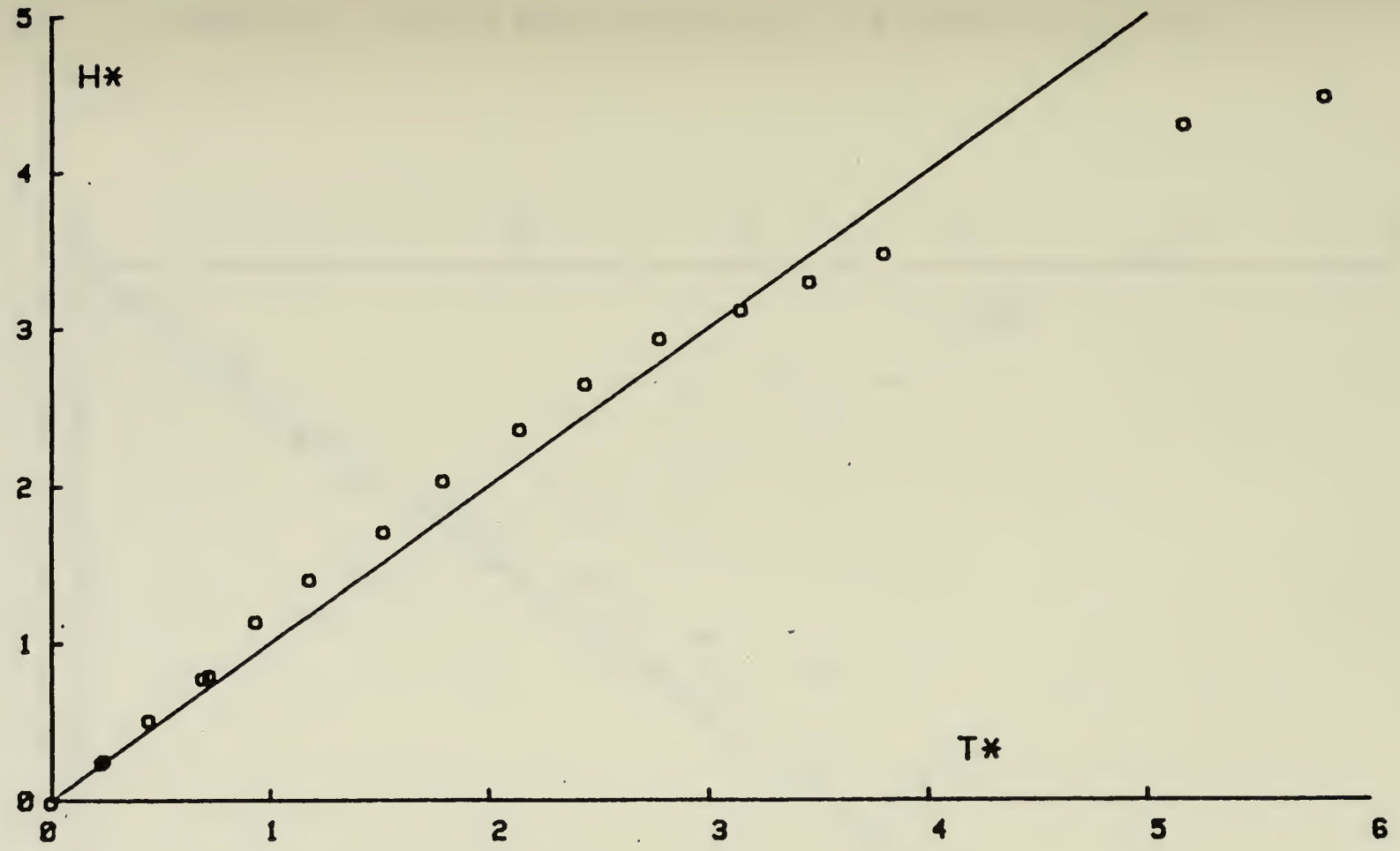

Figure 24. Vortex Rise for RP2 (U = 1.6 ft/sec, X/M = 1000)

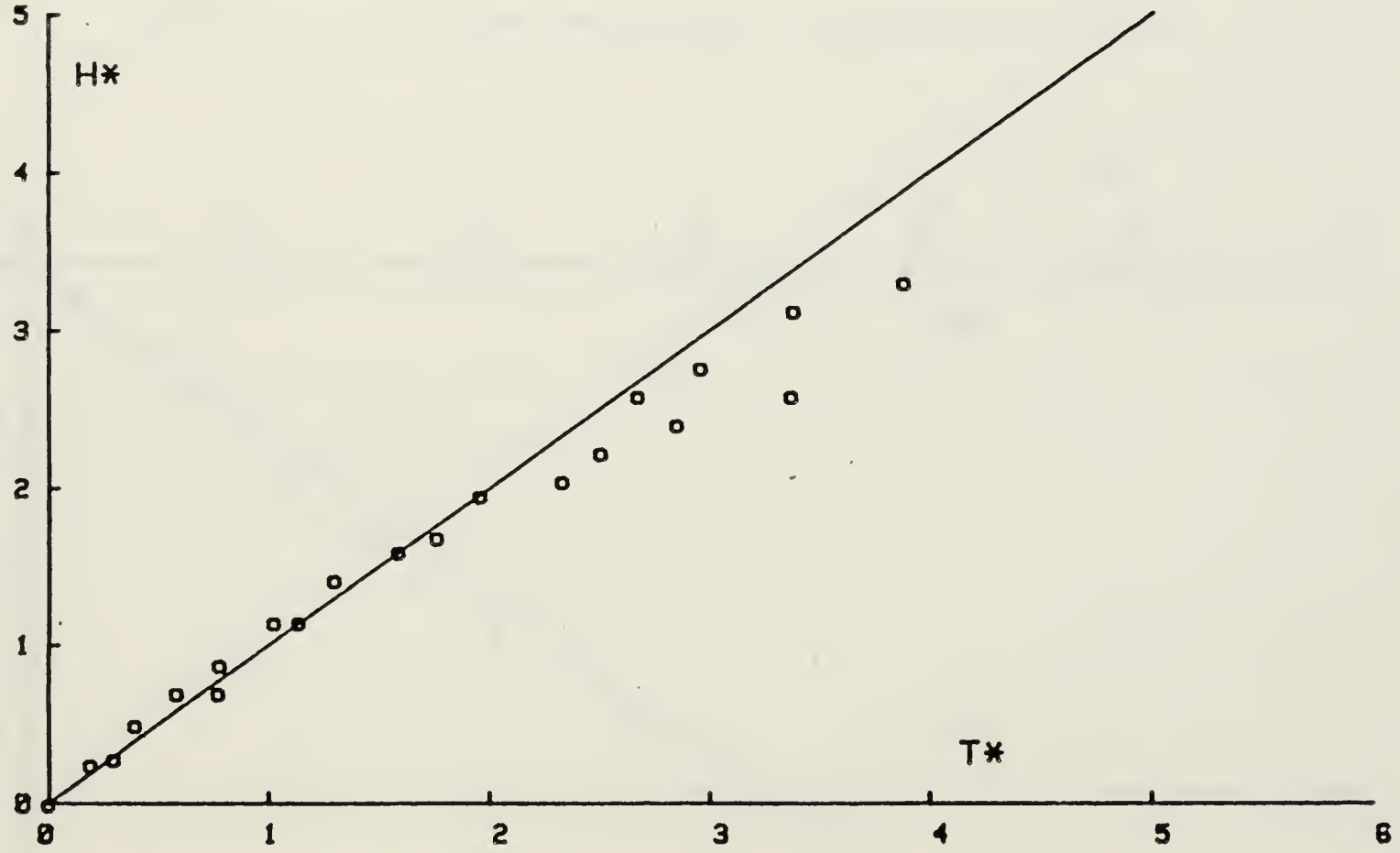

Figure 25. Vortex Rise for RP2 (U = 1.6 ft/sec, X/M = 750)

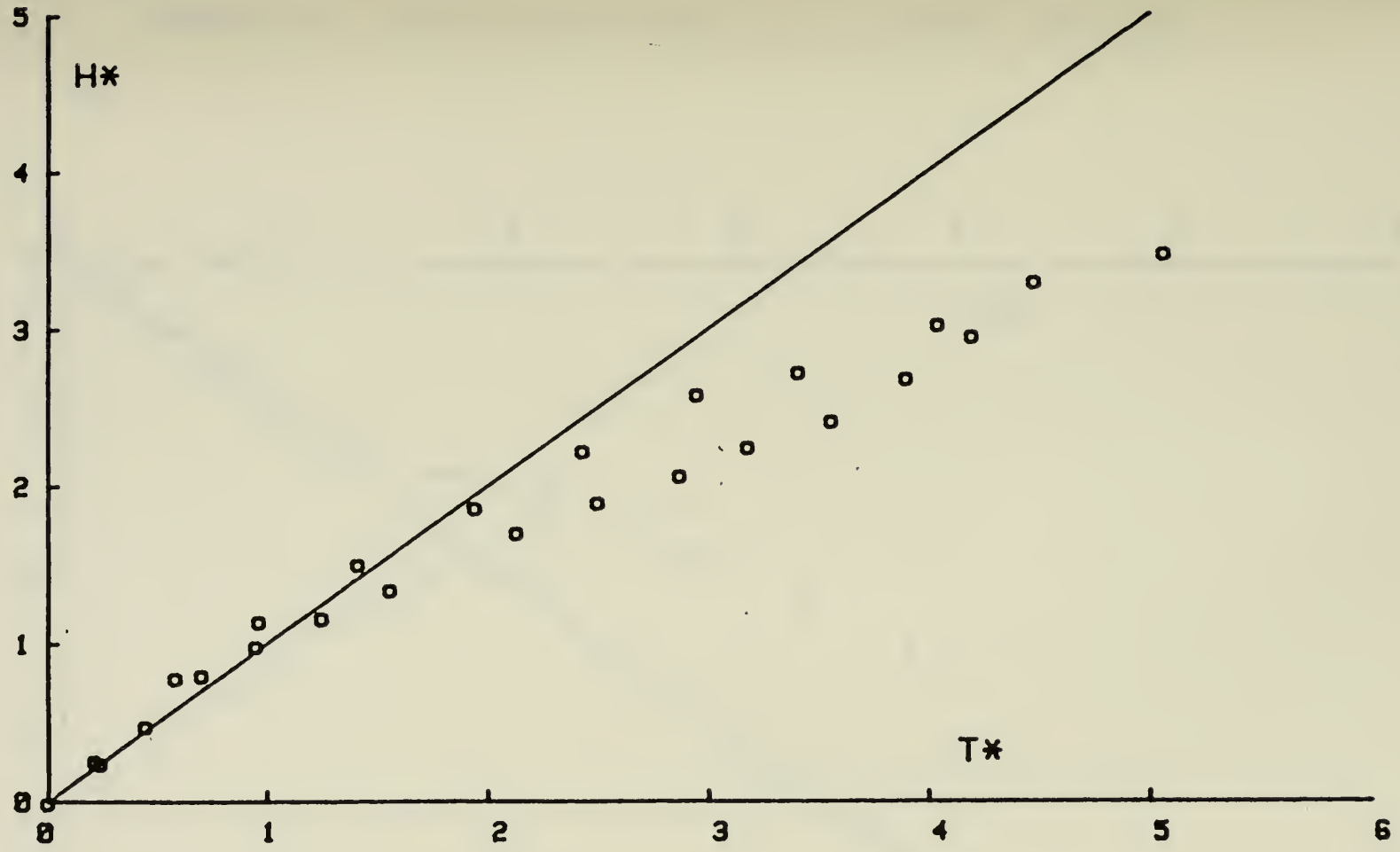

Figure 26. Vortex Rise for RP2 (U = 1.6 ft/sec, X/M = 500)

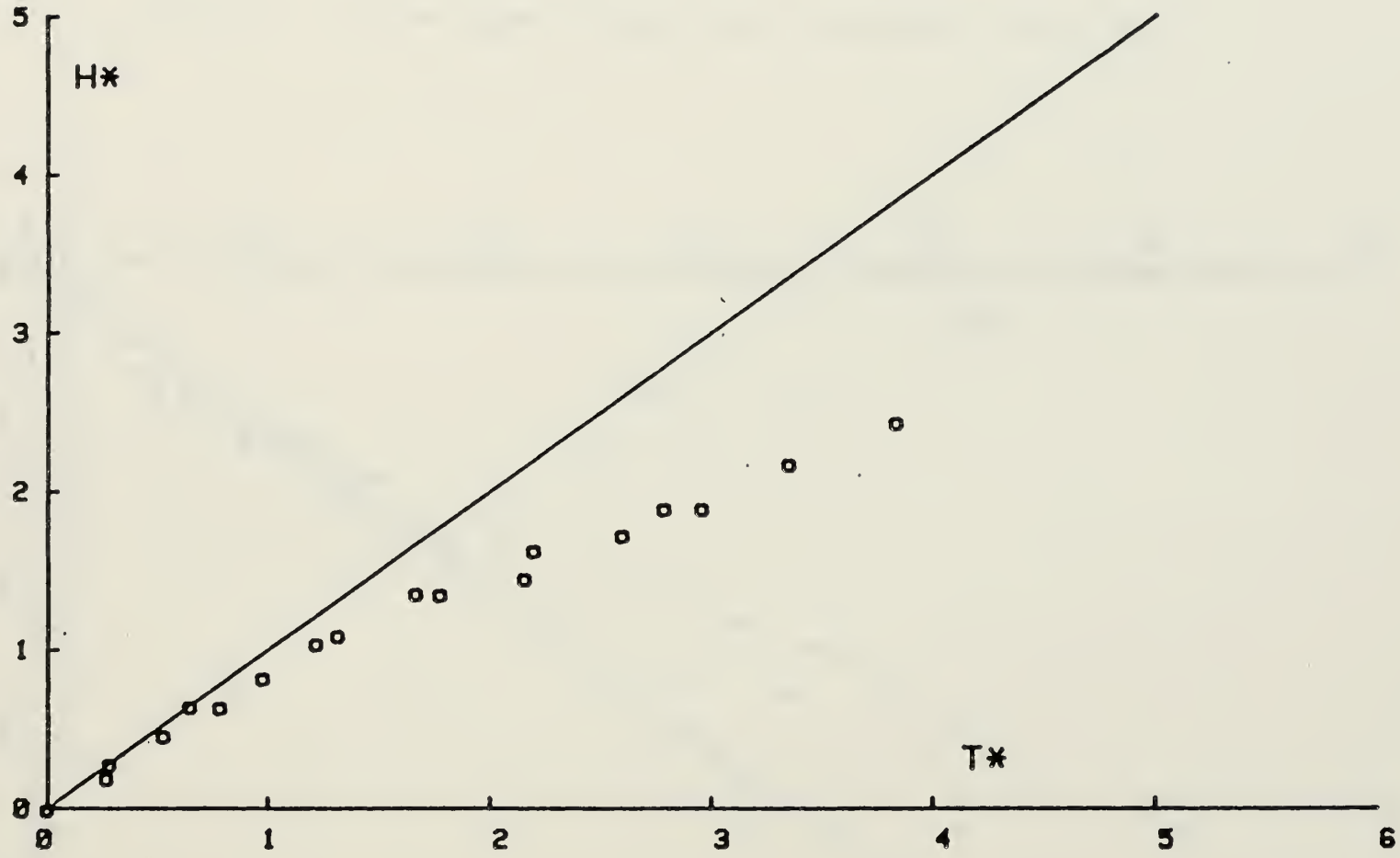

Figure 27. Vortex Rise for RP2 (U = 1.6 ft/sec, X/M = 250)

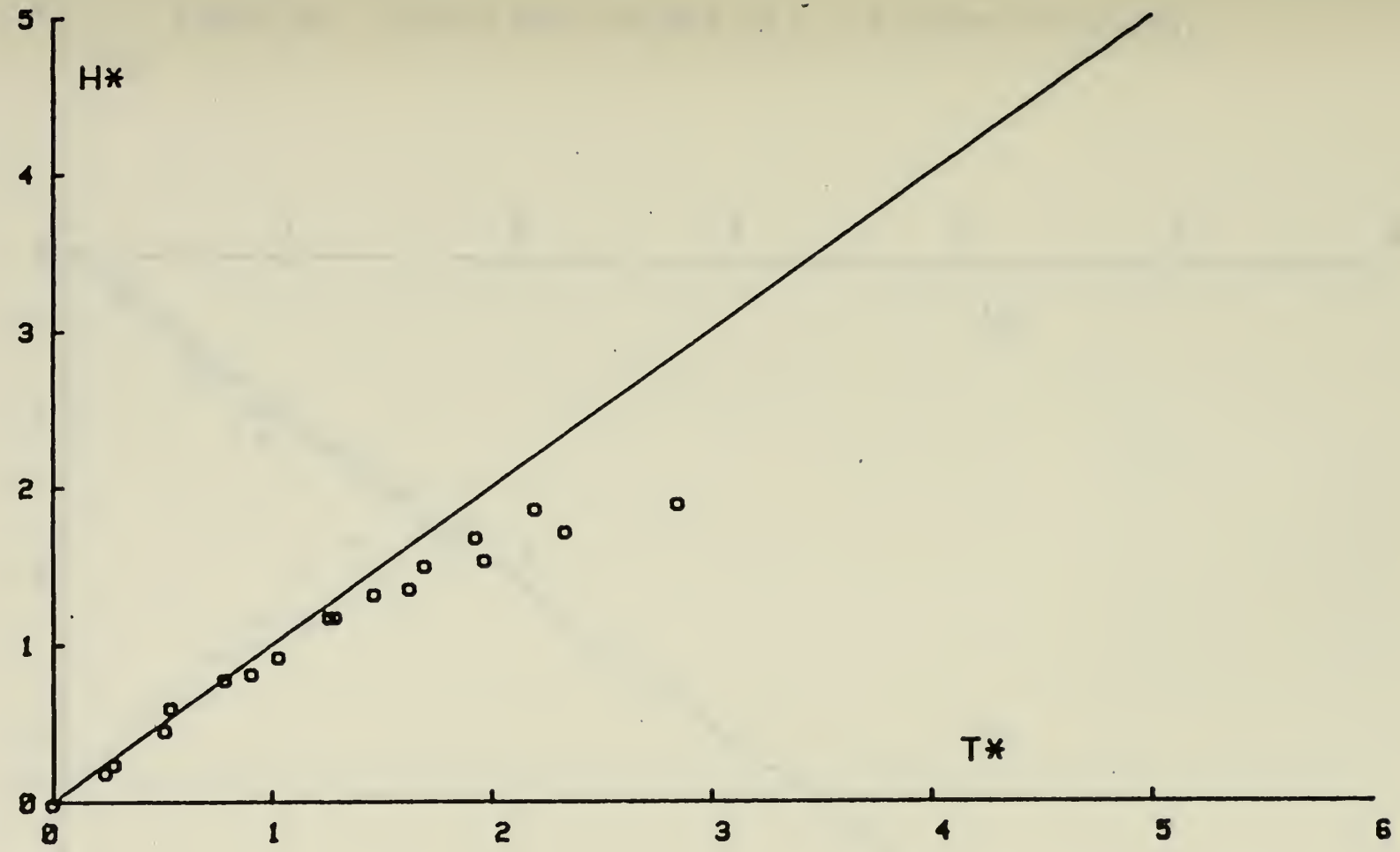

Figure 28. Vortex Rise for RP2 (U = 1.6 ft/sec, X/M = 180)

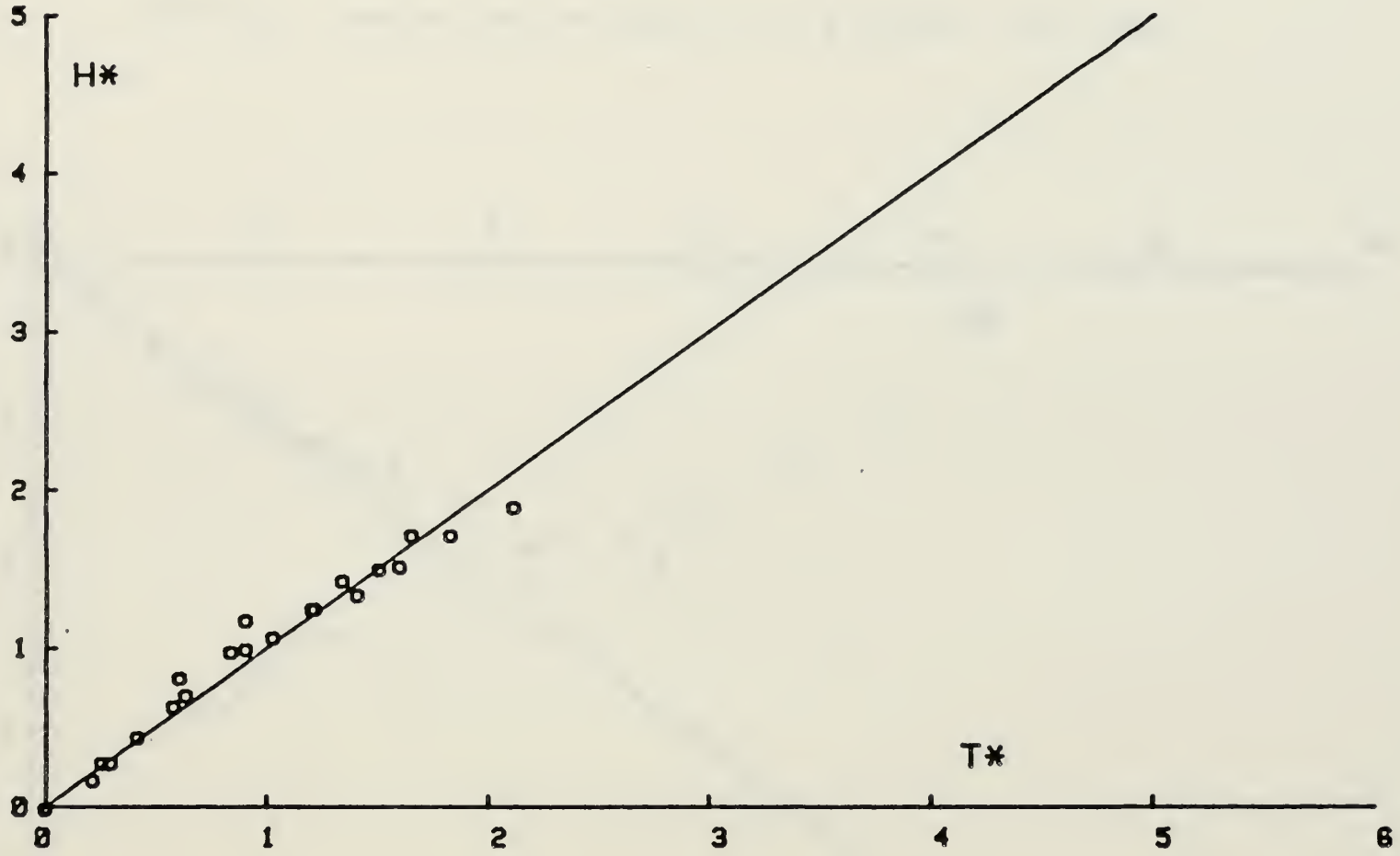

Figure 29. Vortex Rise for RP2 (U = 1.6 ft/sec, X/M = 80)

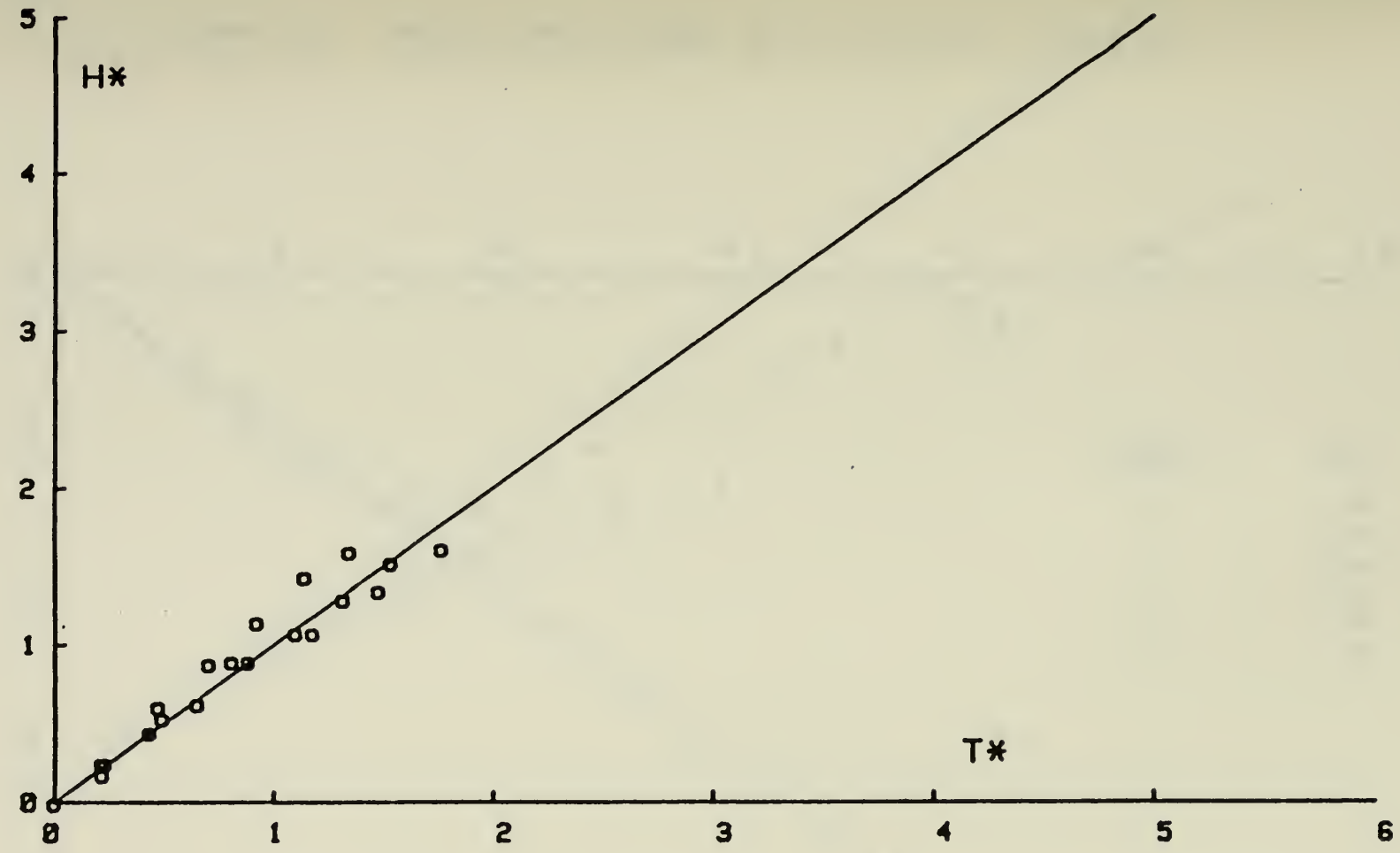

Figure 30. Vortex Rise for RP2 (U = 1.6 ft/sec, X/M = 50)

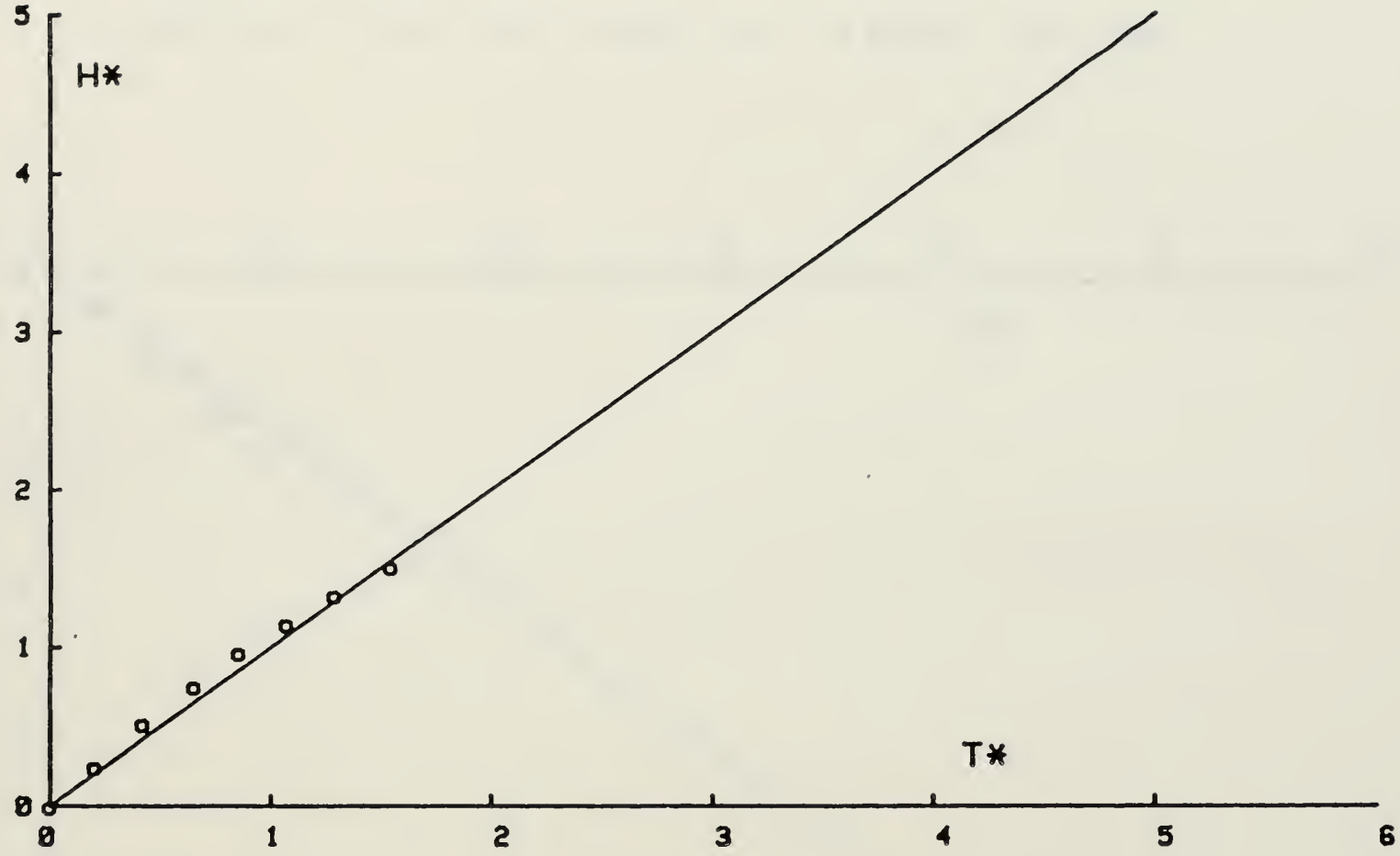

Figure 31. Vortex Rise for RP2 (U = 1.6 ft/sec, X/M = 25)

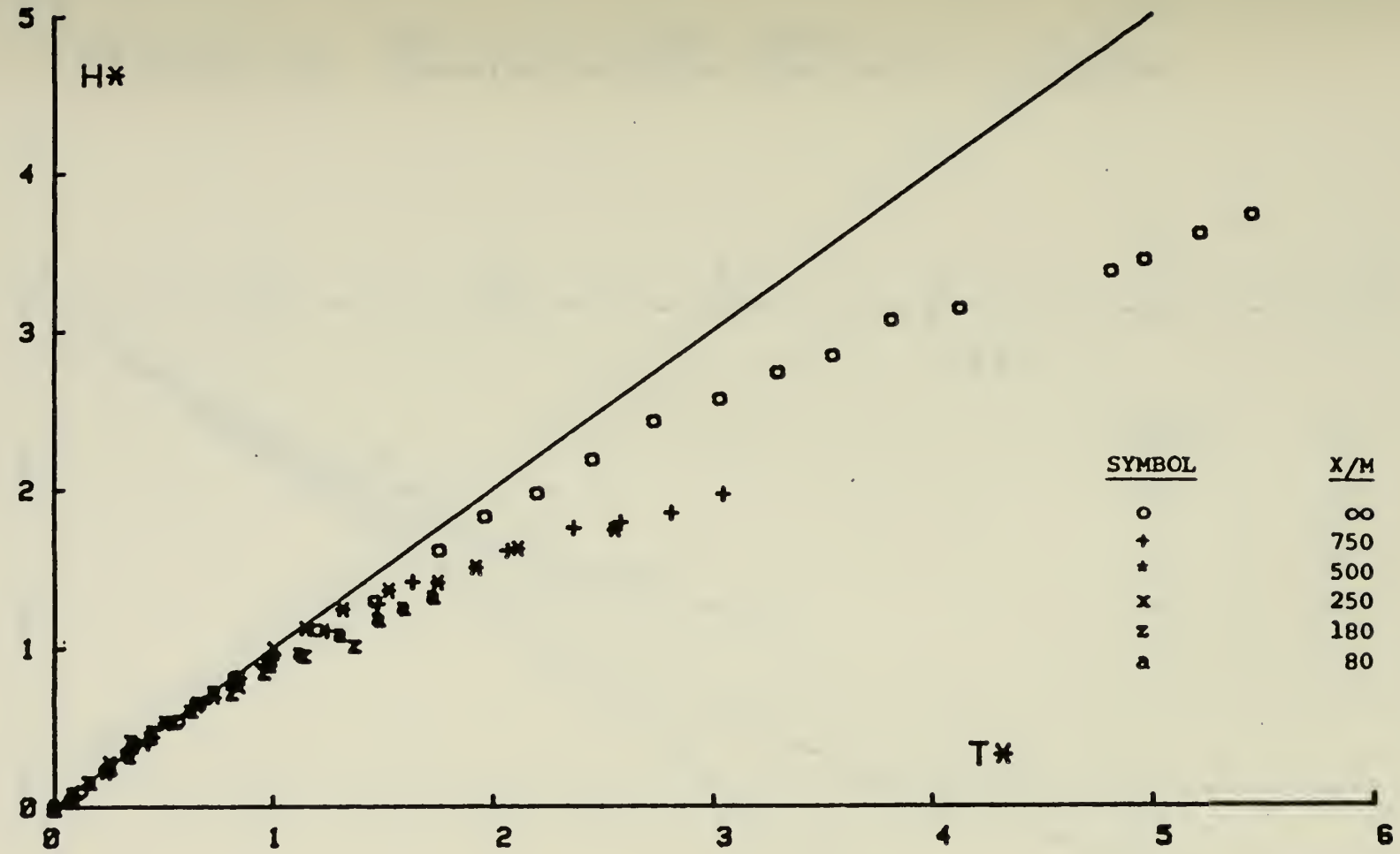

Figure 32a. Comparison of Vortex Rise for RP1 for Various X/M, U = 0.9 ft/sec, Data Points

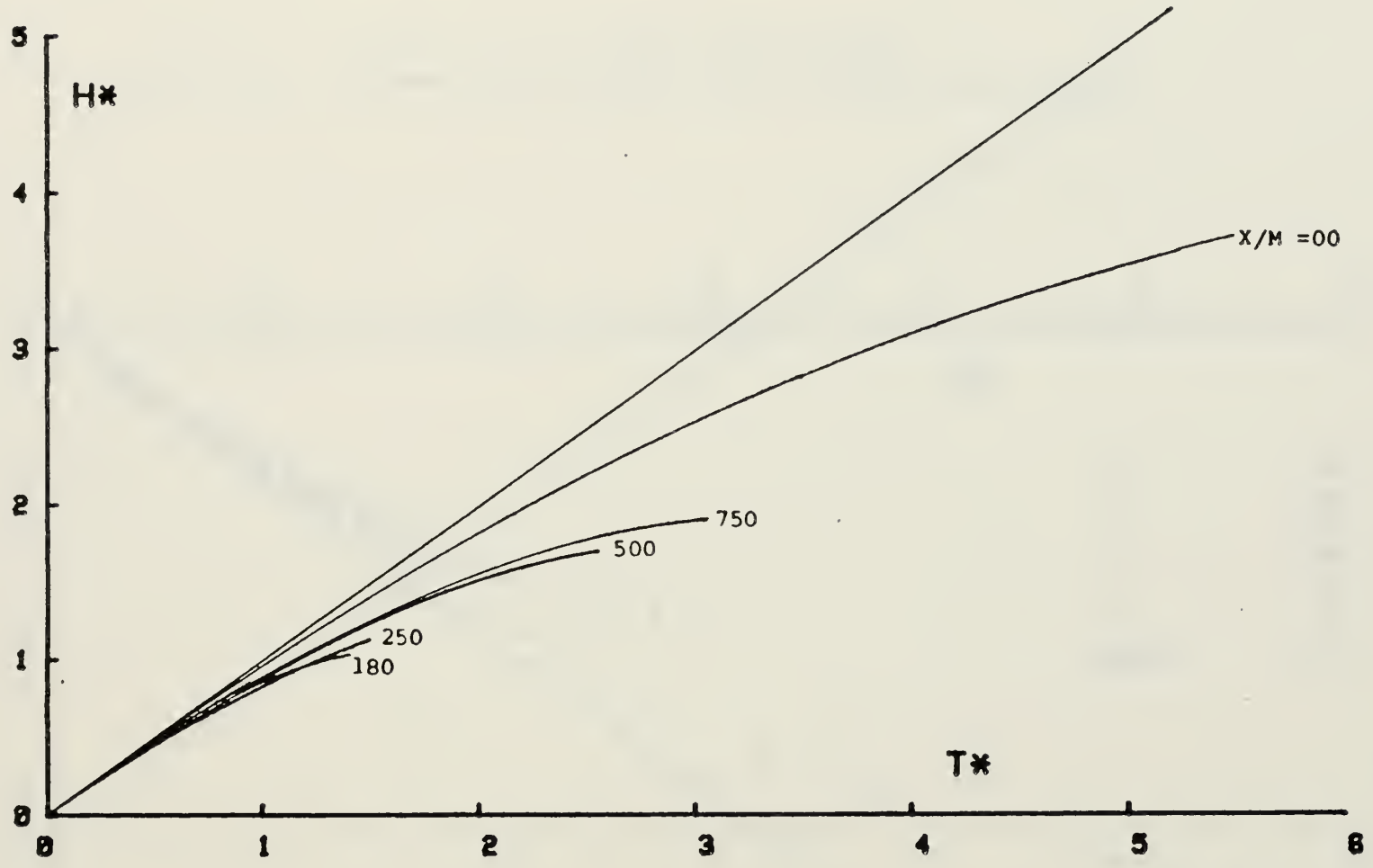

Figure 32b. Comparison of Vortex Rise for RP1 for Various X/M, U = 0.9 ft/sec, Curves

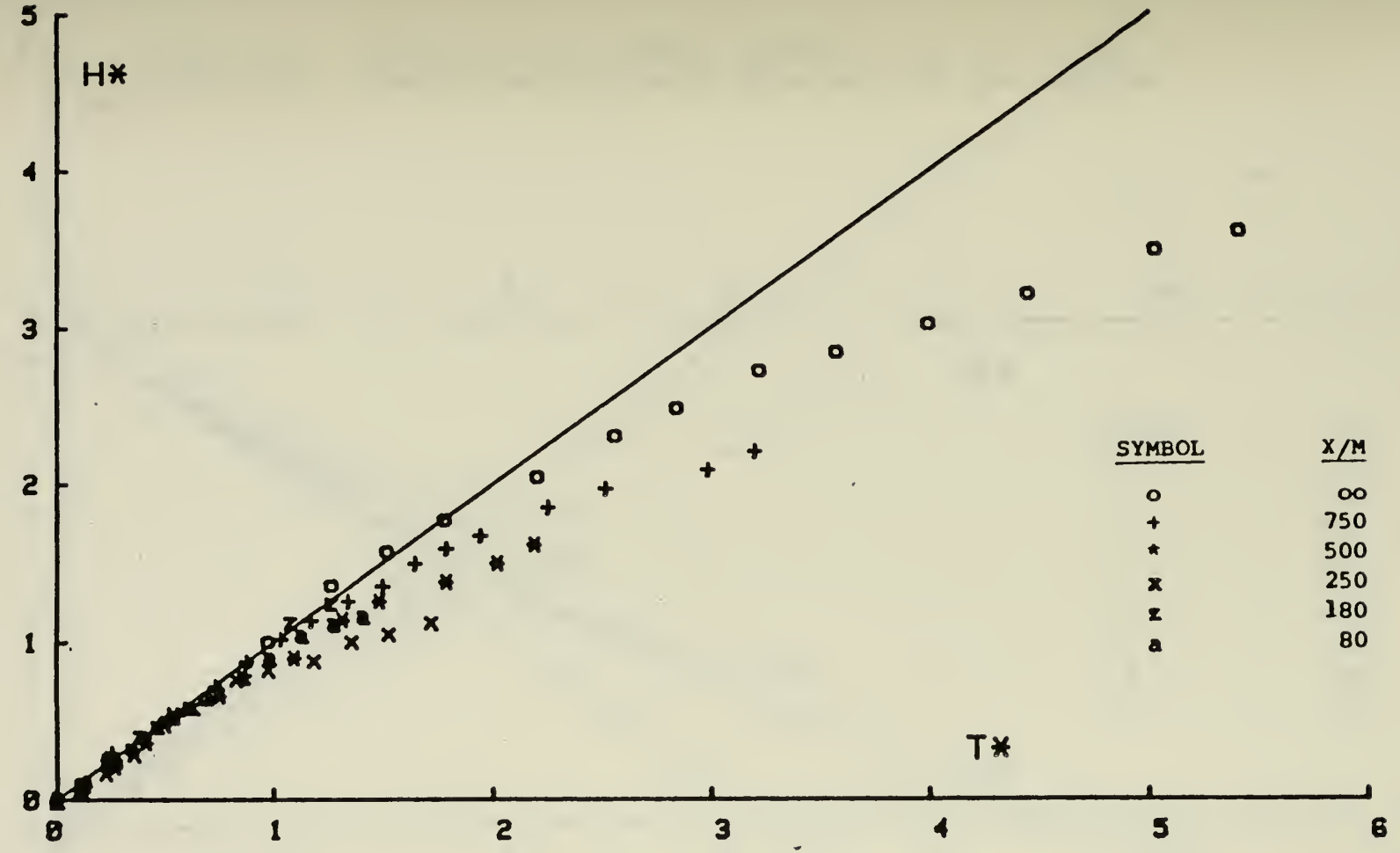

Figure 33a. Comparison of Vortex Rise for RP1 for Various X/M, U = 1.6 ft/sec, Data Points

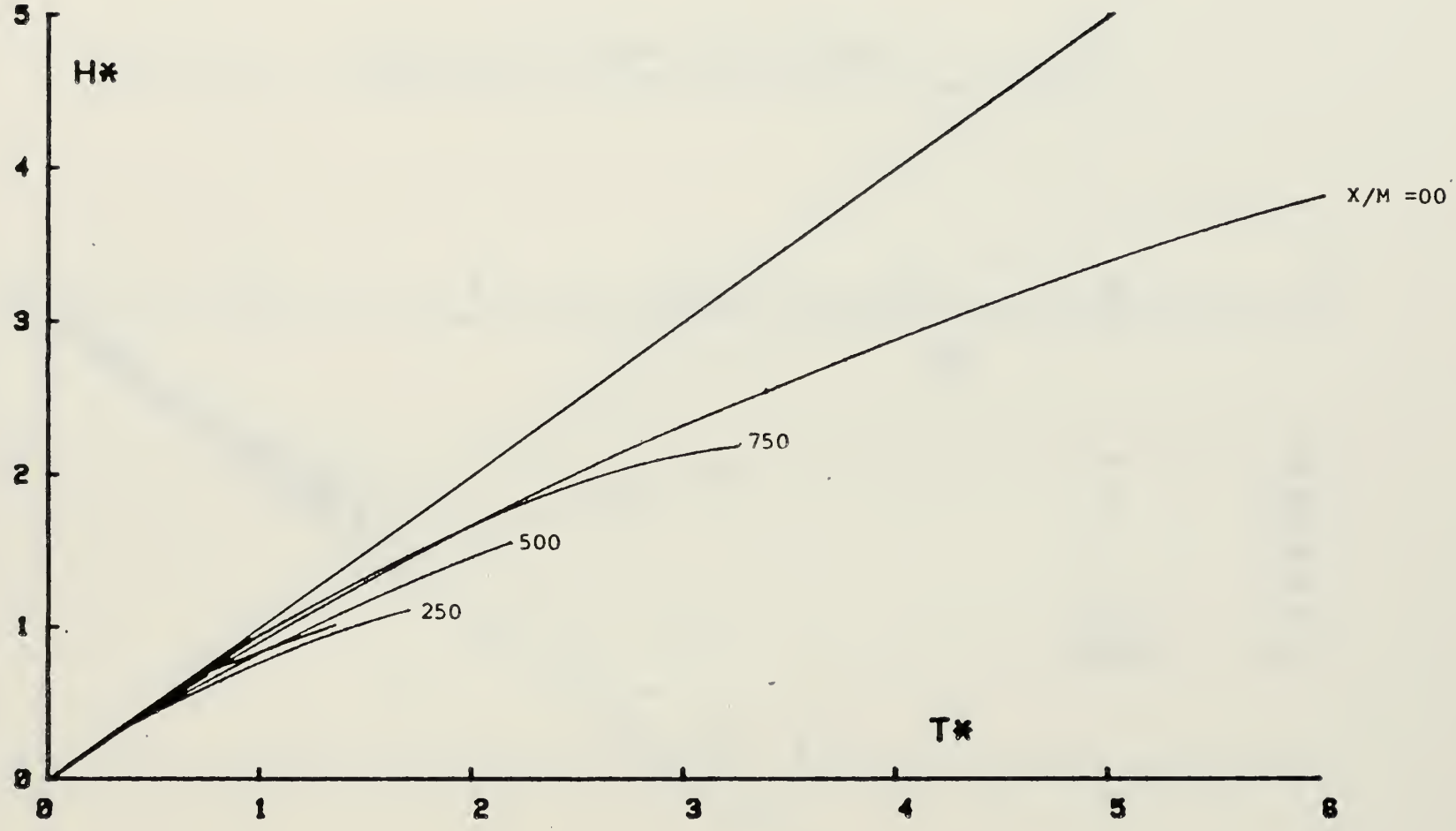

Figure 33b. Comparison of Vortex Rise for RP1 for Various X/M, U = 1.6 ft/sec, Curves

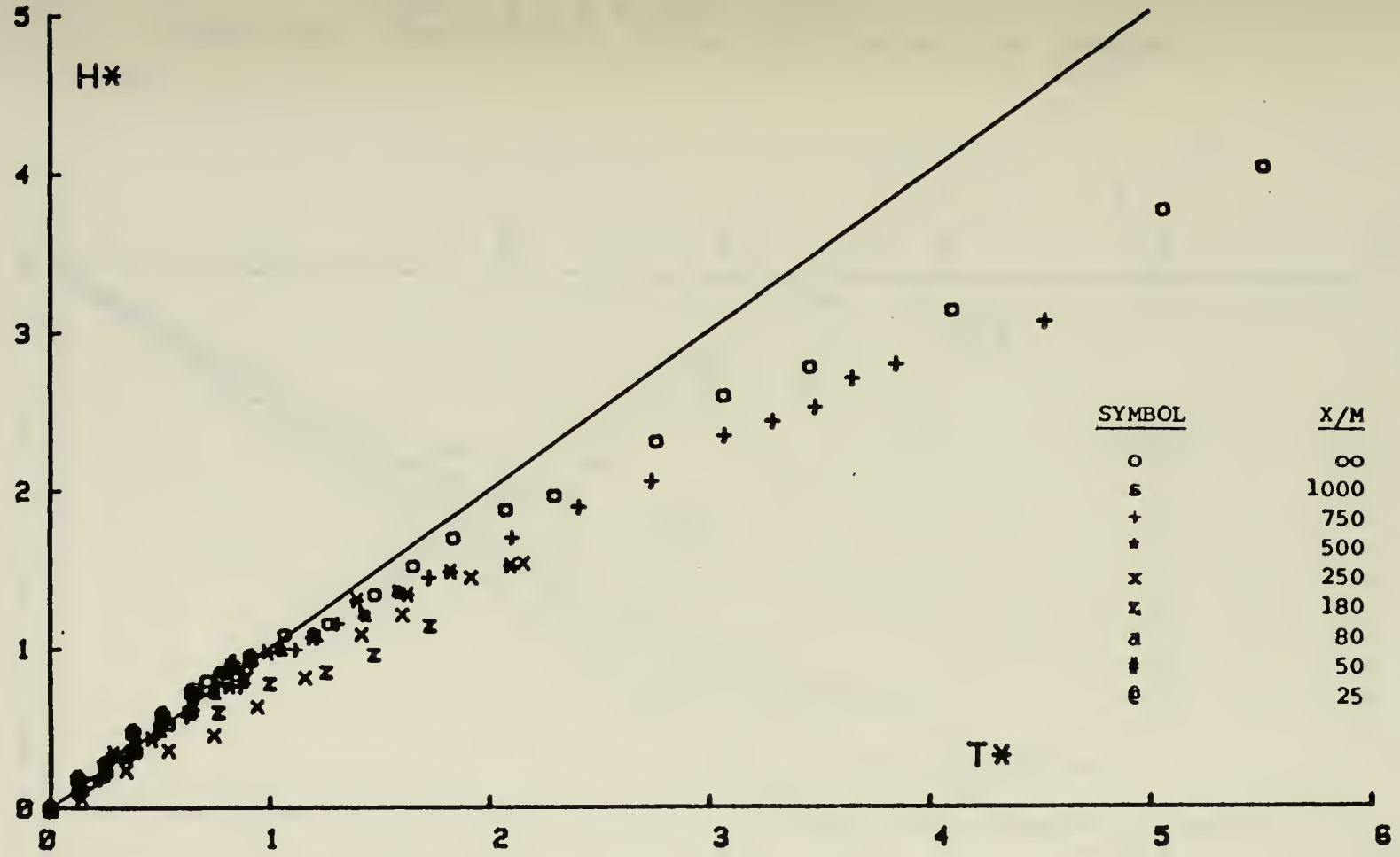

Figure 34a. Comparison of Vortex Rise for RP2 for Various X/M, U = 0.9 ft/sec, Data Points

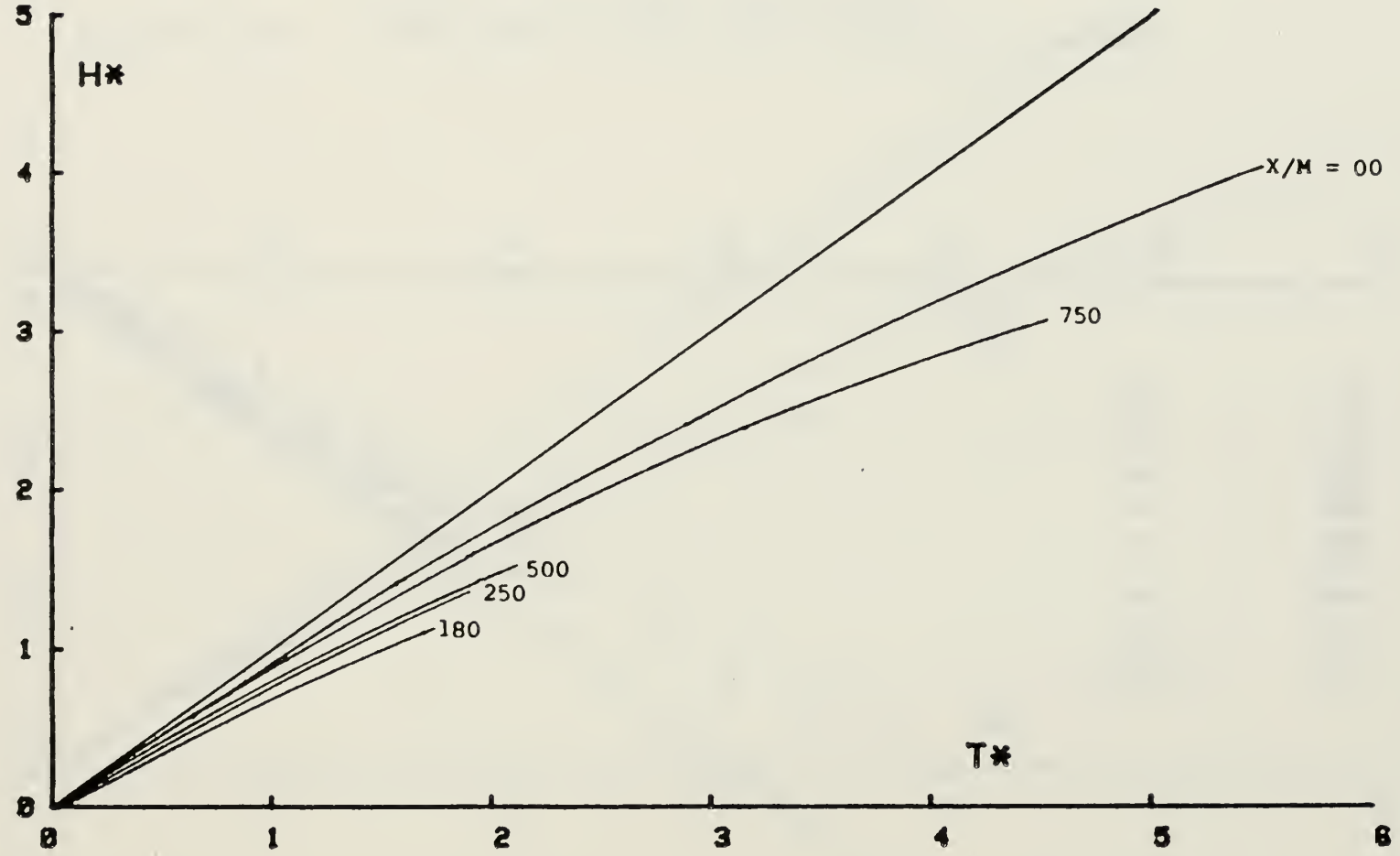

Figure 34b. Comparison of Vortex Rise for RP2 for Various X/M, U = 0.9 ft/sec, Curves

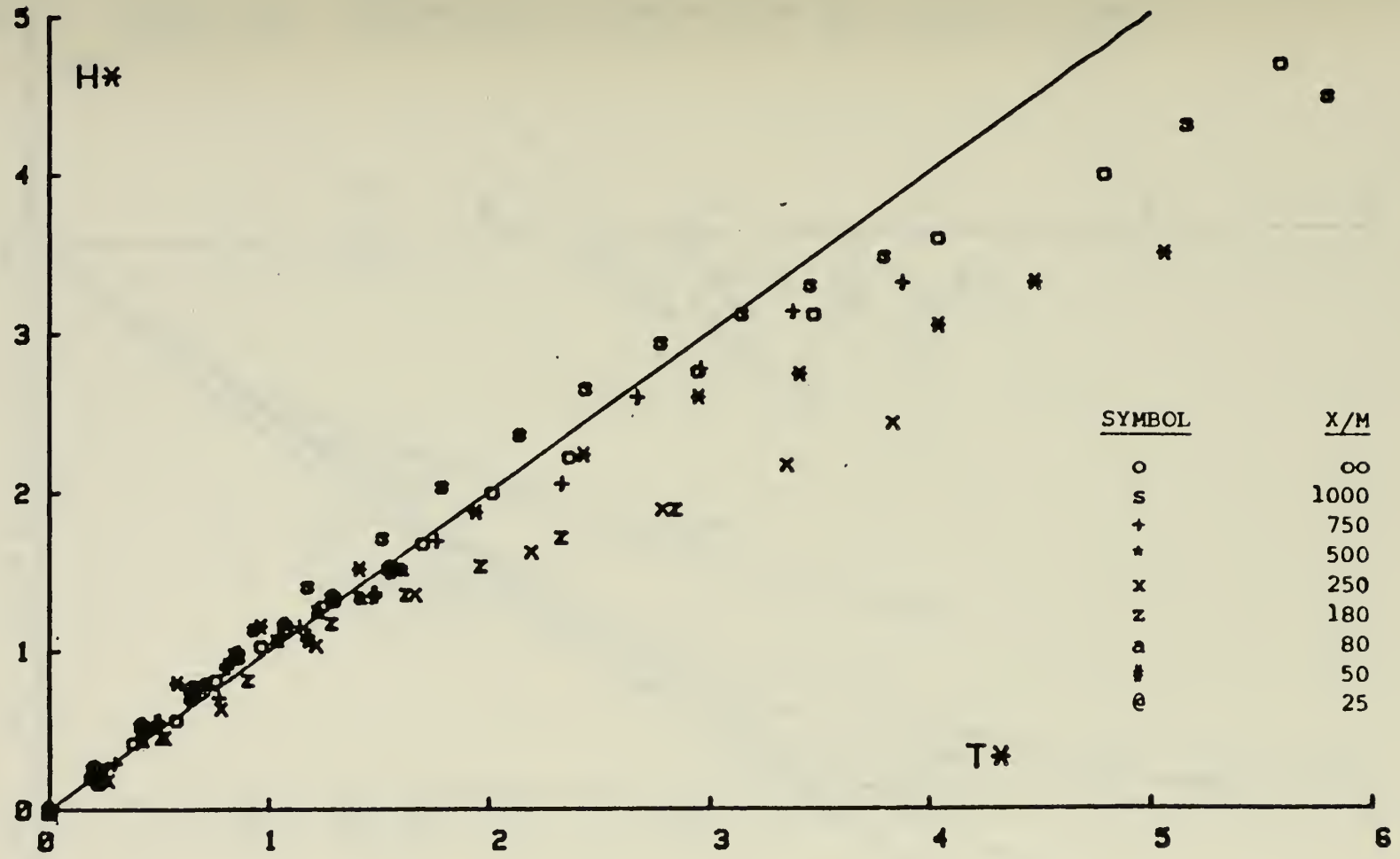

Figure 35a. Comparison of Vortex Rise for RP2 for Various X/M, U = 1.6 ft/sec, Data Points

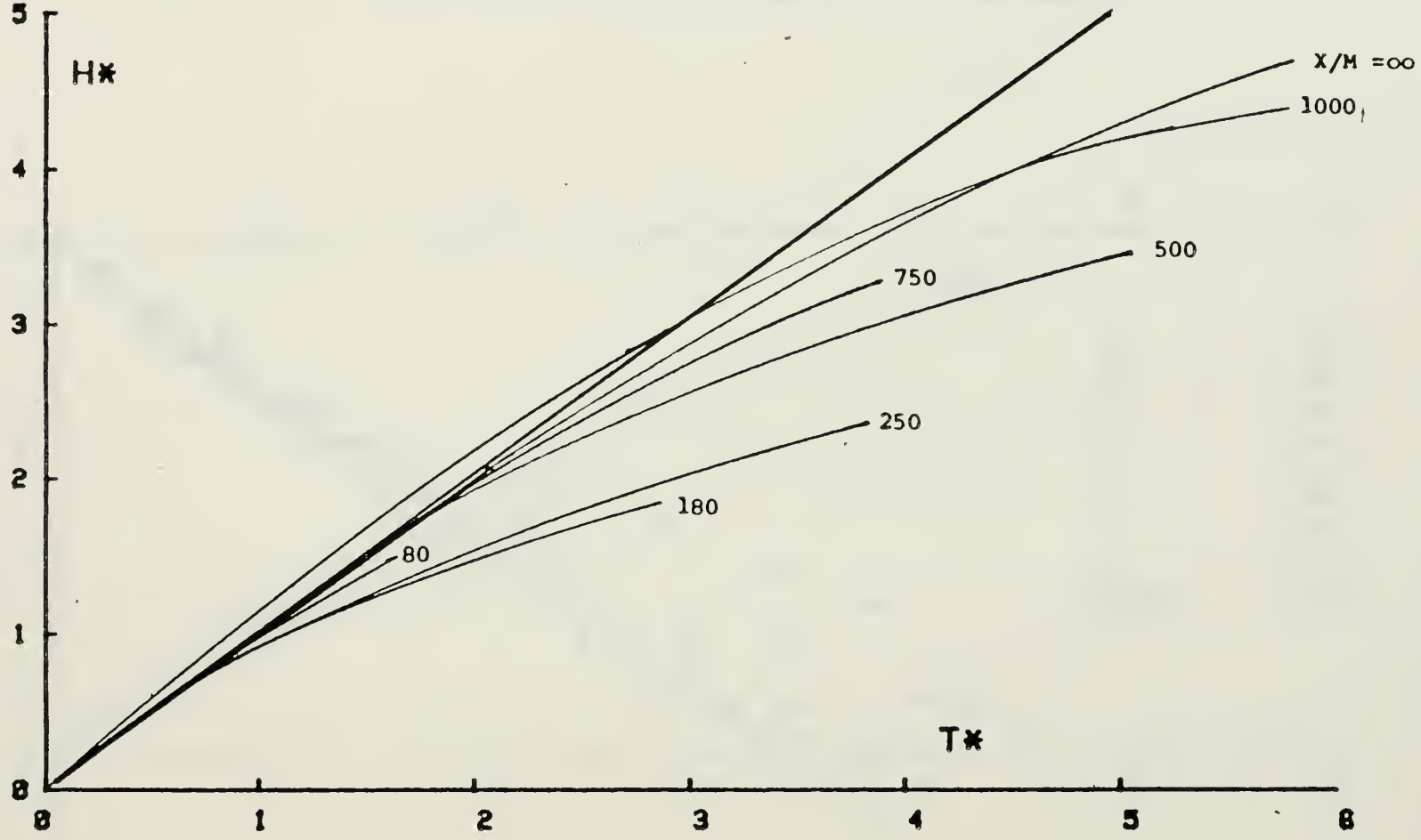

Figure 35b. Comparison of Vortex Rise for RP2 for Various X/M, U = 1.6 ft/sec, Curves

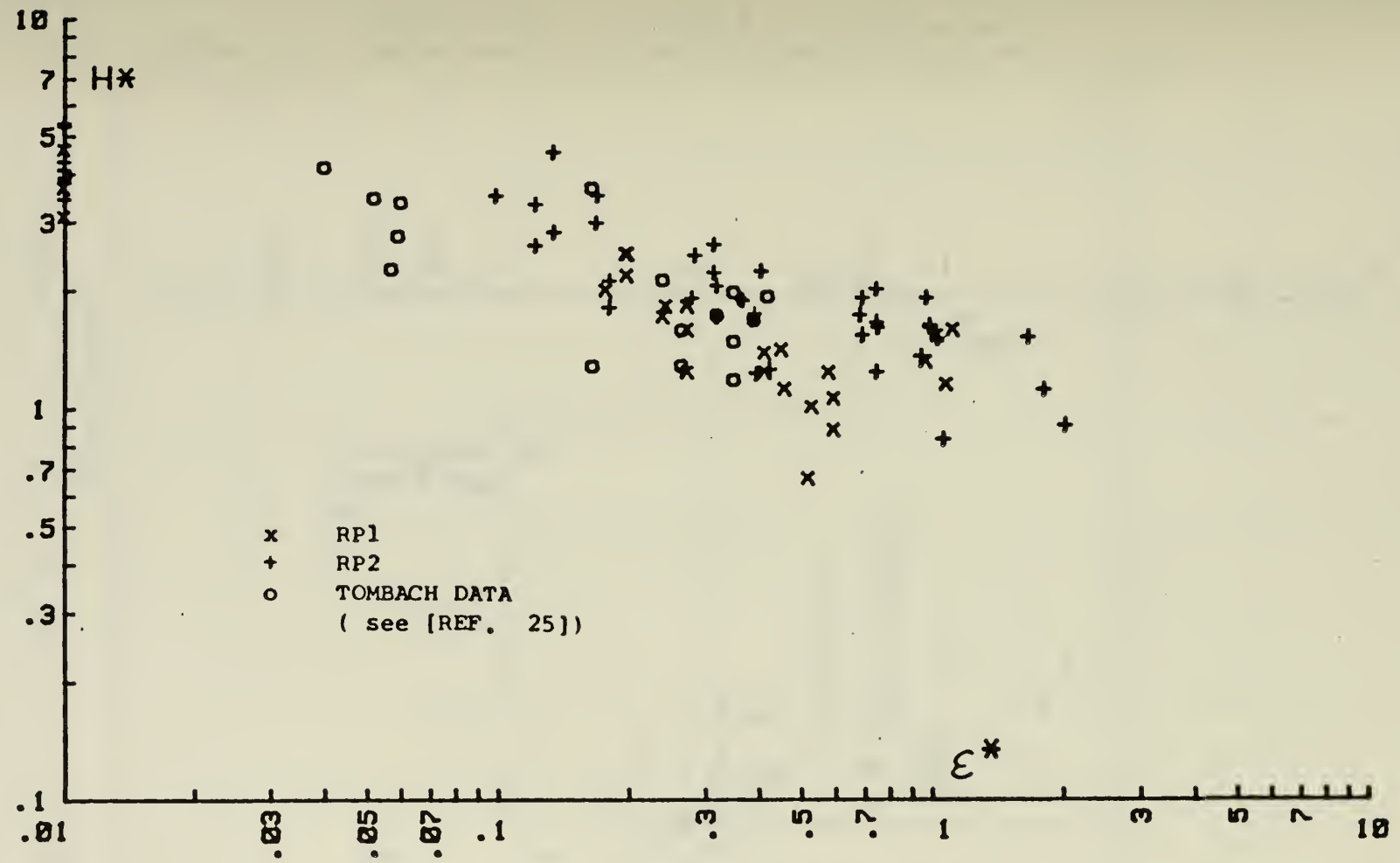

Figure 36. Comparison of H* vs. ε* for RP1, RP2 at U = 0.9 ft/sec and 1.6 ft/sec with Tombach Data

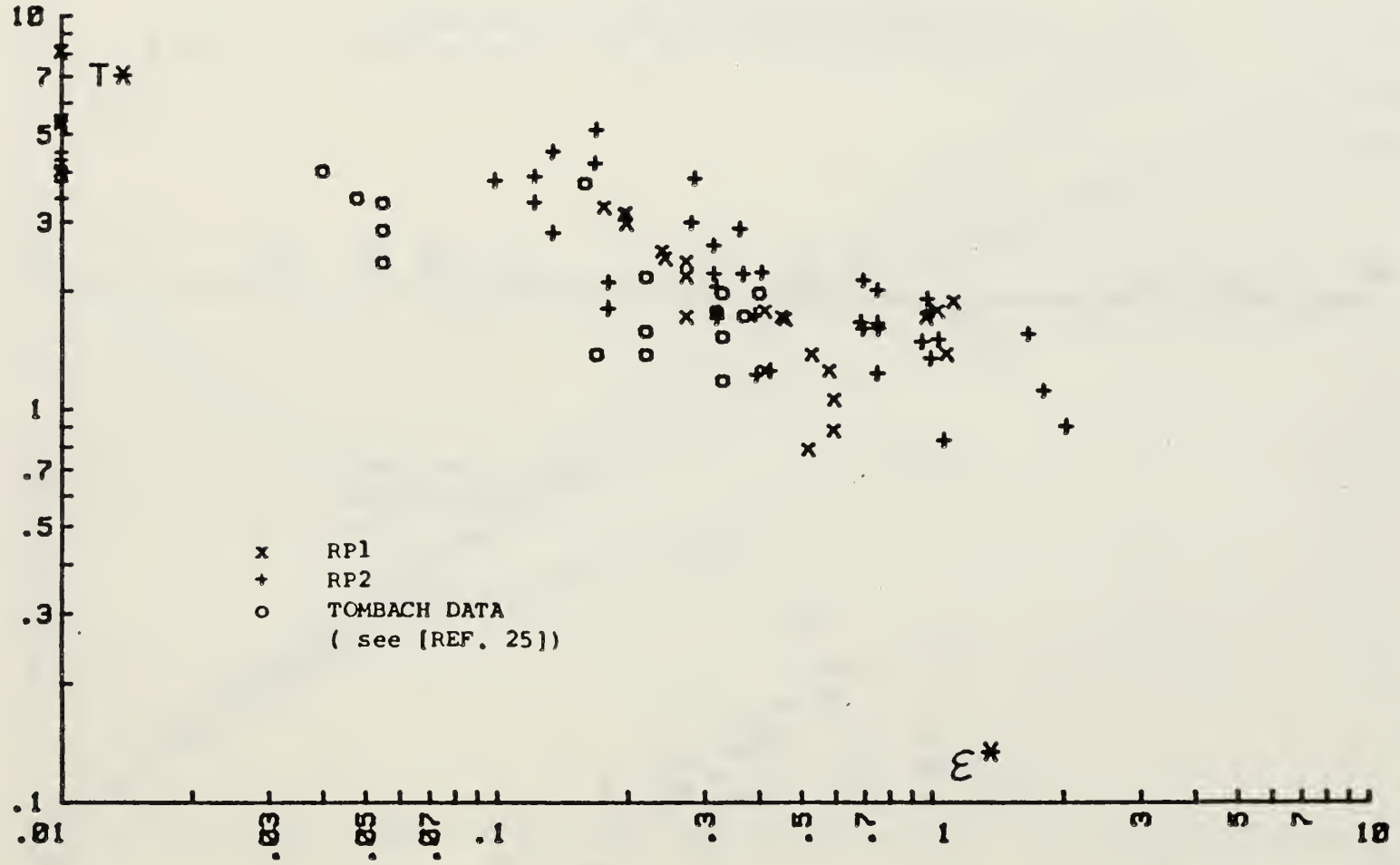

Figure 37. Comparison of T* vs. ε* for RP1, RP2 at U = 0.9 ft/sec and 1.6 ft/sec with Tombach Data

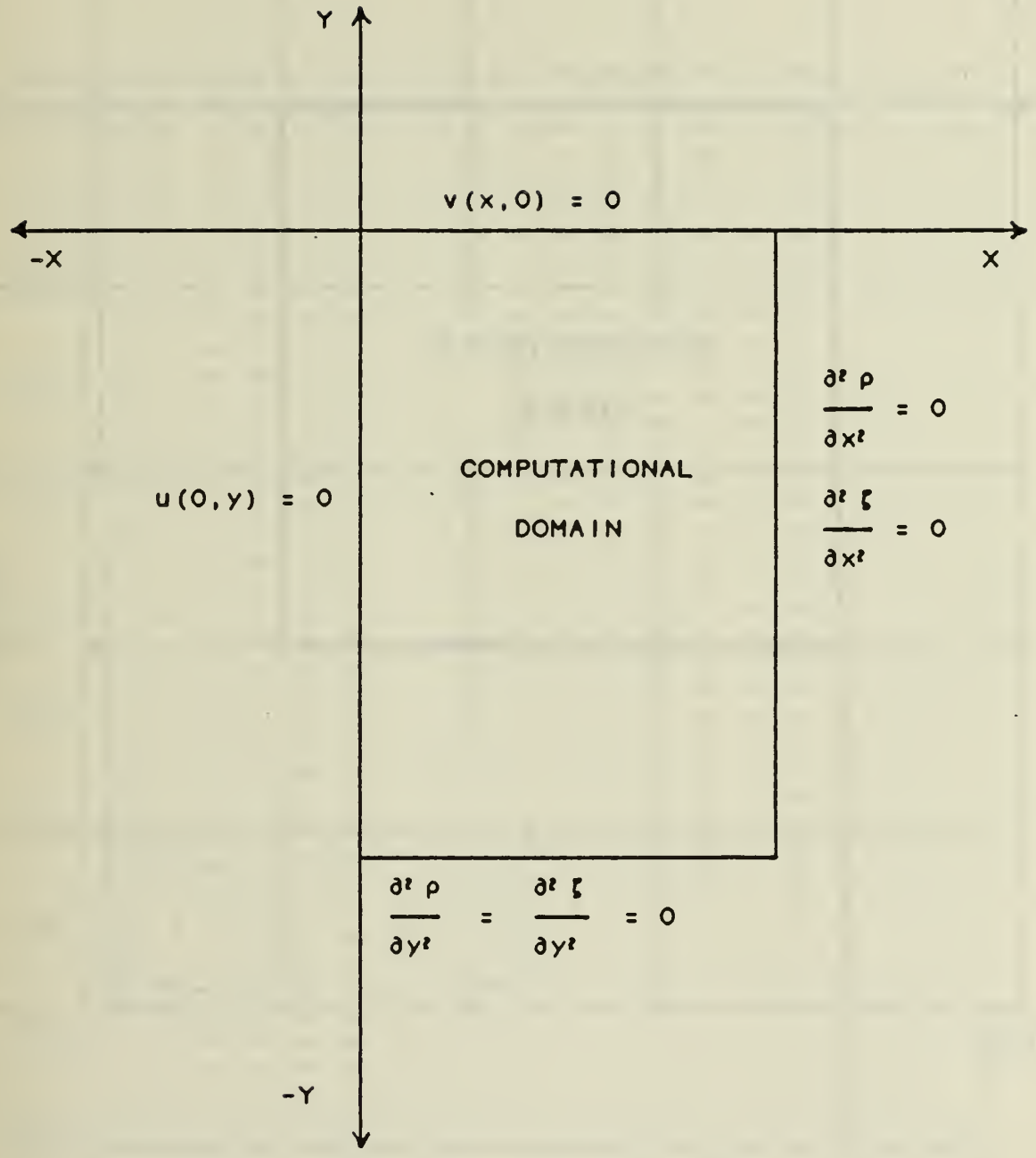

Figure 38a. Numerical Coordinate Axis and Boundary Conditions

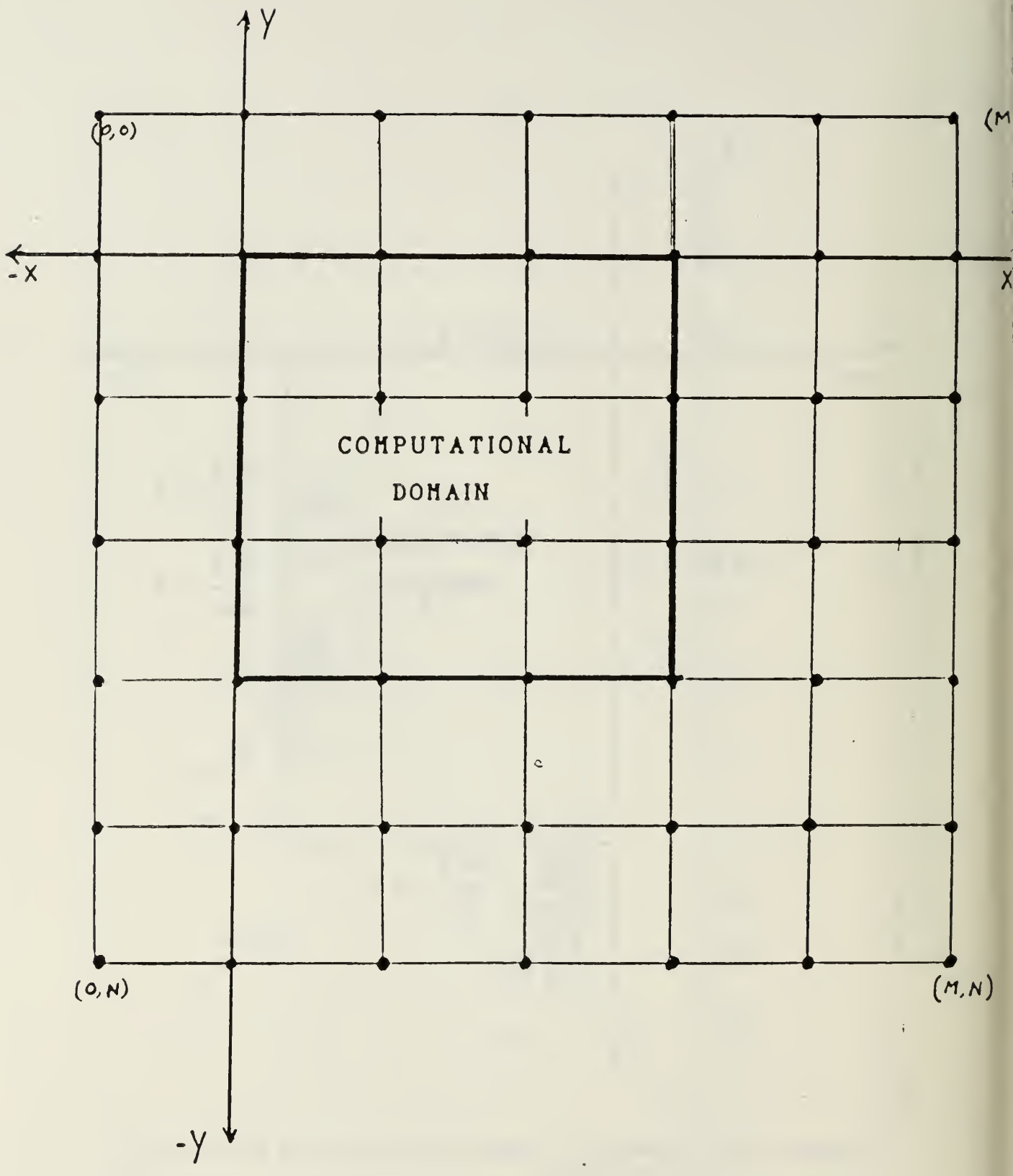

Figure 38b. Numerical Nodal Point Arrangement

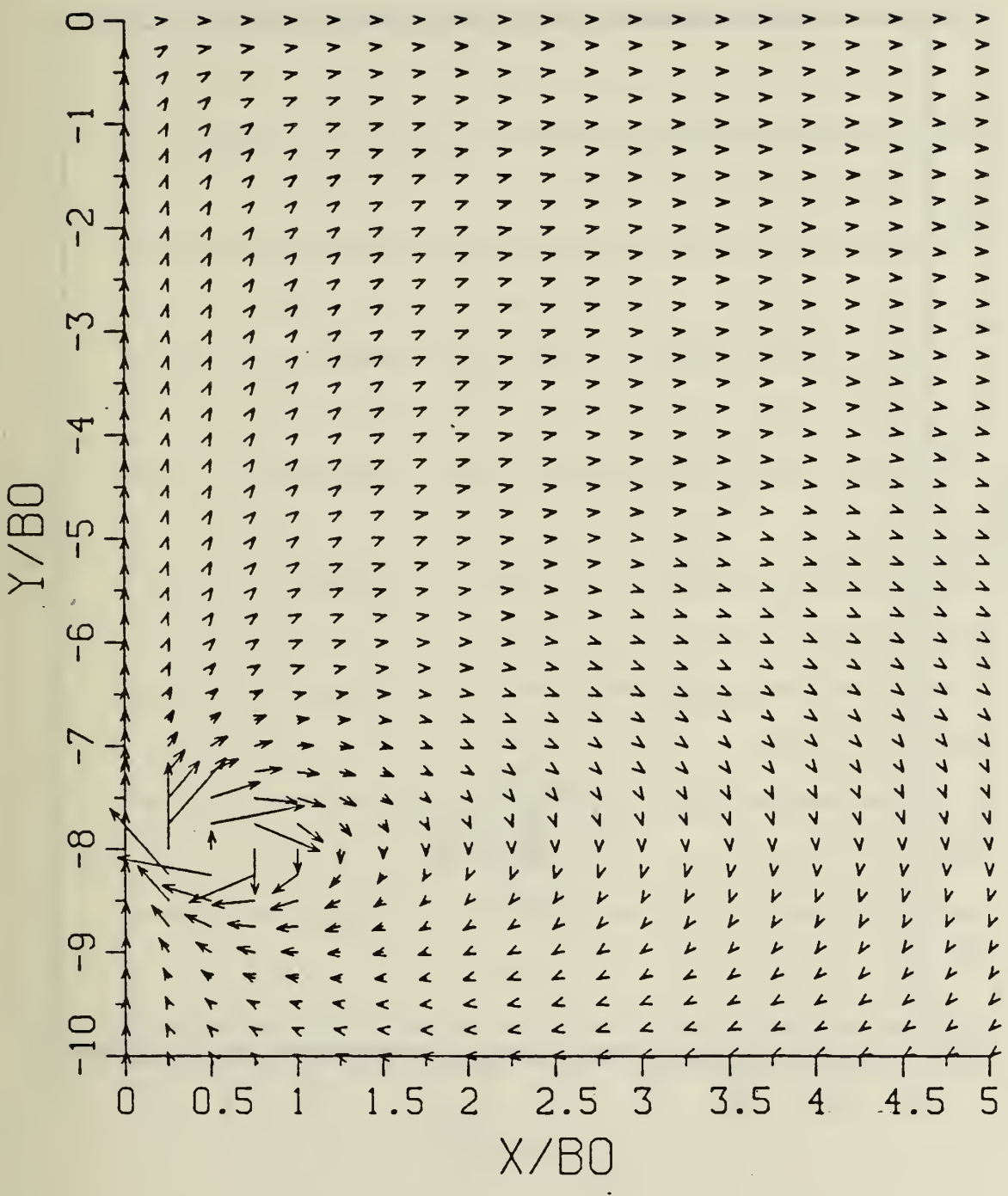

Figure 39a. Velocity Field for T* = 0.0365

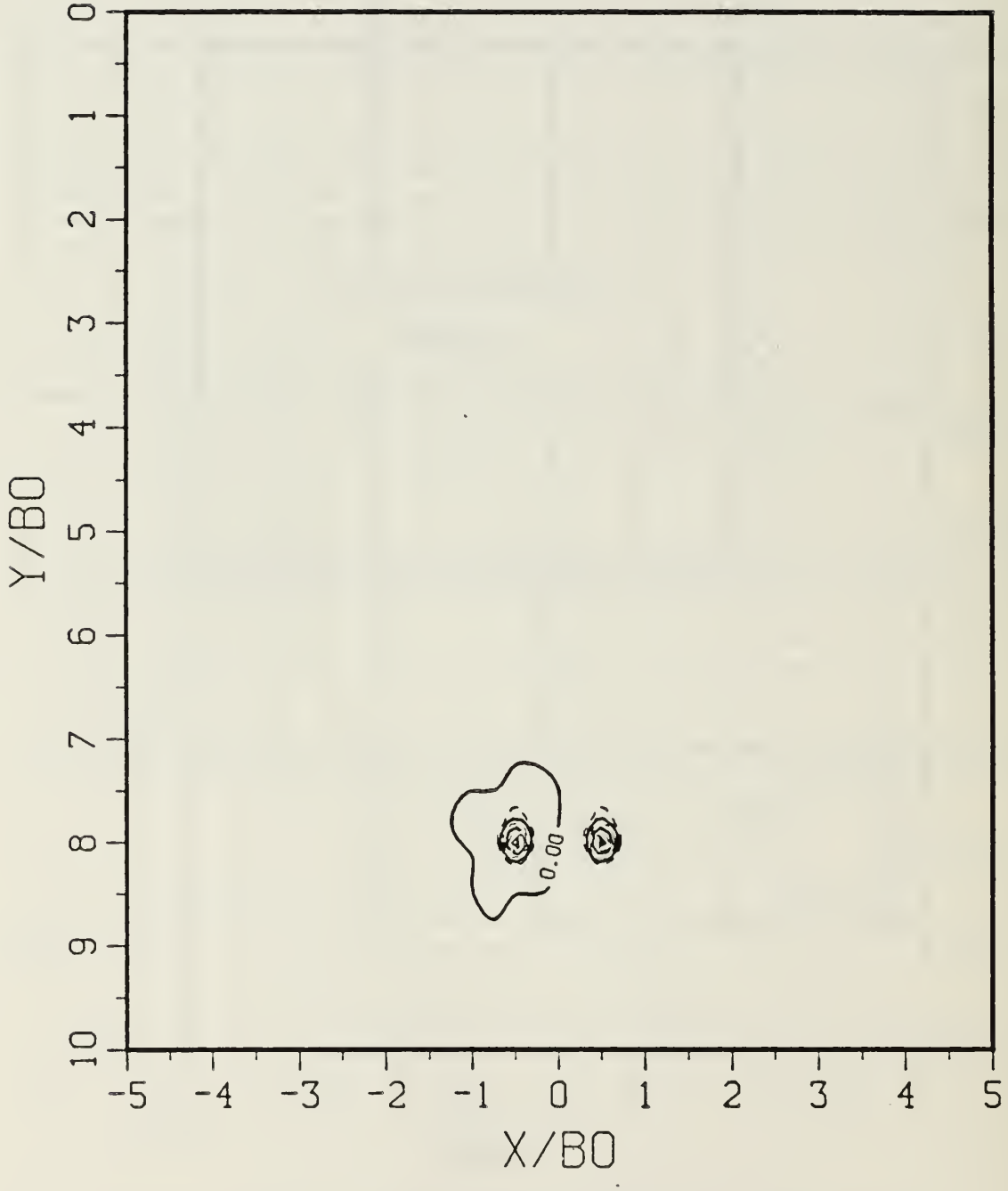

Figure 39b. Vorticity Field for T* = 0.0365

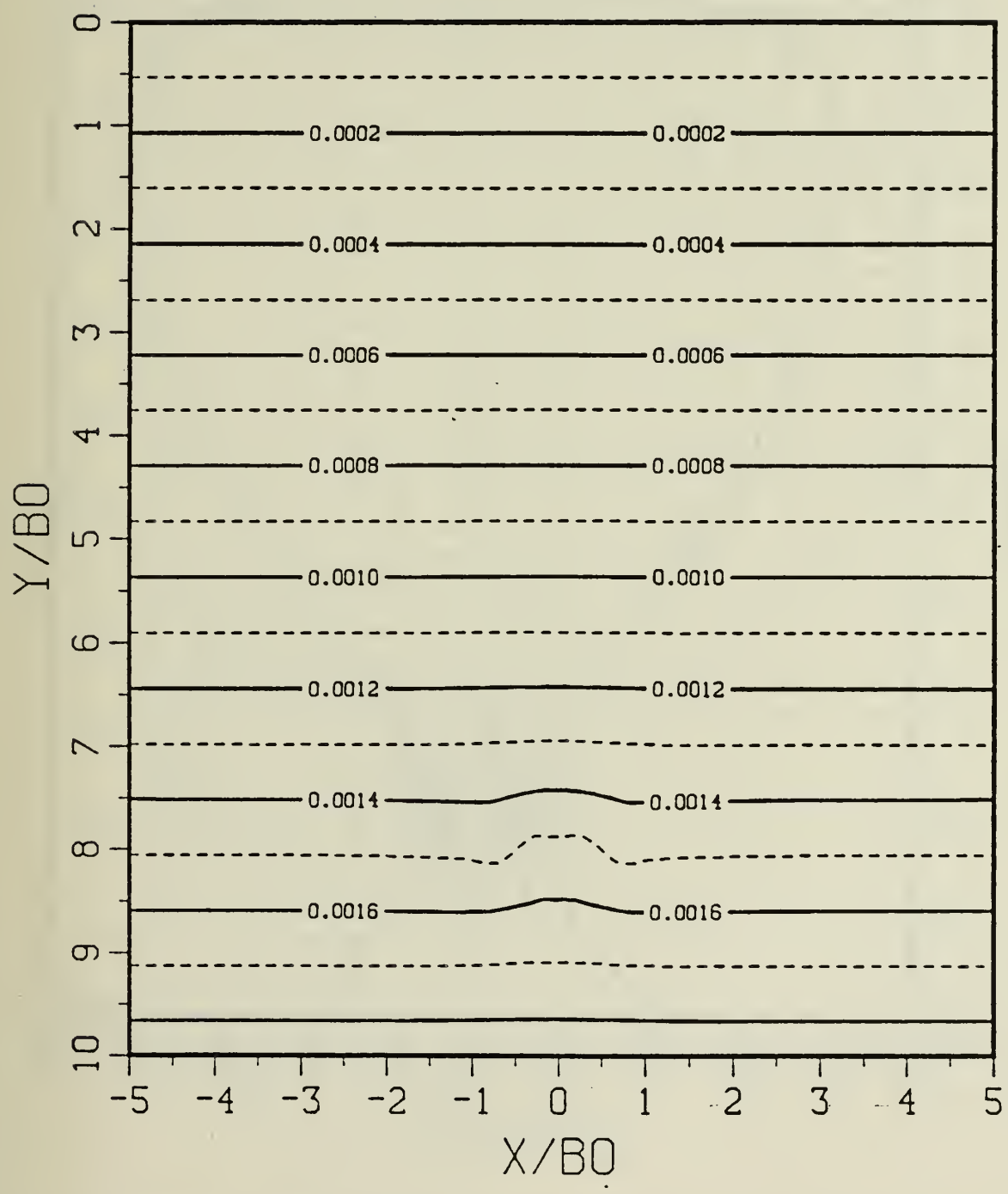

Figure 39c. Constant Density Contours for T* = 0.0365

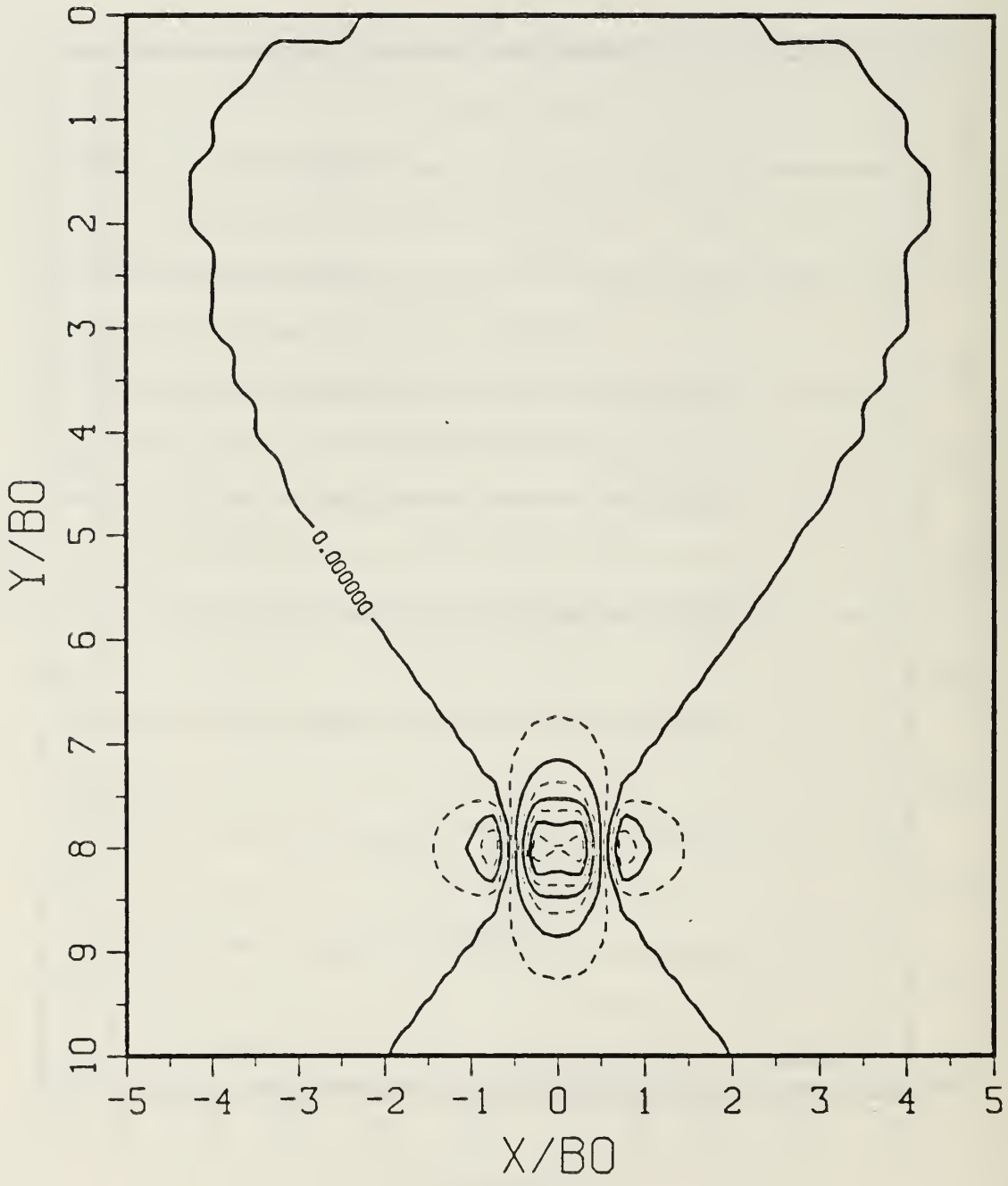

Figure 39d. Density Perturbation Contours for T* = 0.0365

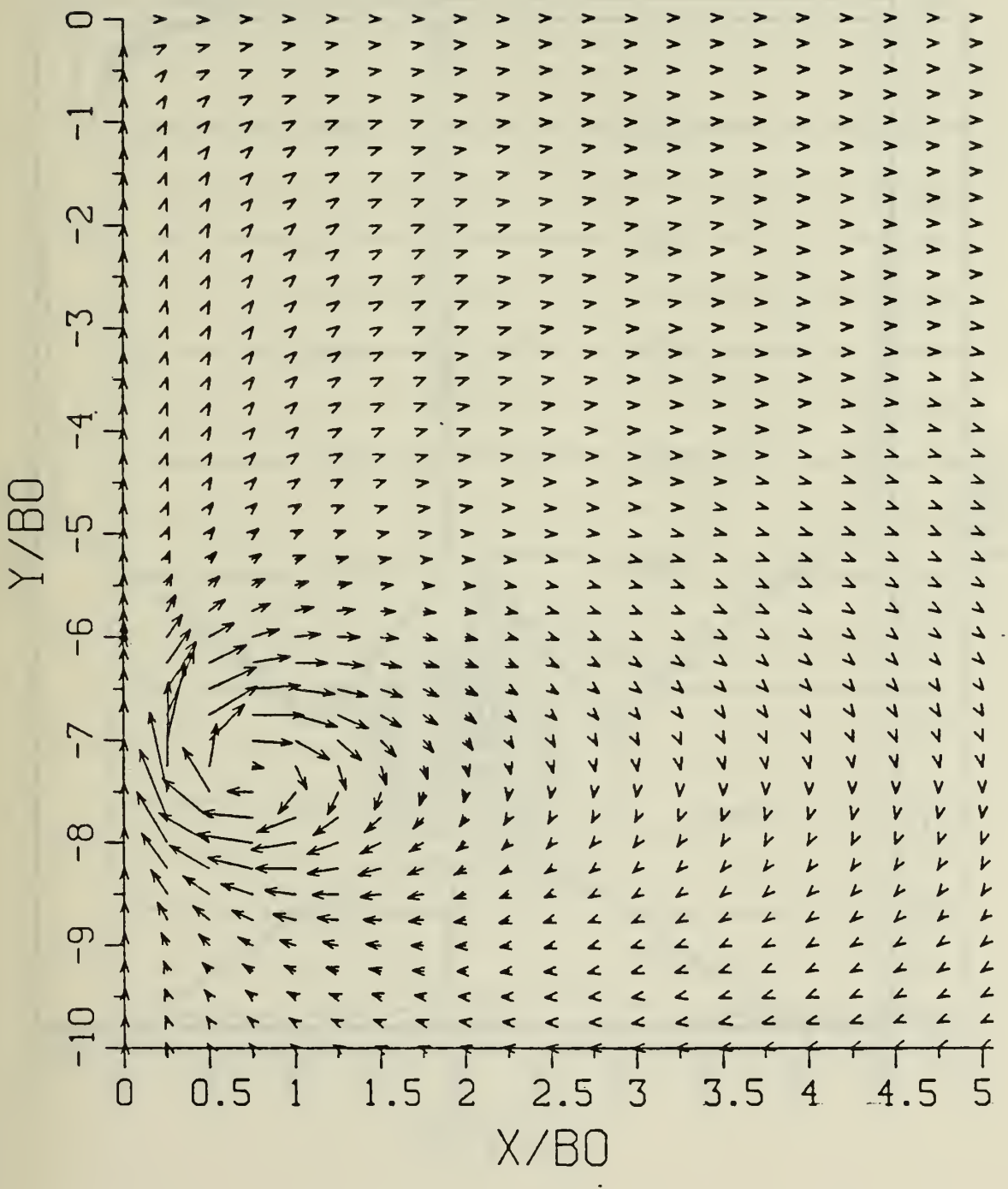

Figure 40a. Velocity Field for T* = 0.728

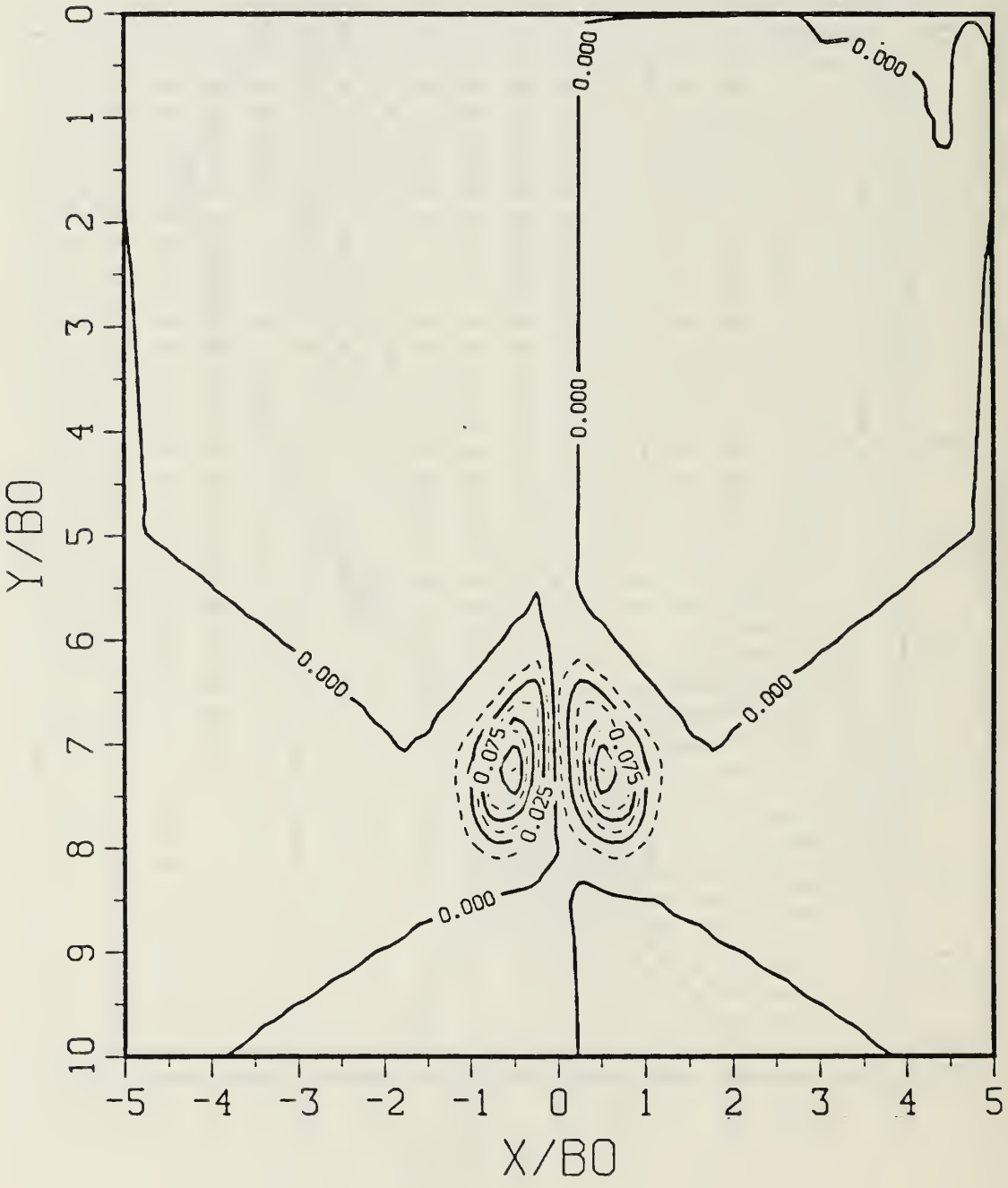

Figure 40b. Vorticity Field for T* = 0.728

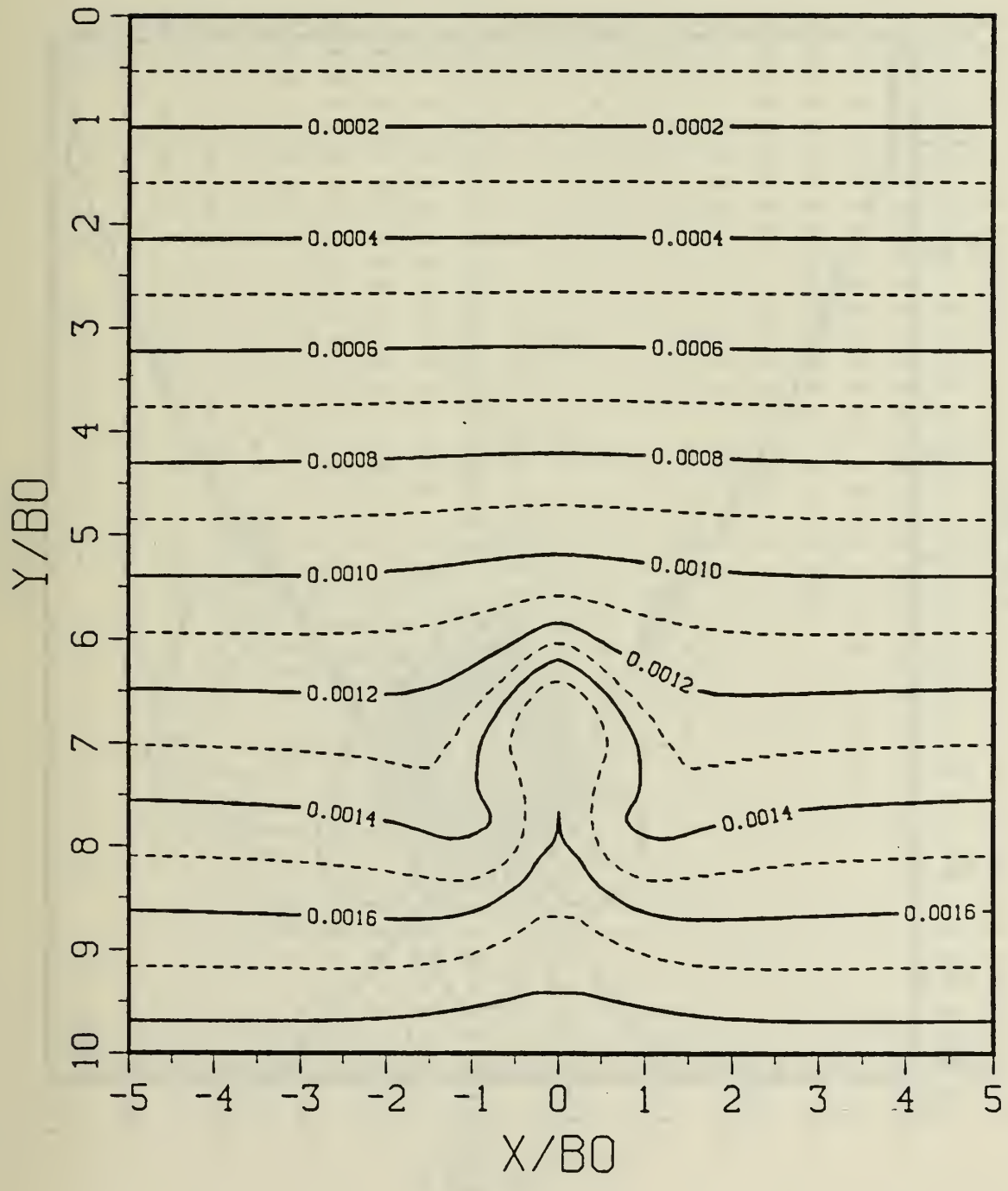

Figure 40c. Constant Density Contours for T* = 0.728

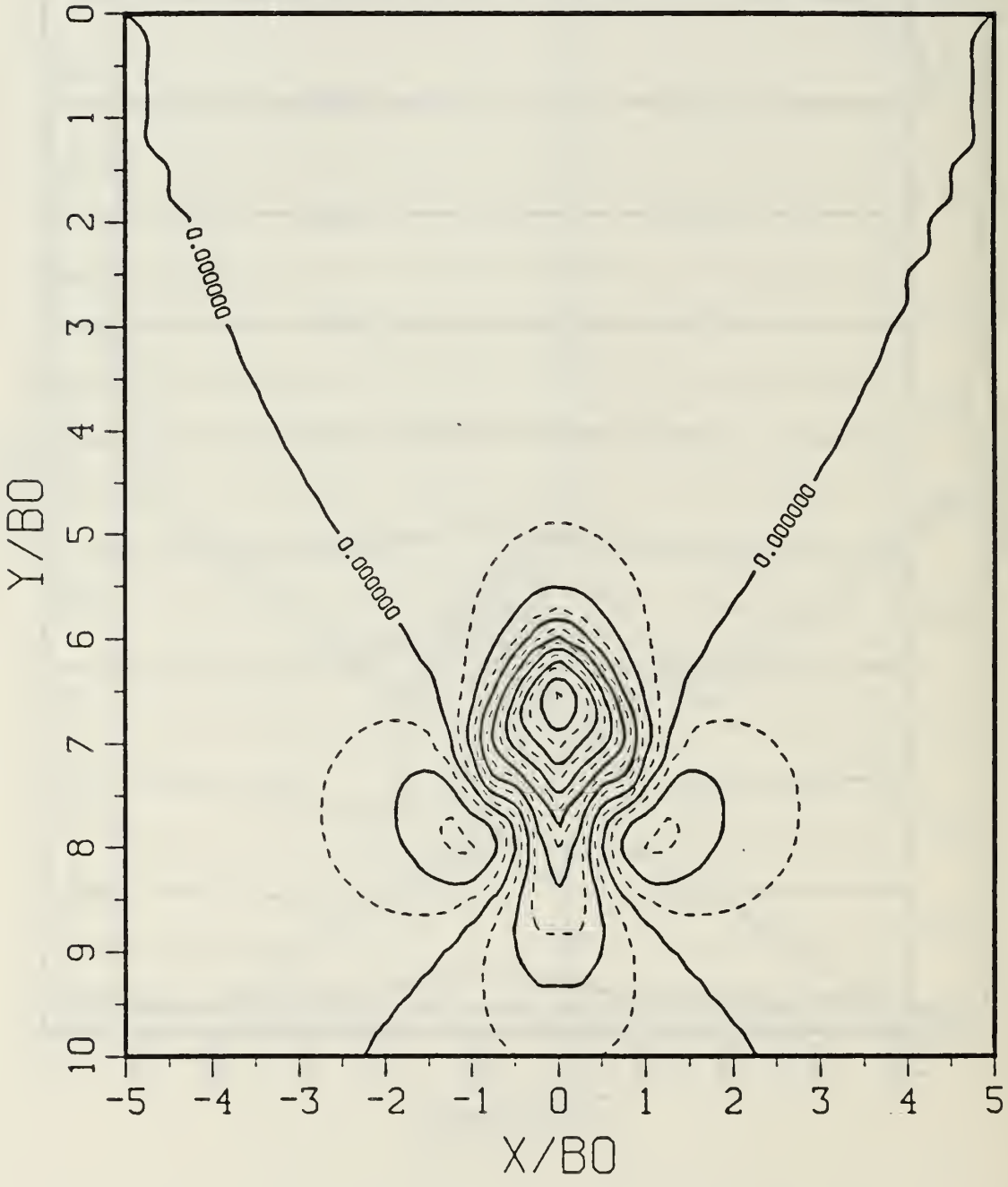

Figure 40d. Density Perturbation Contours for T* = 0.728

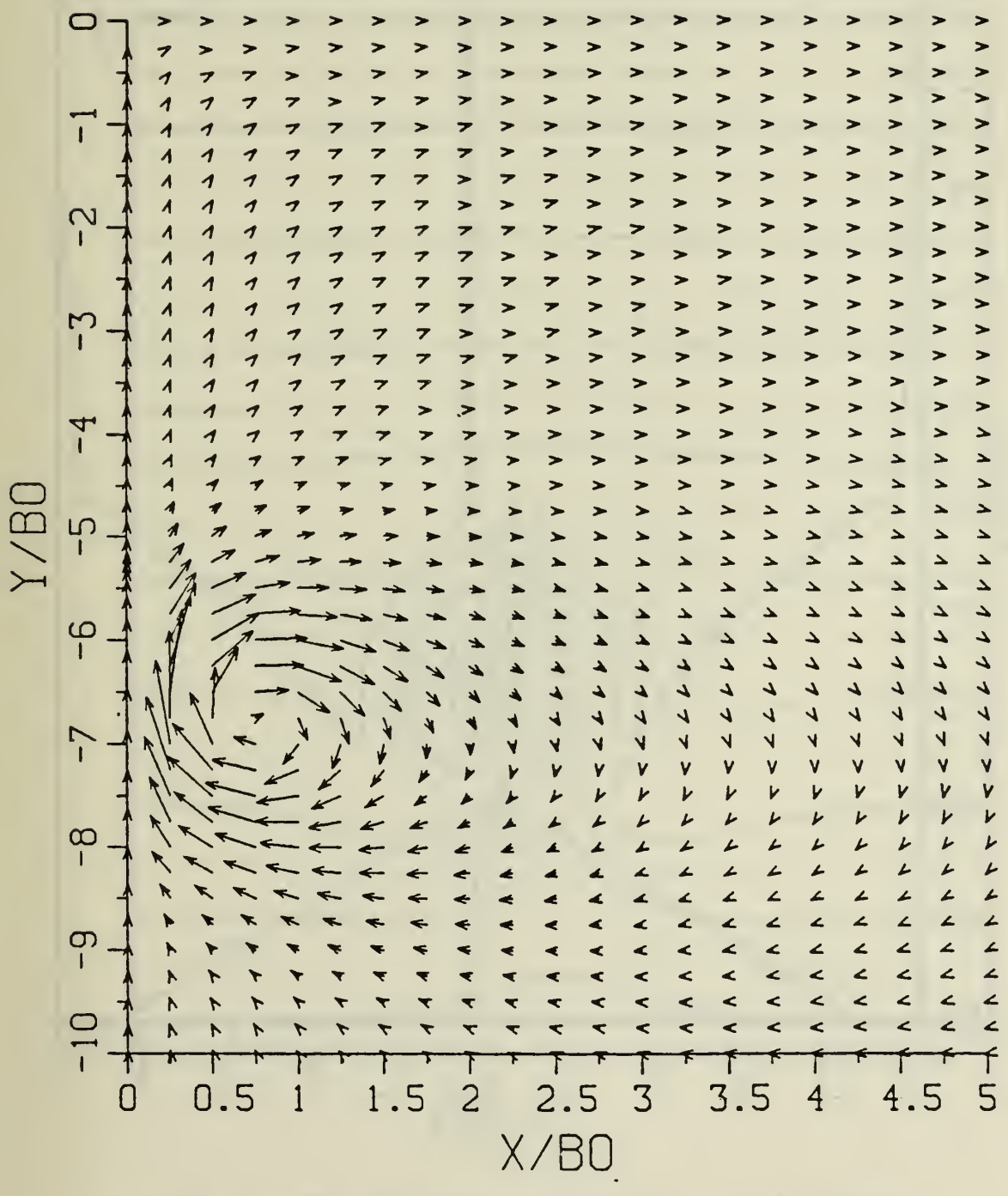

Figure 41a. Velocity Field for T* = 1.46

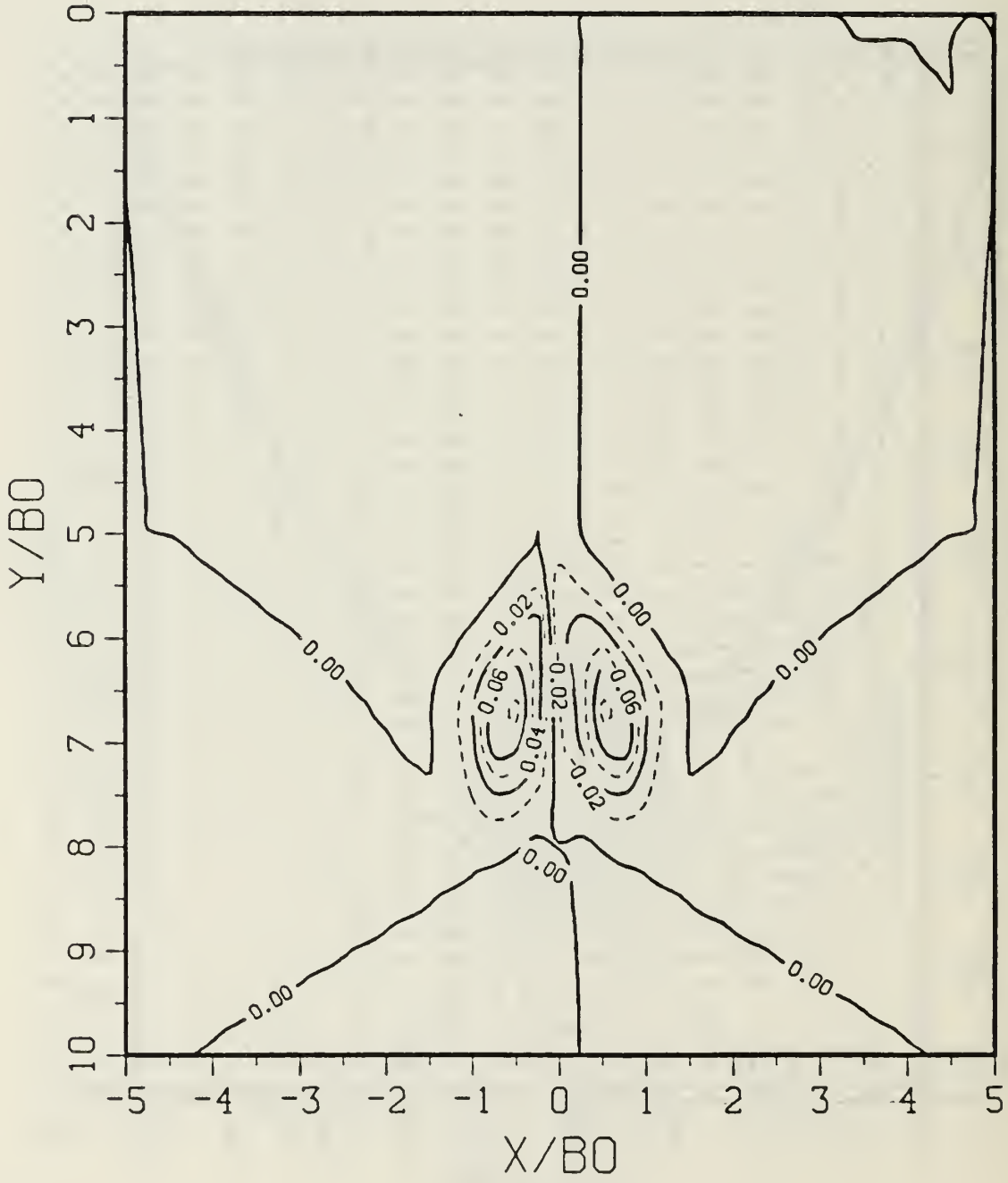
Y/BO
X/BO
0
1
2
3
4
5
6
7
8
9
10
-5
-4
-3
-2
-1
0
1
2
3
4
5
0.00
0.00
0.00

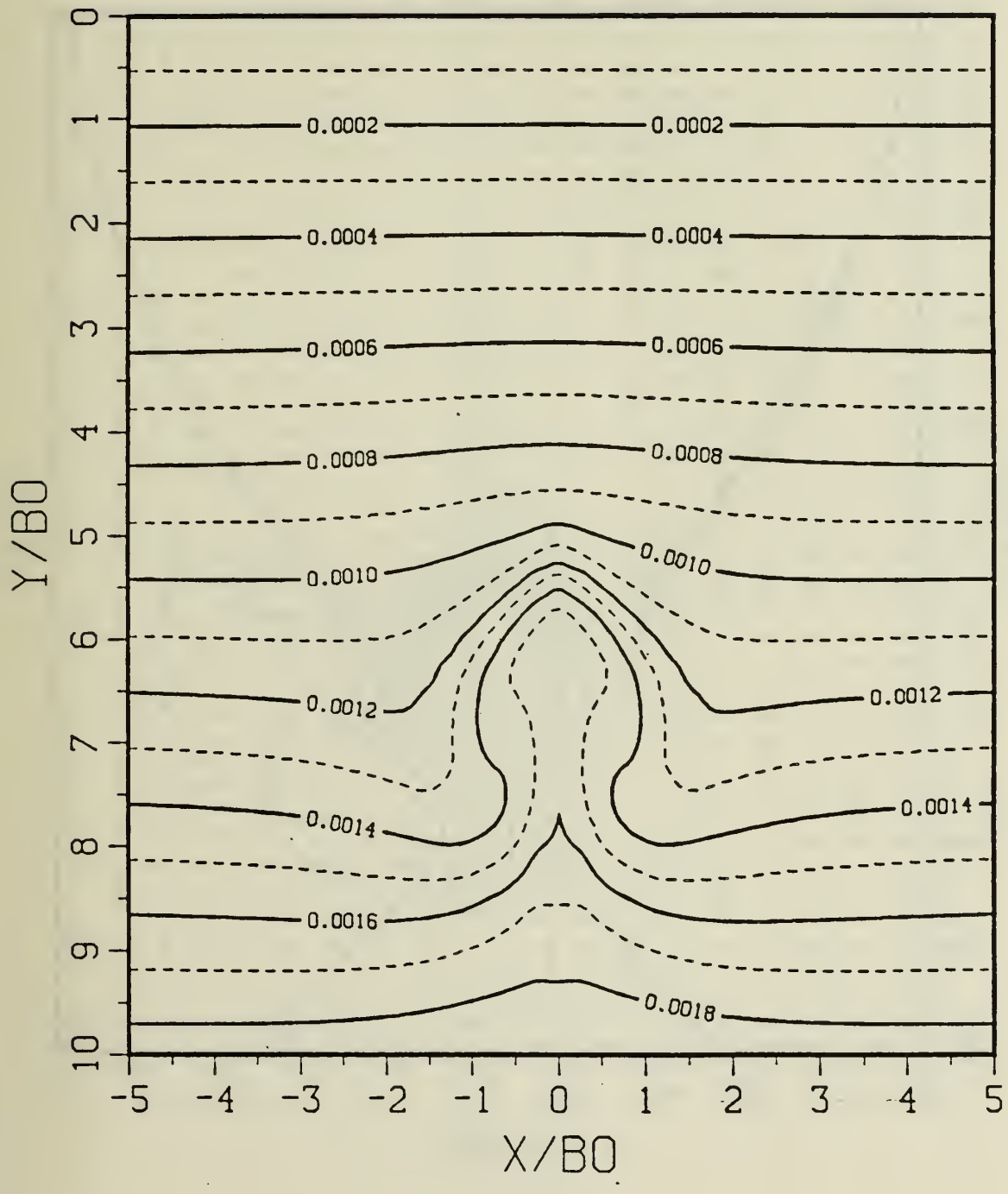

Figure 41c. Constant Density Contours for T* = 1.46

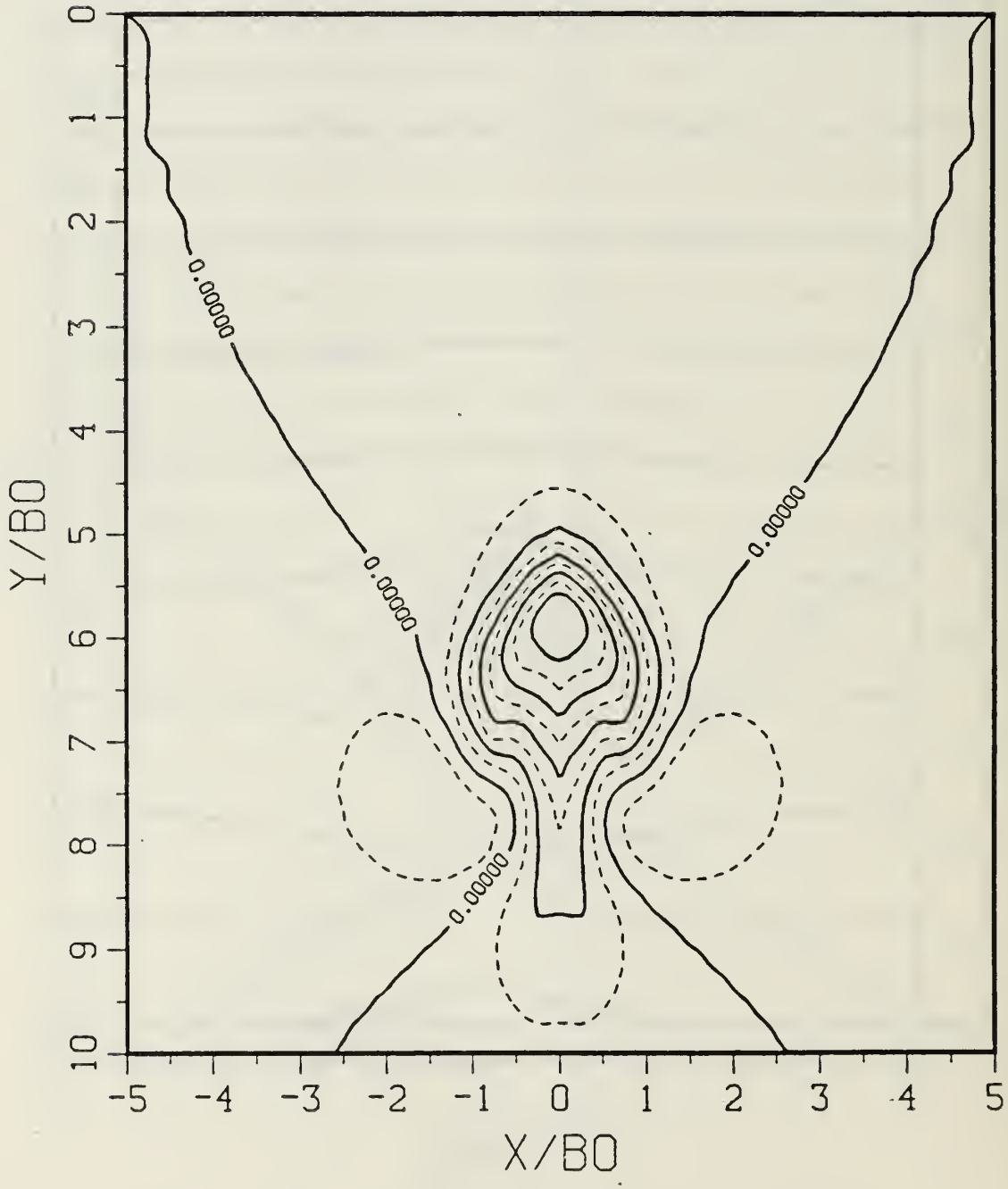

Figure 41d. Density Perturbation Contours for T* = 1.46

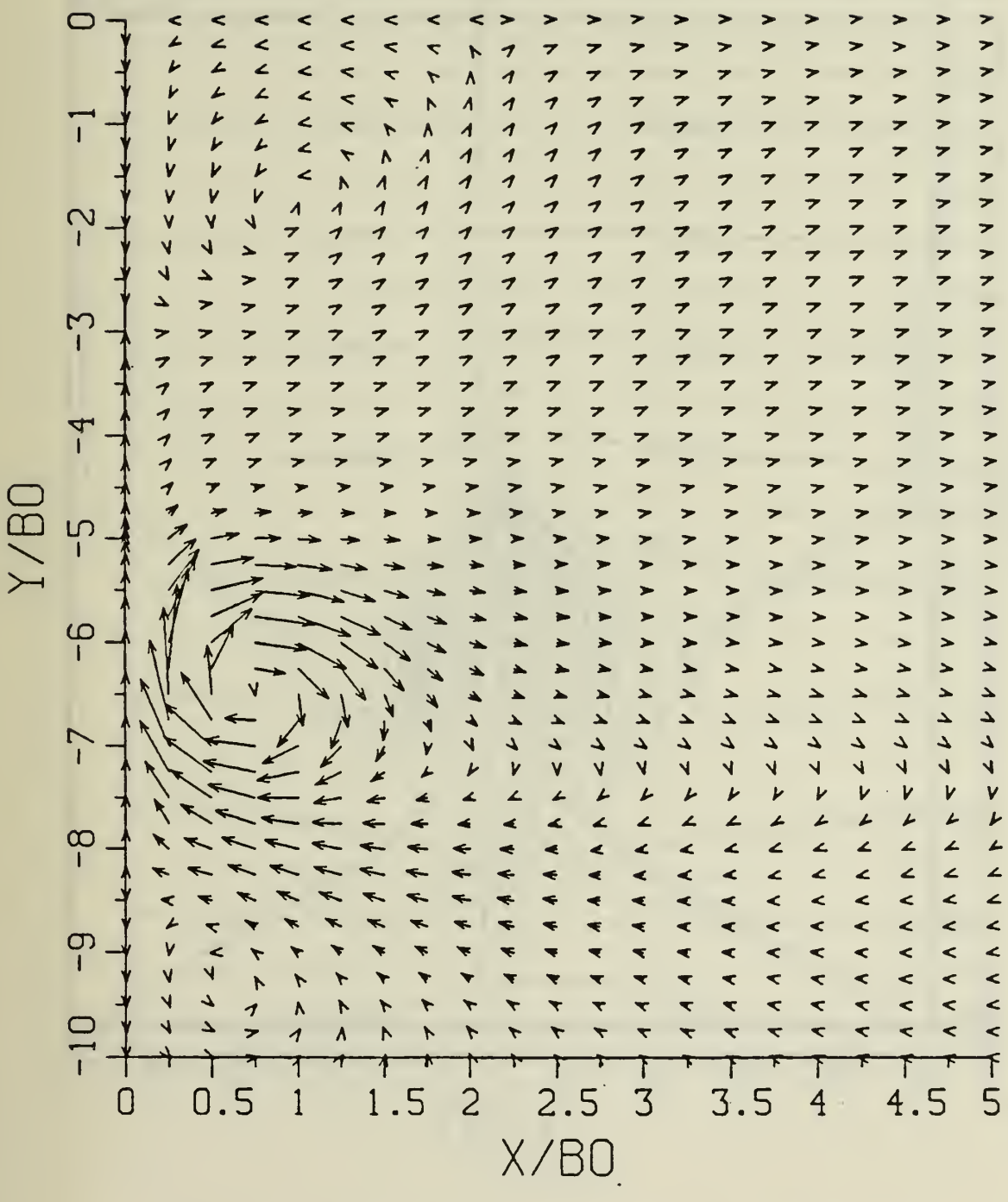

Figure 42a. Velocity Field for T* = 2.18

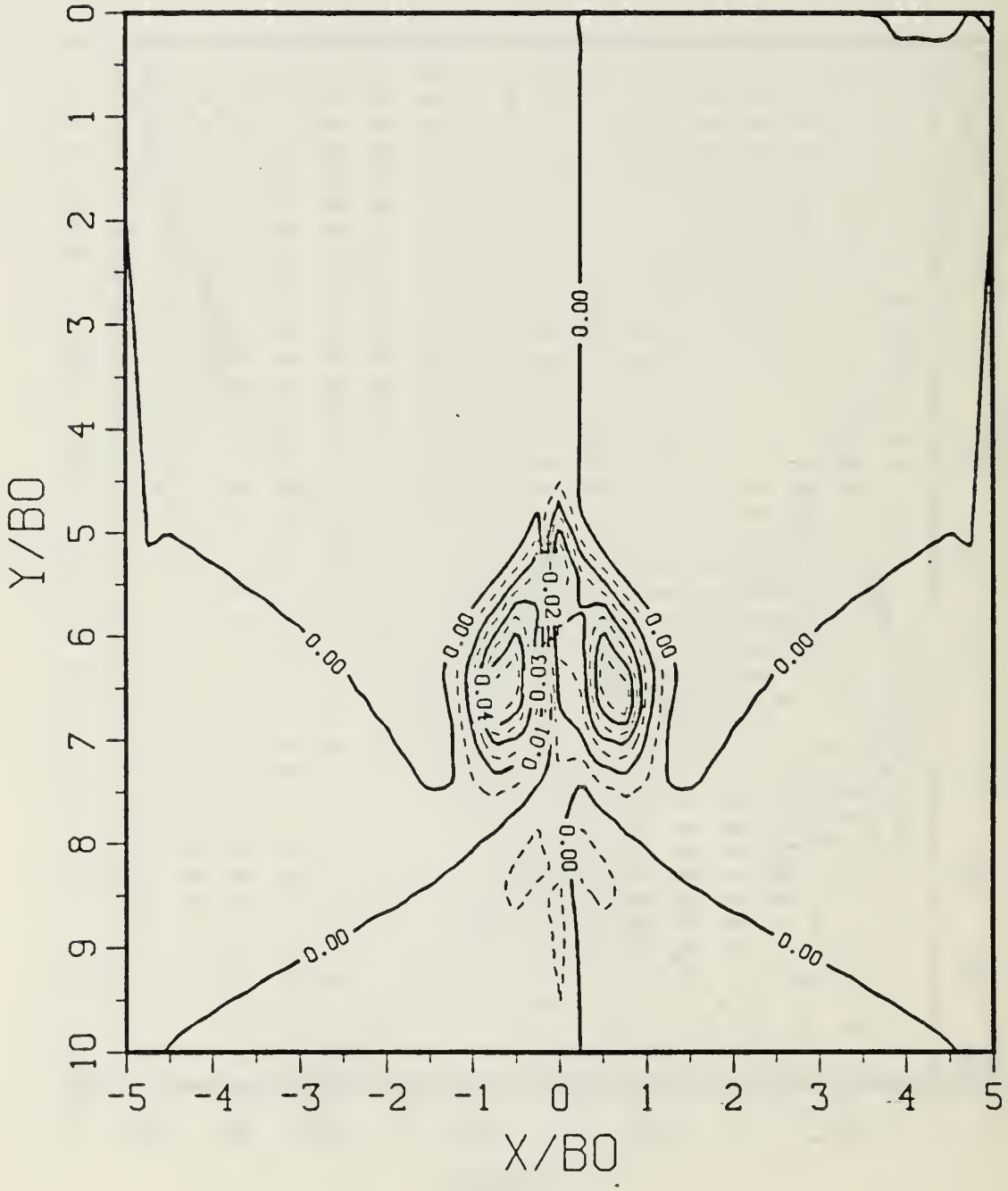

Figure 42b. Vorticity Field for T* = 2.18

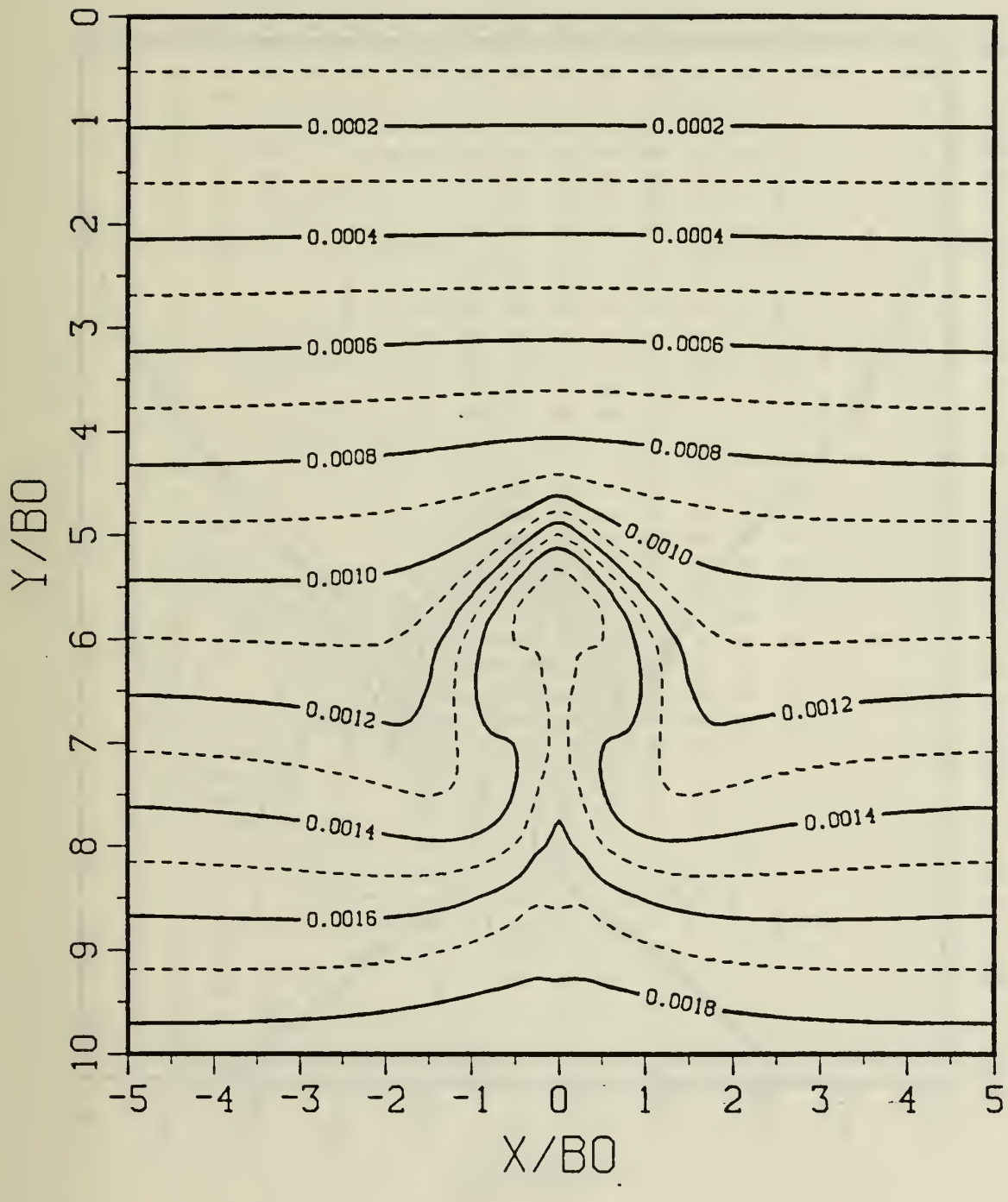

Figure 42c. Constant Density Contours for T* = 2.18

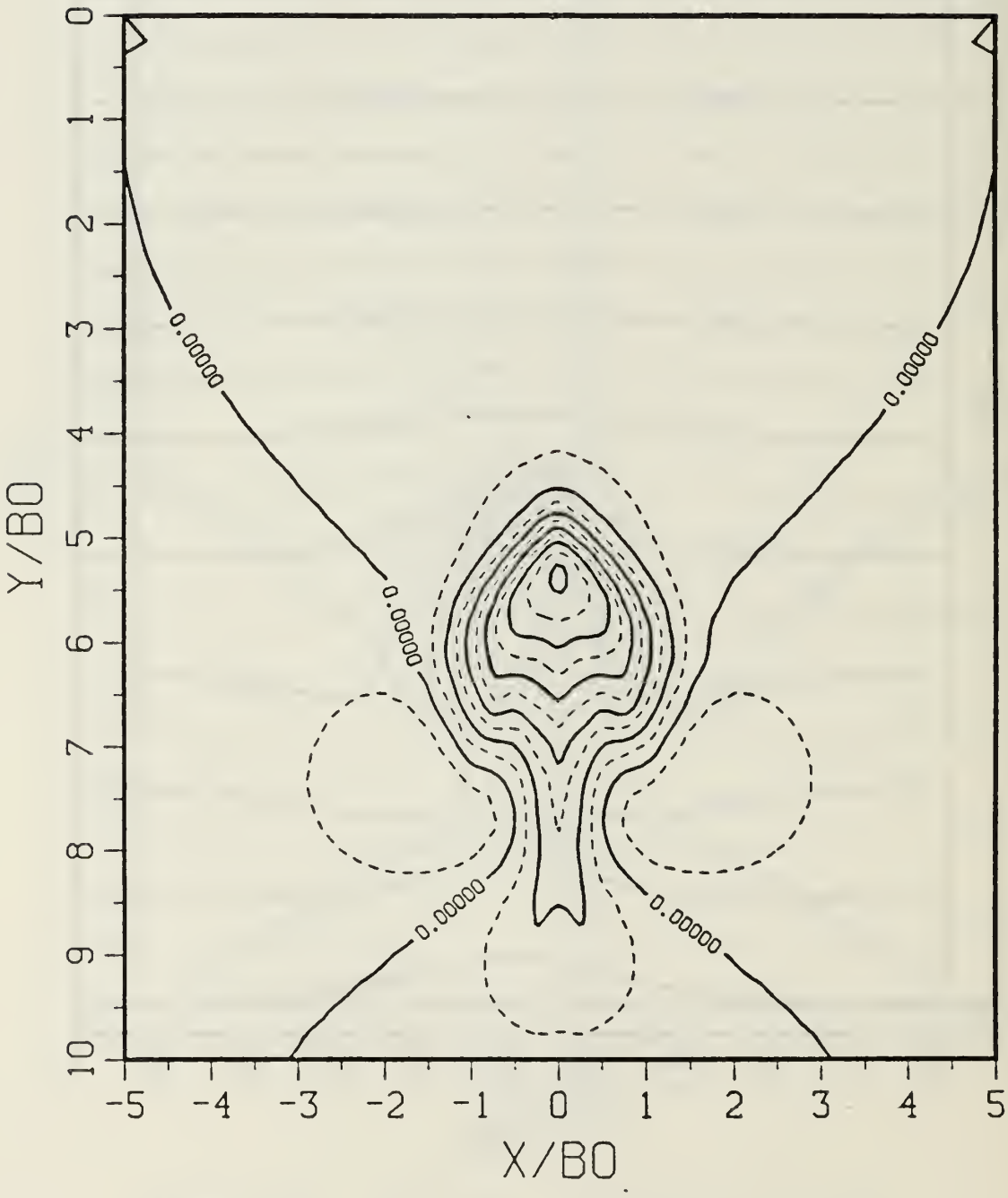

Figure 42d. Density Perturbation Contours for T* = 2.18

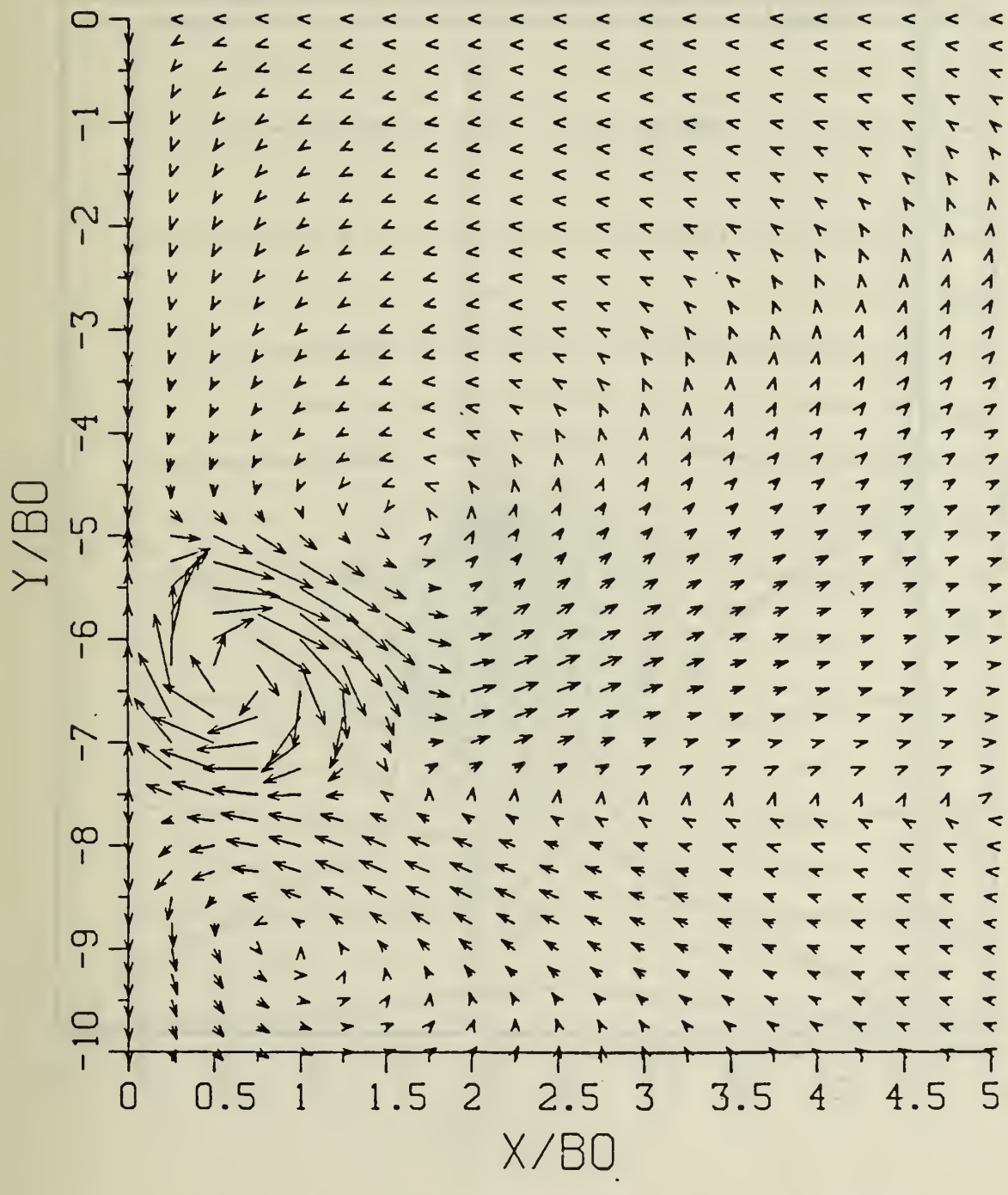

Figure 43a. Velocity Field for T* = 2.9

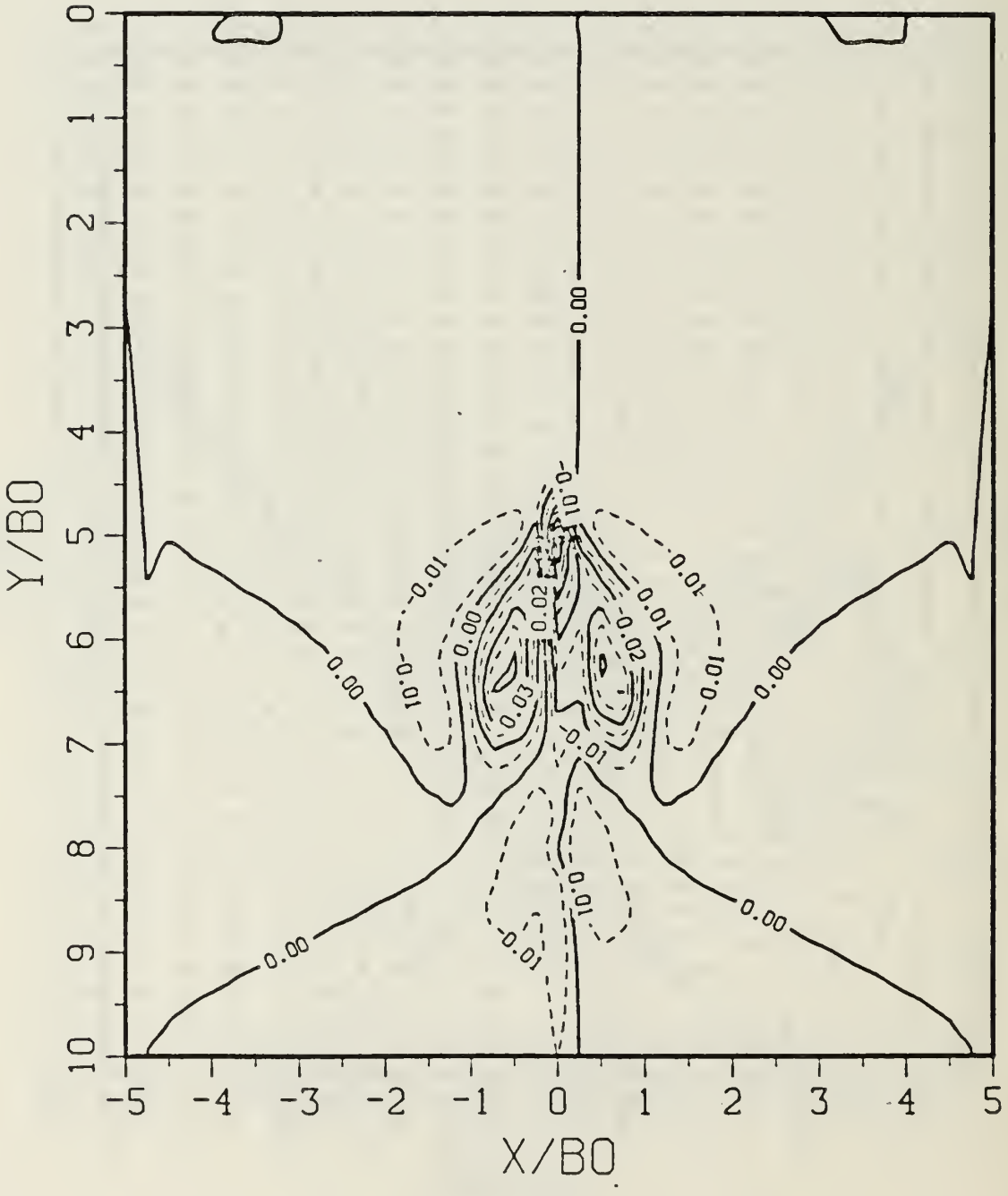

Figure 43b. Vorticity Field for T* = 2.9

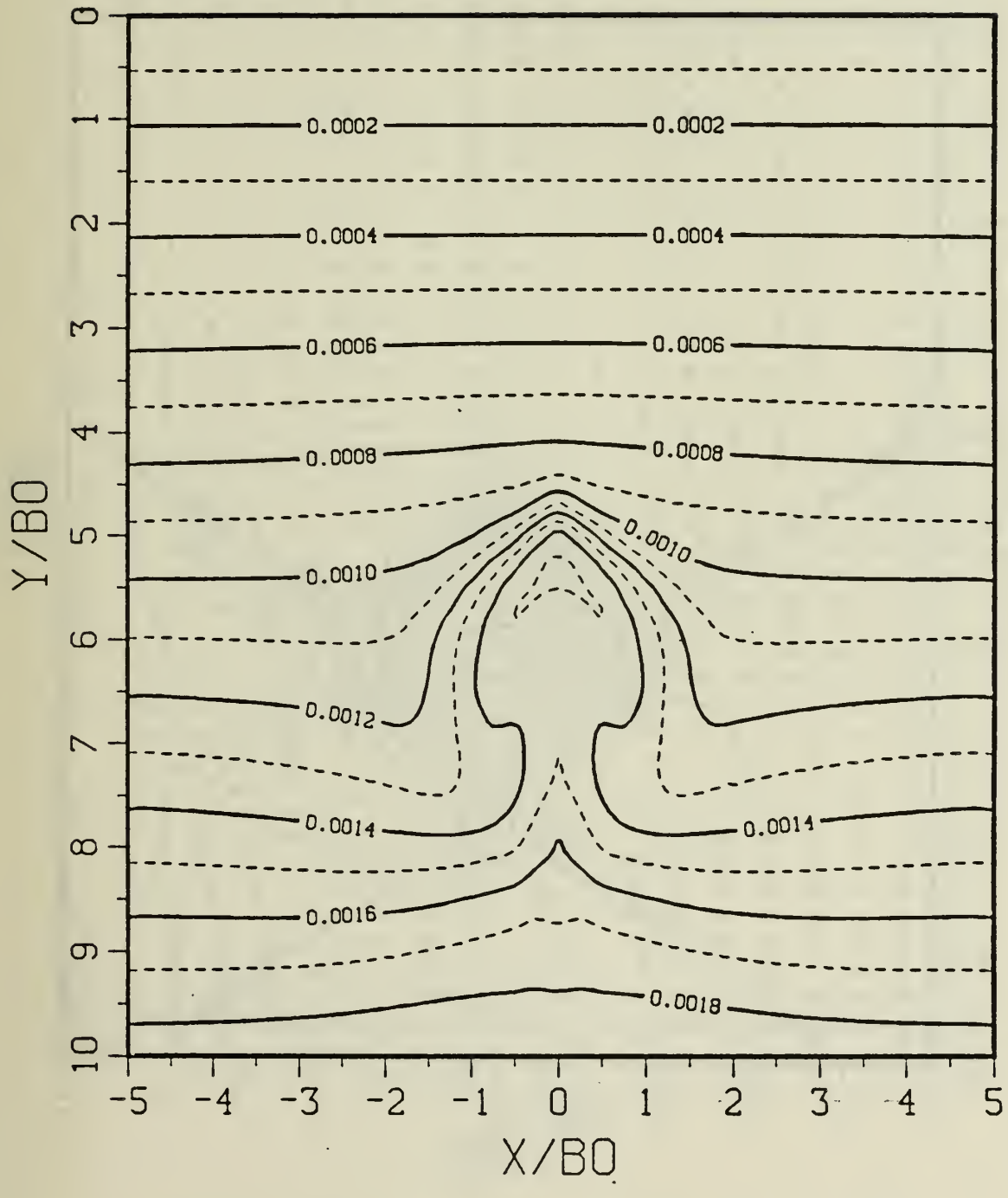

Figure 43c. Constant Density Contours for T* = 2.9

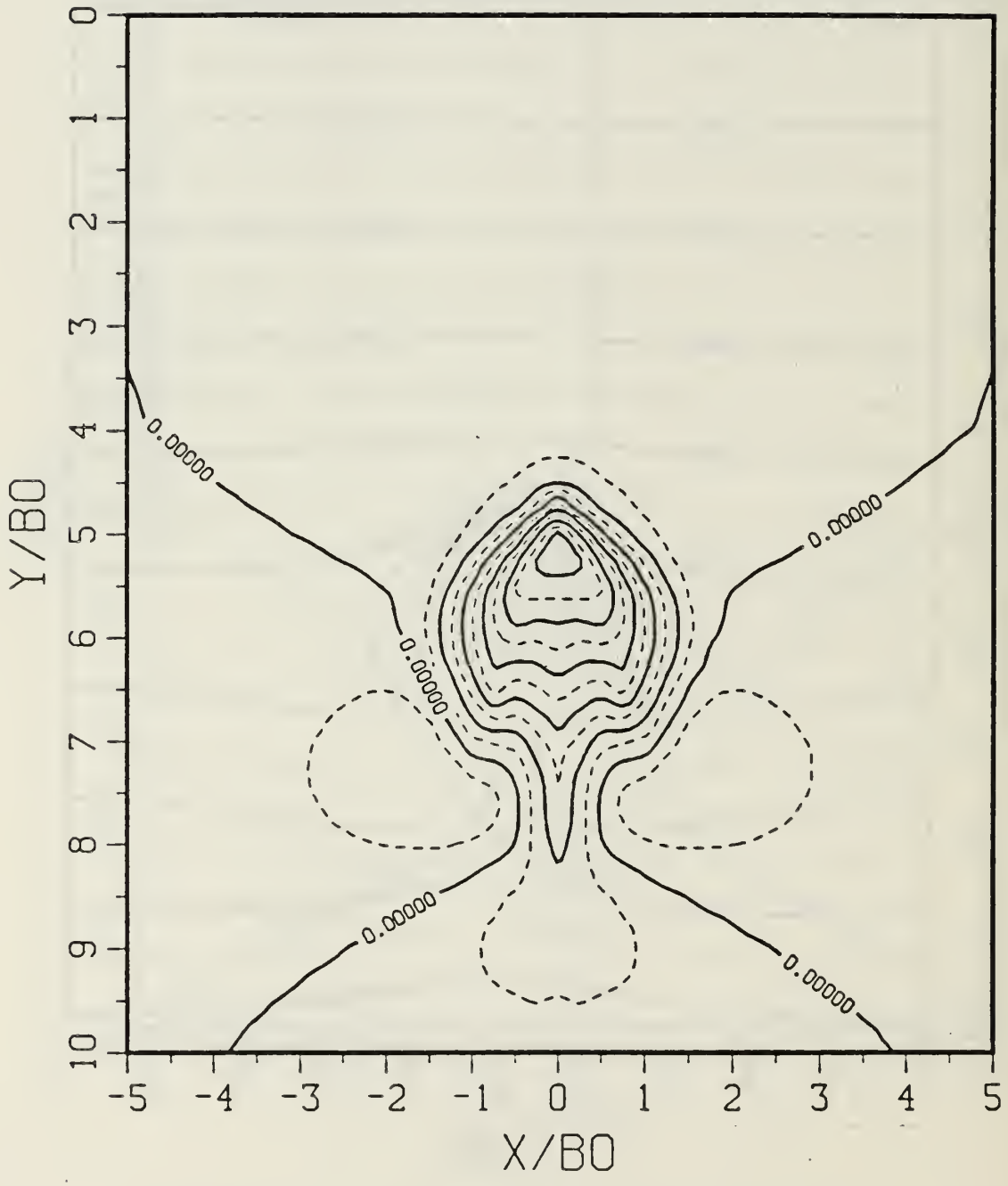

Figure 43d. Density Perturbation Contours for T* = 2.9

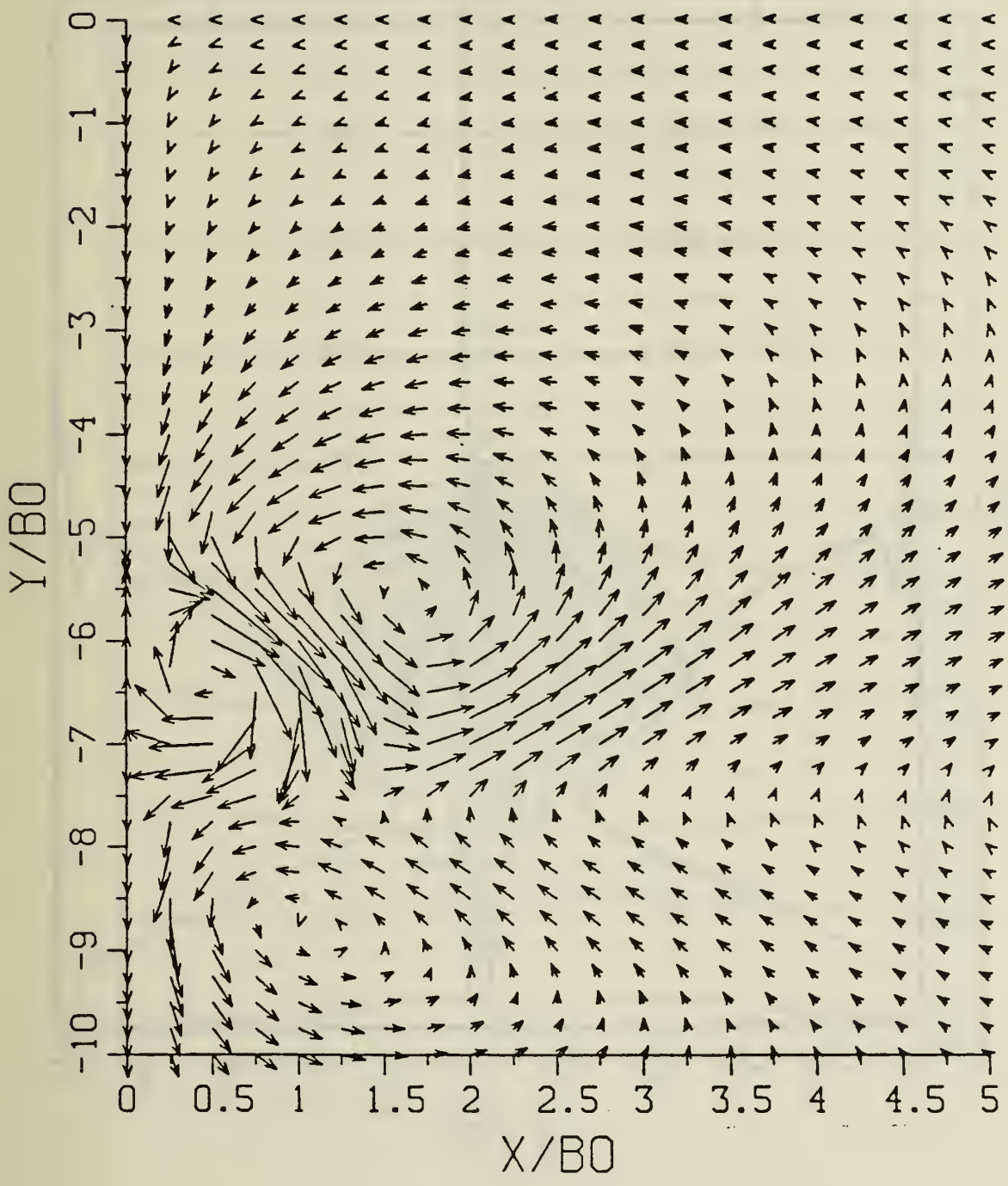

Figure 44a. Velocity Field for T* = 3.64

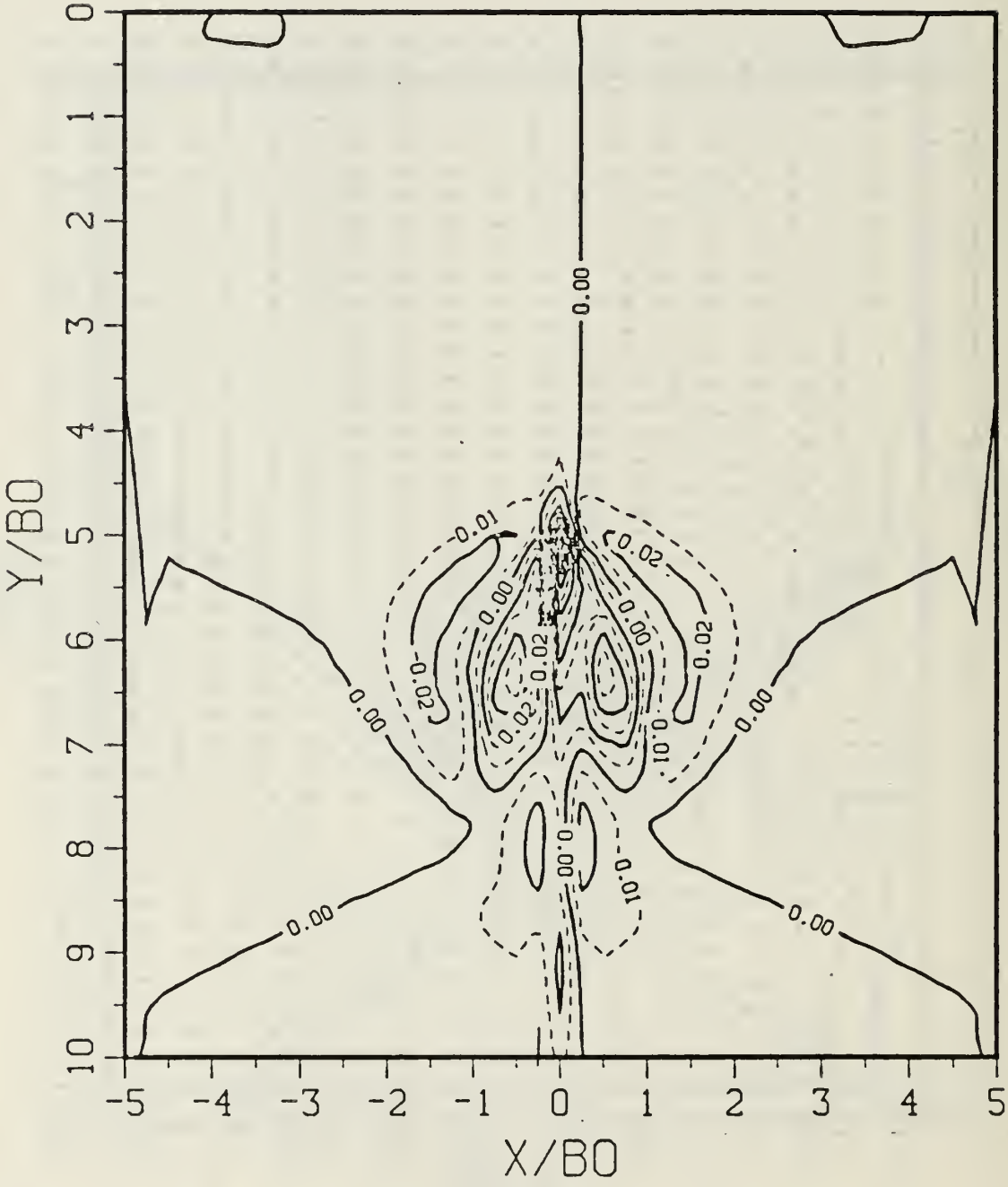

Figure 44b. Vorticity Field for T* = 3.64

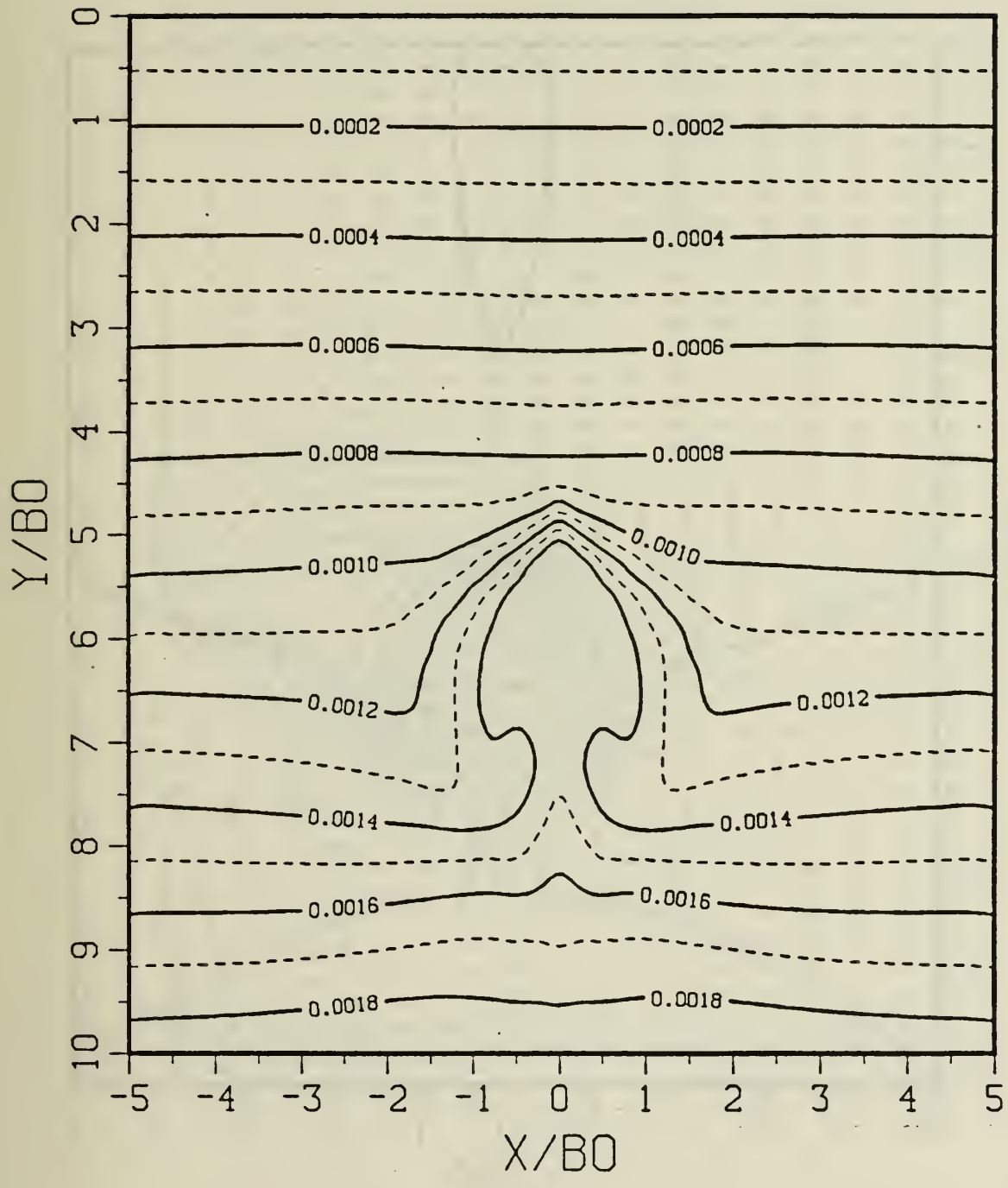

Figure 44c. Constant Density Contours for T* = 3.64

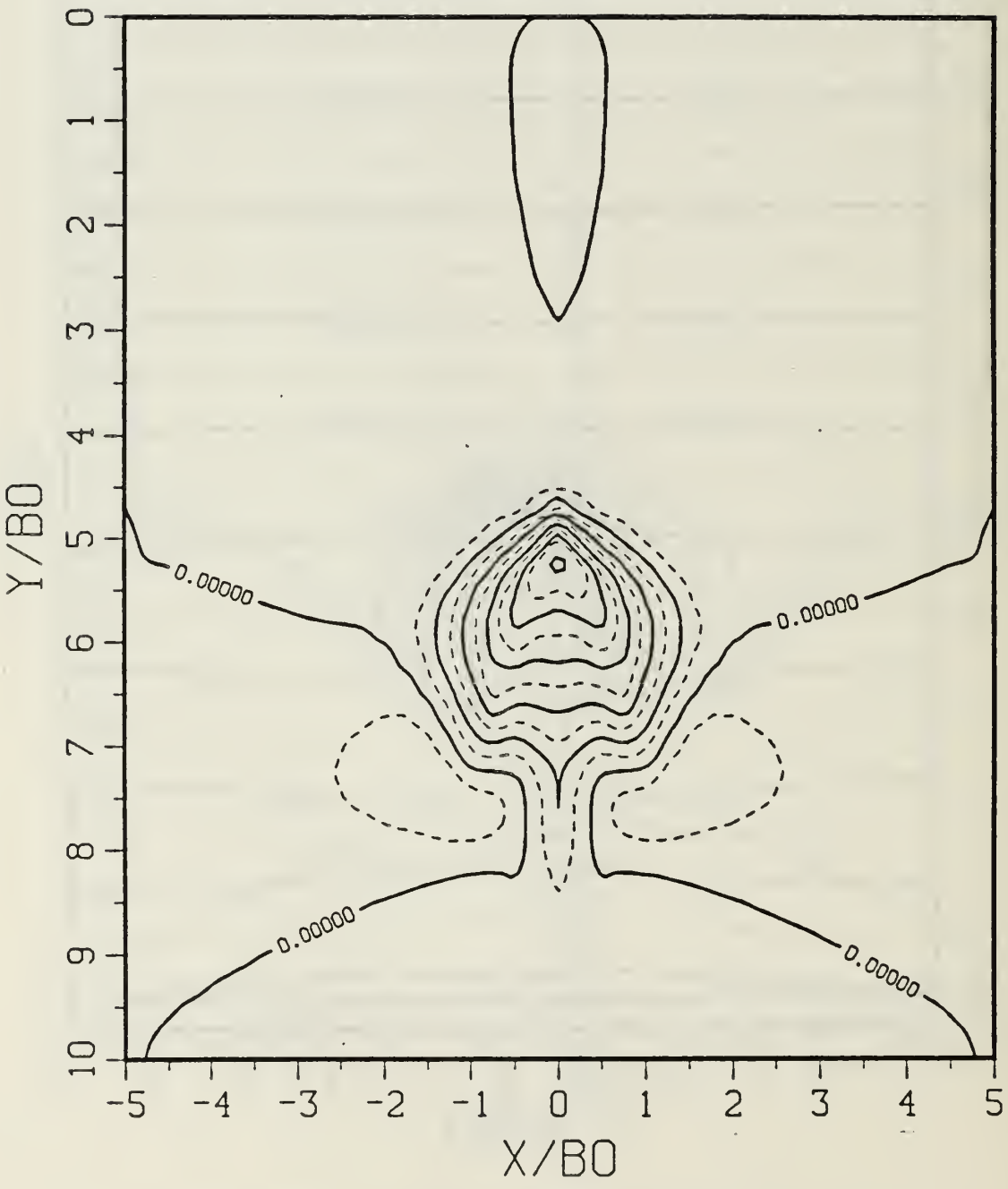

Figure 44d. Density Perturbation Contours for T* = 3.64

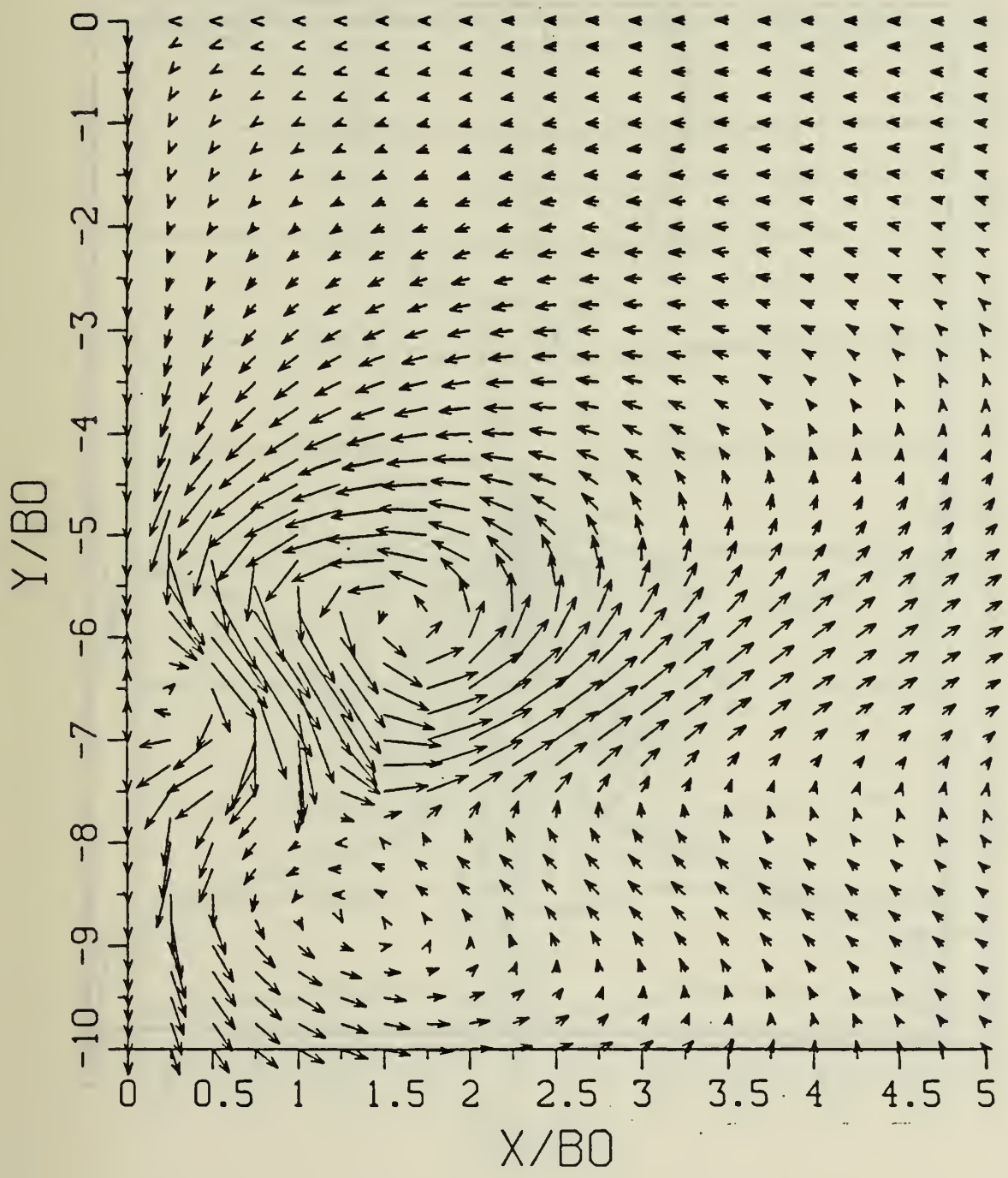

Figure 45a. Velocity Field for T* = 4.4

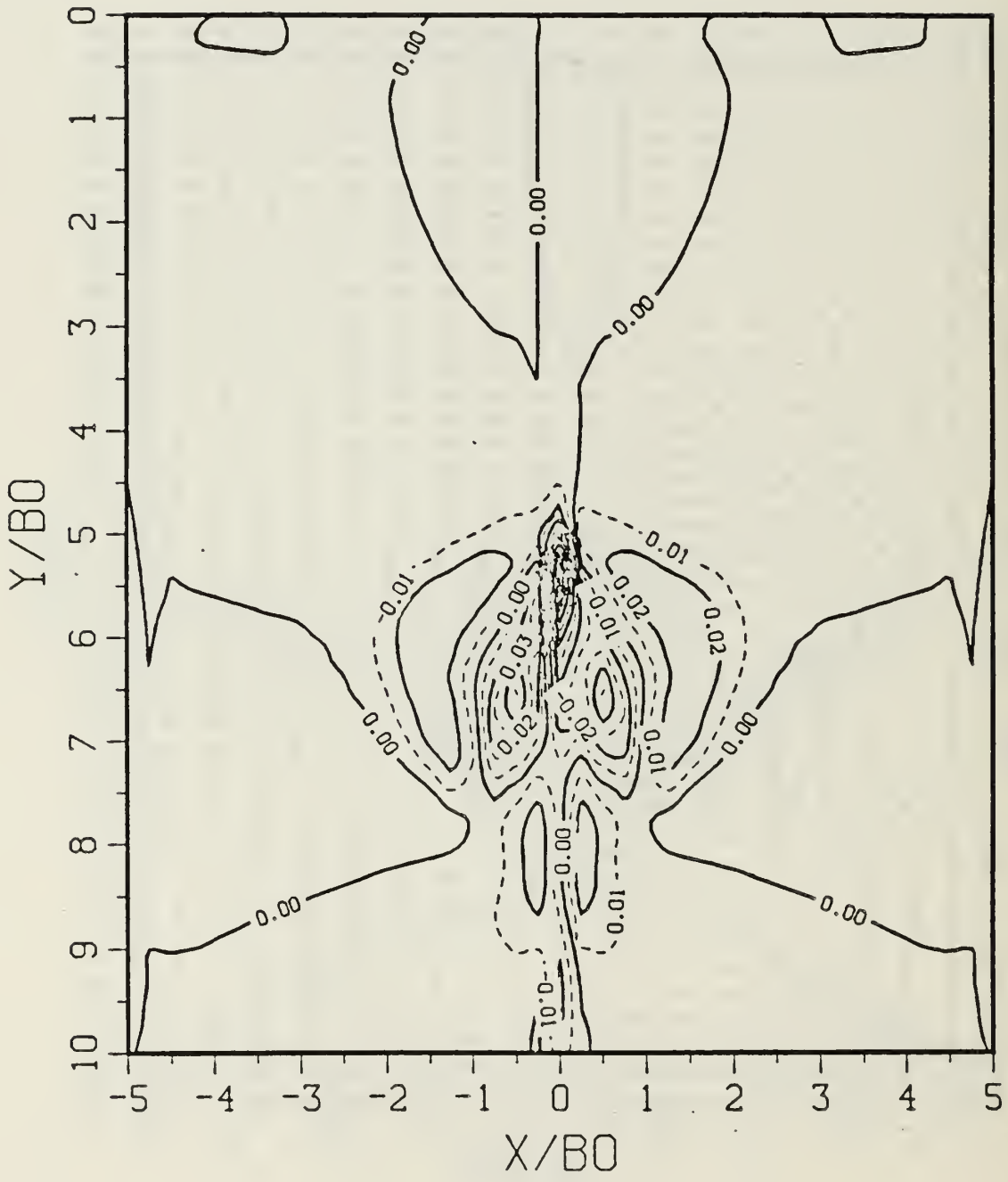

Figure 45b. Vorticity Field for T* = 4.4

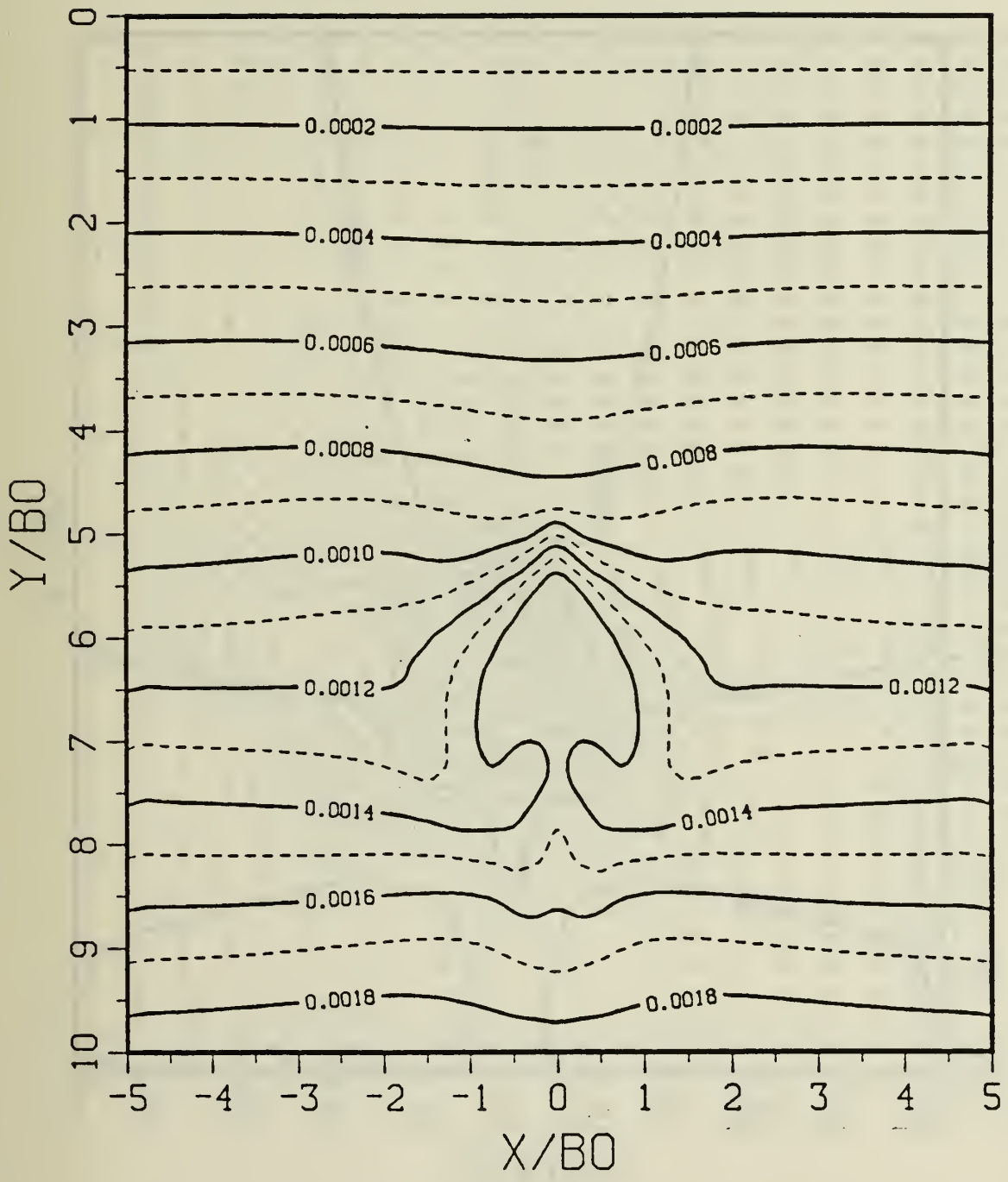

Figure 45c. Constant Density Contours for T* = 4.4

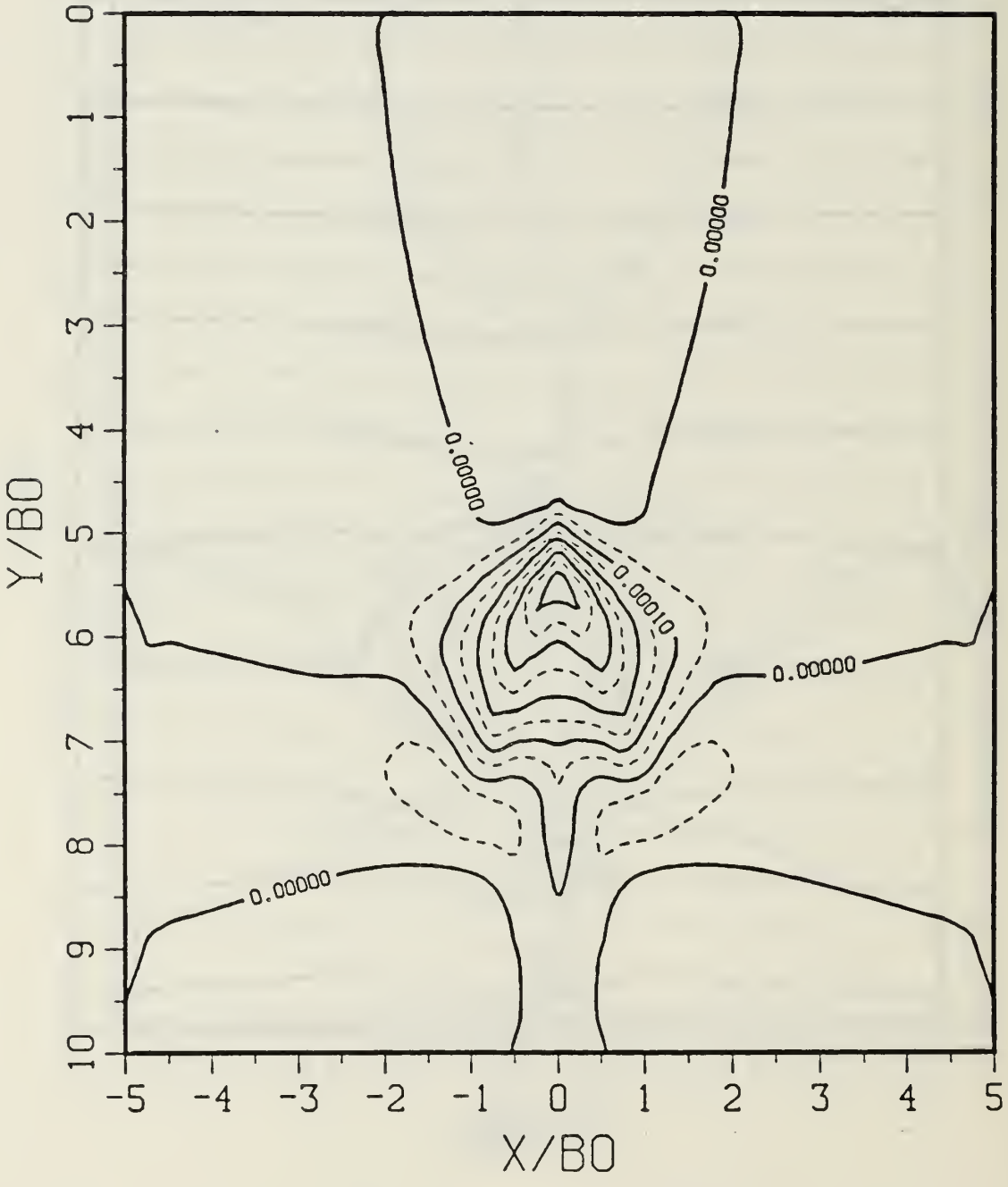

Figure 45d. Density Perturbation Contours for T* = 4.4

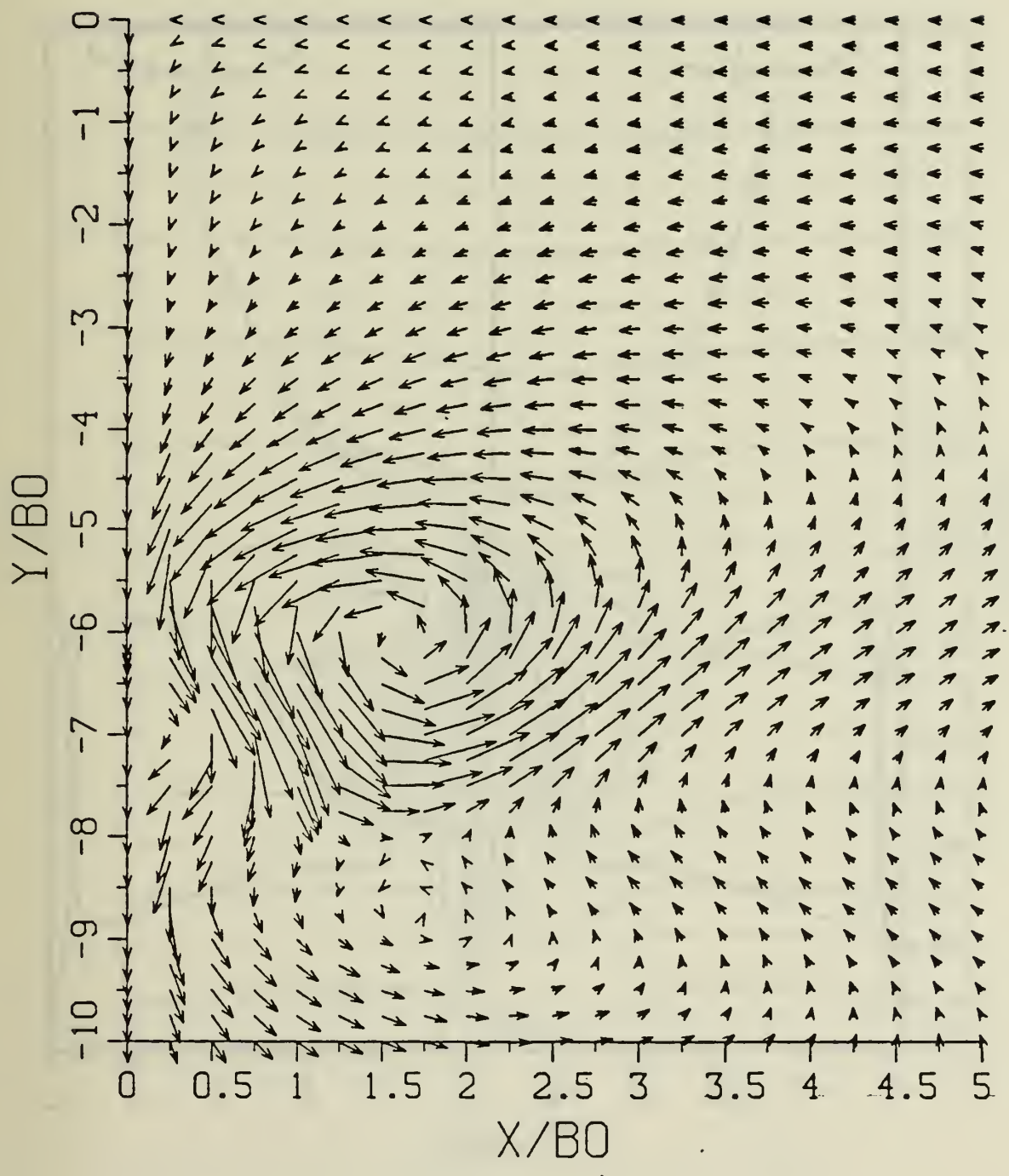

Figure 46a. Velocity Field for T* = 5.1

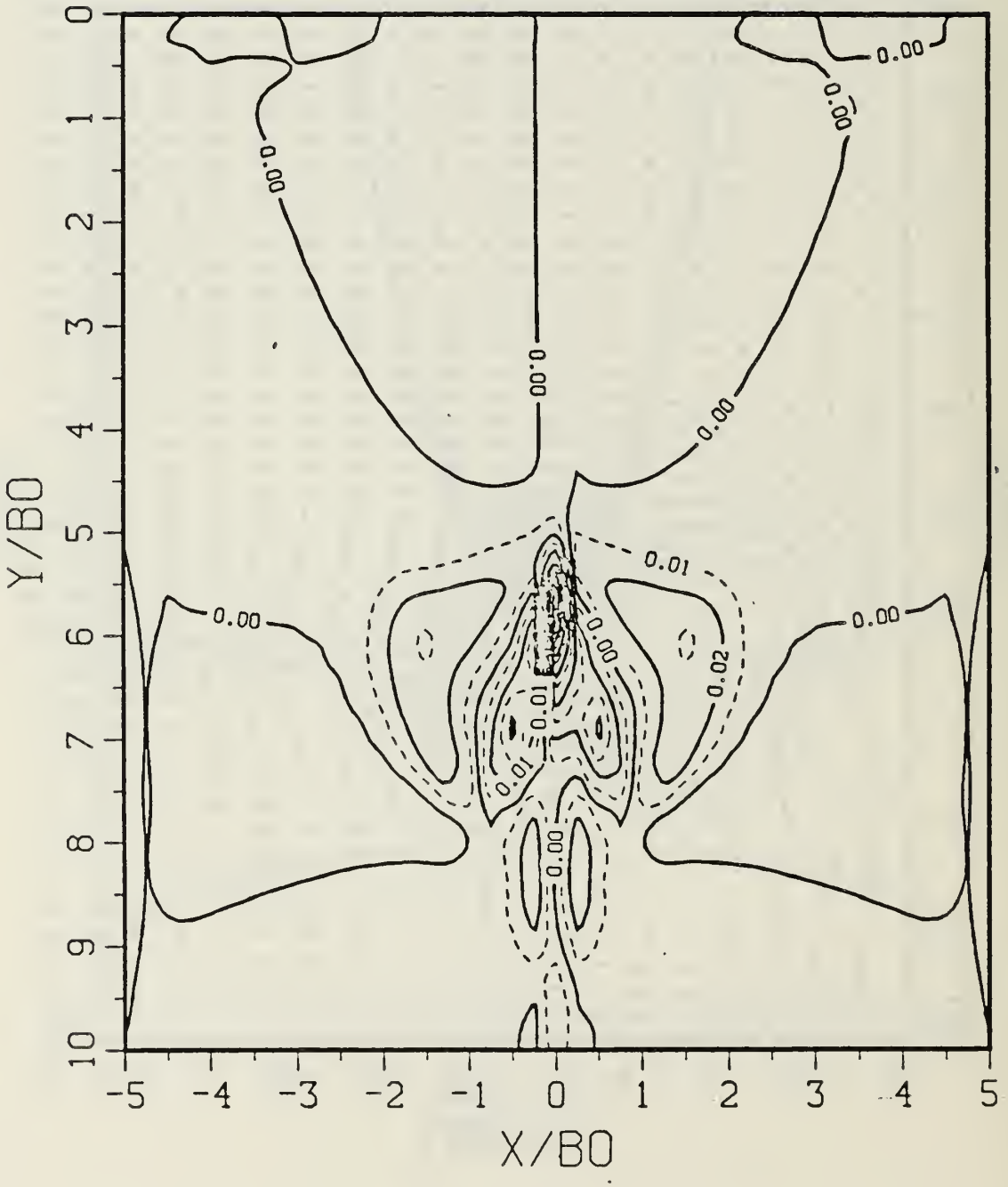

Figure 46b. Vorticity Field for T* = 5.1

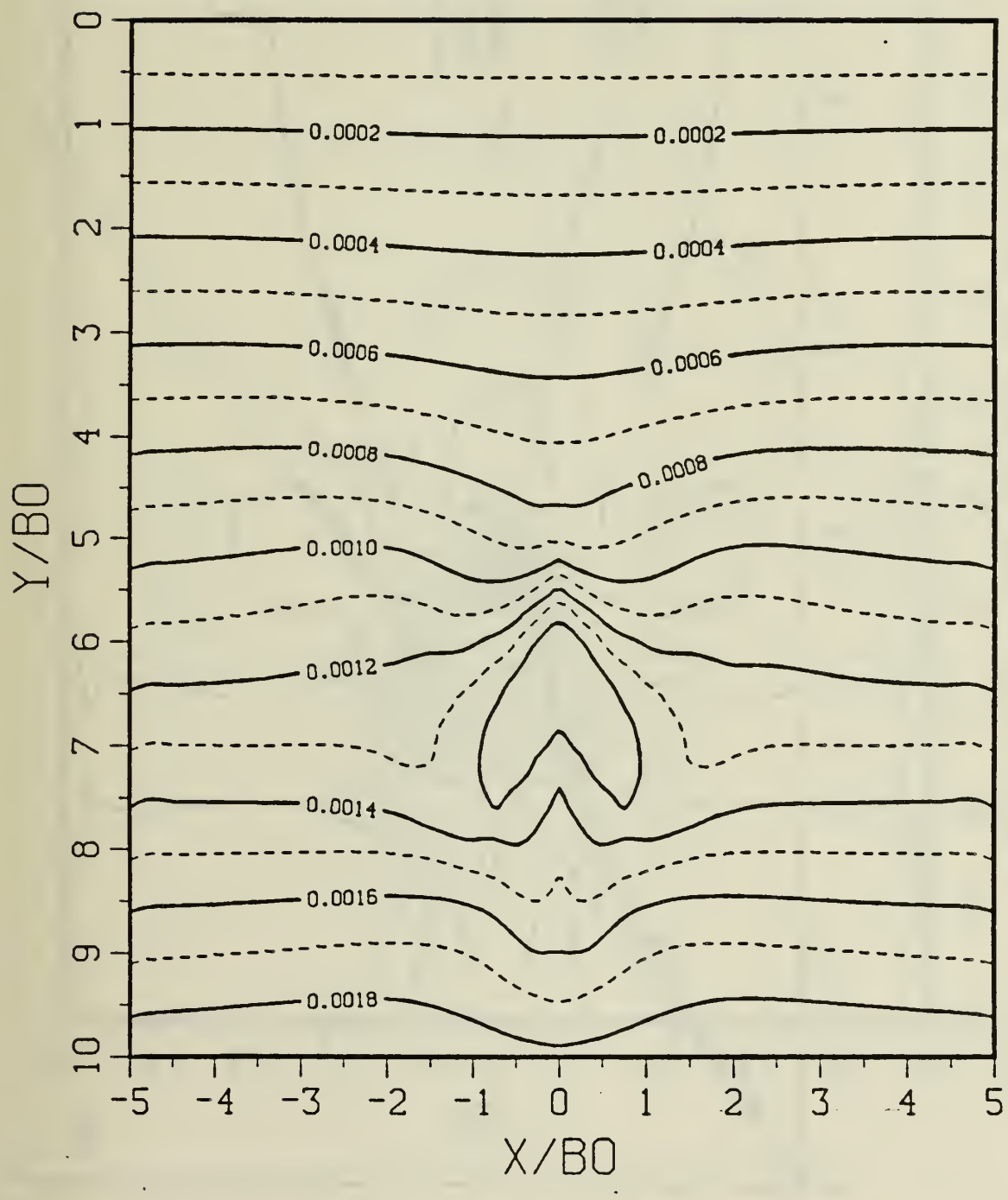

Figure 46c. Constant Density Contours for T* = 5.1

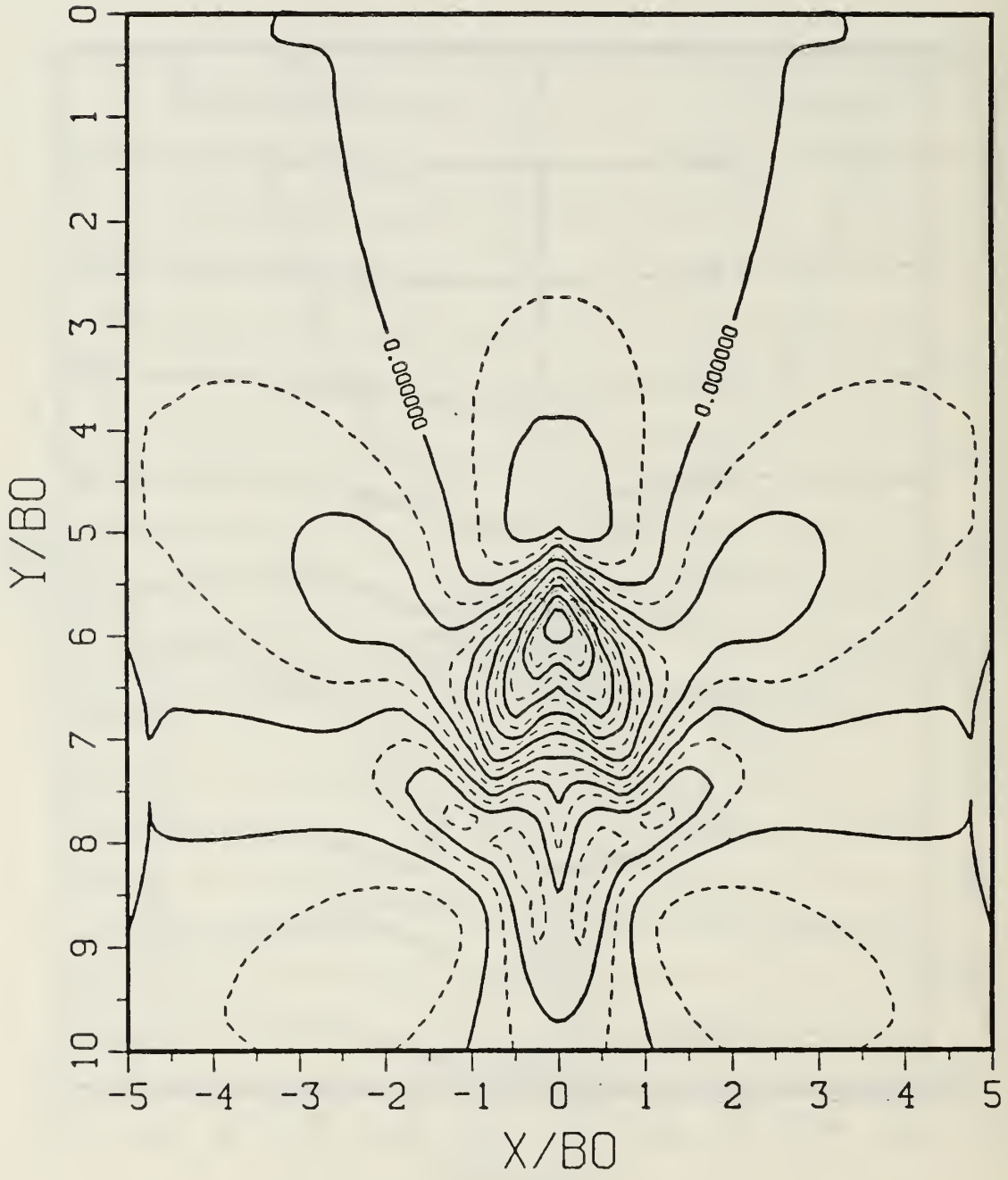

Figure 46d. Density Perturbation Contours for T* = 5.1

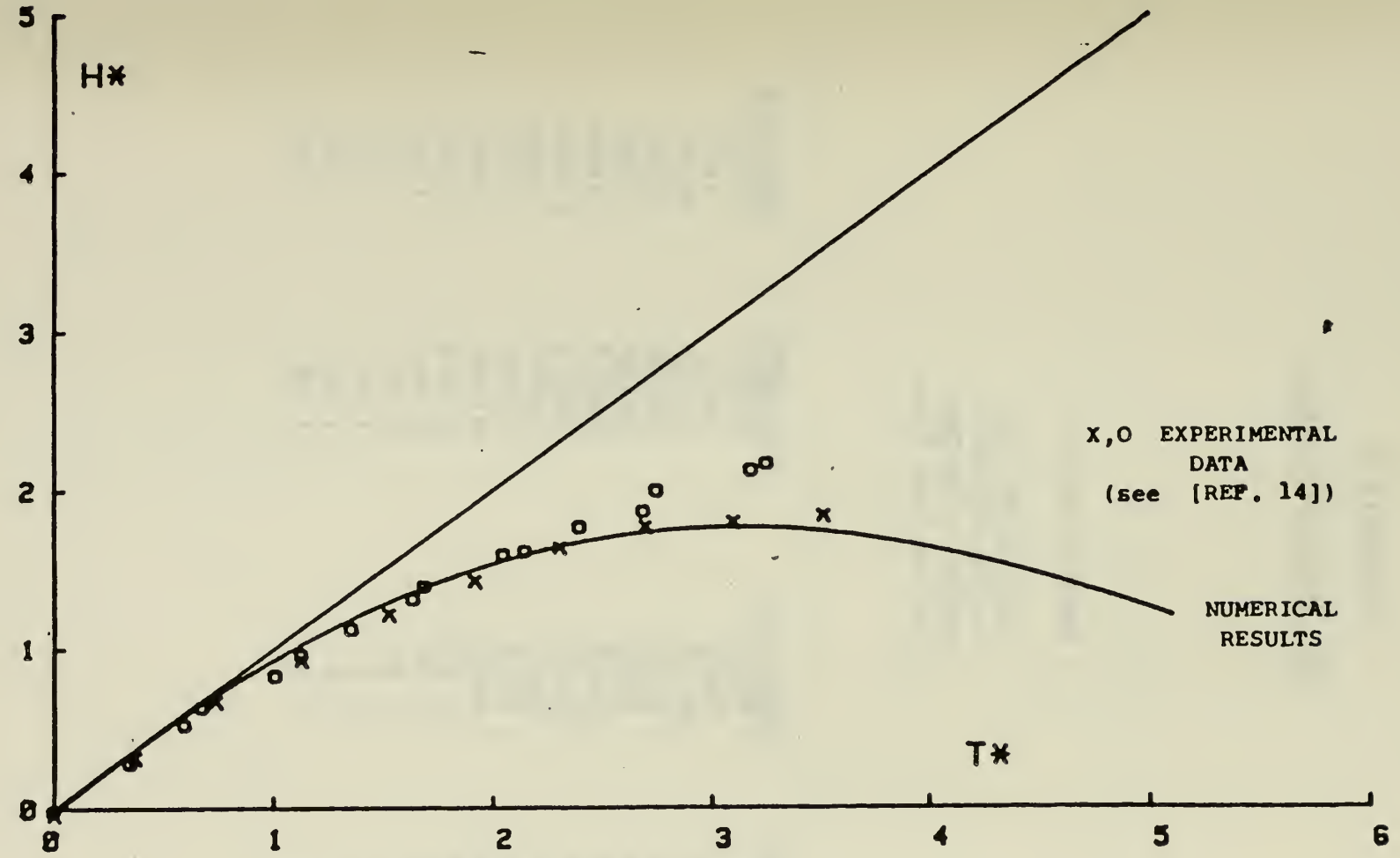

Figure 47. Comparison of Numerical and Experimental Results for SP = 0.75, $\dot{F}_v$ = 0.018

APPENDIX B

RP1 TABULATED DATA

Model: RP1

b_o = 5.34 in
U = 1.6 ft/s
ALPHA = 10 Deg
V_o = 0.028 ft/s

EPSILON*	T*	EPSILON*	H*
0.01	8.2	0.01	4.7
0.01	5.4	0.01	3.15
0.197	3.17	0.197	2.5
0.198	3.2	0.198	2.2
0.199	3.0	0.199	2.5
0.273	1.74	0.273	1.25
0.273	2.2	0.273	1.6
0.273	2.4	0.273	1.84
0.451	1.74	0.451	1.43
0.459	1.72	0.459	1.13
0.595	0.893	0.595	0.89
0.595	1.07	0.595	1.07
0.58	1.27	0.58	1.25
1.12	1.9	1.12	1.6
1.03	1.8	1.03	1.55
1.08	1.4	1.08	1.17

Model: RP1

b_o = 5.34 in
U = 0.9 ft/s
ALPHA = 10 Deg
V_o = 0.018 ft/s

EPSILON*	T*	EPSILON*	H*
0.01	5.5	0.01	3.74
0.01	4.1	0.01	3.15
0.178	3.3	0.178	2.02
0.24	2.55	0.24	1.73
0.24	2.45	0.24	1.84
0.413	1.27	0.413	1.25
0.413	1.8	0.413	1.4
0.53	1.4	0.53	1.02
0.53	0.8	0.53	0.67
0.97	1.73	0.97	1.33

APPENDIX C

RP 2 TABULATED DATA

Model: RP2

b_o = 3.53 in
U = 0.9 ft/s
ALPHA = 10 Deg
V_o = 0.021 ft/s

EPSILON*	T*	EPSILON*	H*
0.01	4.3	0.01	3.16
0.01	3.44	0.01	3.4
0.01	5.4	0.01	3.5
0.01	4.1	0.01	3.1
0.01	3.8	0.01	2.5
0.134	2.8	0.134	2.37
0.134	4.5	0.134	3.05
0.18	2.1	0.18	1.5
0.18	1.8	0.18	1.2
0.314	2.6	0.314	1.9
0.319	1.7	0.319	1.7
0.314	2.2	0.314	1.55
0.319	2.04	0.319	1.98
0.392	1.22	0.392	0.97
0.39	1.73	0.39	1.15
0.404	2.22	0.404	1.6
0.422	1.25	0.422	1.2
0.745	1.23	0.745	1.1
0.75	1.6	0.75	1.4
0.745	2.0	0.745	1.9
0.745	1.65	0.745	1.7
1.03	1.5	1.03	1.55
1.06	0.83	1.06	0.9
0.97	1.9	0.97	1.8
1.8	1.11	1.8	1.1
2.02	0.9	2.02	0.9

Model: RP2

b_o = 3.53 in
U = 1.6 ft/s
ALPHA = 12 Deg
V_o = 0.04 ft/s

EPSILON*	T*	EPSILON*	H*
0.01	4.5	0.01	3.91
0.01	8.4	0.01	5.29
0.01	5.6	0.01	4.74
0.099	3.8	0.099	3.48
0.123	3.35	0.123	2.59
0.123	3.89	0.123	3.3
0.168	4.2	0.168	2.96
0.169	5.1	0.169	3.48
0.279	2.97	0.279	1.9
0.284	3.85	0.284	1.87
0.36	2.86	0.36	1.9
0.366	2.2	0.366	1.87
0.692	2.12	0.692	1.9
0.682	1.66	0.682	1.72
0.692	1.6	0.692	1.53
0.945	1.48	0.945	1.35
0.989	1.77	0.989	1.62
0.989	1.35	0.989	1.6
1.66	1.55	1.66	1.51

APPENDIX D

TOMBACH DATA

EXPERIMENTAL DATA COMPILED FROM DATA REPORTED BY TOMBACH
(SEE [REF. 24])

EPSILON*	T*	EPSILON*	H*
0.040	4.1	0.040	4.2
0.048	3.5	0.052	3.5
0.055	3.4	0.060	3.4
0.055	2.9	0.059	2.8
0.055	2.4	0.057	2.3
0.160	3.8	0.165	3.7
0.220	2.2	0.240	2.15
0.220	1.6	0.350	2.0
0.220	1.4	0.420	1.95
0.170	1.4	0.320	1.75
0.330	2.0	0.390	1.7
0.400	2.0	0.265	1.6
0.320	1.8	0.350	1.5
0.370	1.75	0.165	1.3
0.330	1.55	0.265	1.3
0.330	1.2	0.350	1.2

APPENDIX E

NUMERICAL ANALYSIS PROGRAM LISTING

```
C*****************************************************************
C
C      _              PROGRAM VOR1SPL
C
C        5 MARCH 86
C
C*****************************************************************
C
C     PURPOSE:
C
C      THIS PROGRAM NUMERICALLY SIMULATES THE RISE OF A TRAILING
C       VORTEX PAIR SHED OFF A LIFTING SURFACE SUBMERGED IN A
C       DENSITY STRATIFIED MEDIUM.
C-----------------------------------------------------------------
C
C     TO RUN THIS PROGRAM:
C
C    1) GO TO "INPUT PARAMETERS" SECTION OF CODE AND CHANGE ANY PROBLEM
C       PARAMETERS ( SP, FV, DT, ZTMAX, MP, NP, ISAVE) DESIRED.
C
C    2) SET MAXIMUM TIME IN DATA STATEMENT MAXSTP;
C       EX:  DATA  MAXSTP /N/
C                  ( WHERE N= MAXIMUM NUMBER OF TIME STEPS)
C
C    3) SET INTERVALS FOR PLOTTING BY ENTRIES IN DATA STATEMENT NPLOT;
C       EX:  DATA NPLOT/ 1,2,8,12,20,40,50,75/.
C            ( THIS PLOTS OUTPUT AT THE 1ST,2ND,8TH,12TH,40TH,50TH,AND
C                       75TH PROGRAM TIME STEP)
C
C    4) CHOOSE  WHAT OUTPUT DEVICE TO USE, EITHER TEK 618 OR COMPRES
C       (METAFILE OUTPUT) BY GOING TO  GRAPHIC DEVICE SECTION OF PROGRAM
C       AND COMMENTING OUT WHICH OF TWO DEVICES YOU DONT WANT TO USE.
C
C    5) COMPILE PROGRAM UNDER VS FORTRAN USING THIS COMMAND;
C
C       FORTVS  VOR1SPL  (OPT(3)
C
C       ( NOTE: THIS OPTIMIZES CODE AT LEVEL 3 )
C
C    6) GO TO APPROPRIATE TERMINAL AND RUN UNDER DISSPLA.
C            A.  WHEN THE DISSPLA EXEC PROMPTS YOU ASK FOR 5 CYLINDERS OF
C                 TEMPORARY DISK STORAGE.
C            B.  WHEN THE EXEC PROMPTS YOU YOU MAY WISH TO ISSUE:
C
C                FILEDEF  06  DISK  VOR1OUT LISTING (PERM
C
C                IN ORDER TO REROUTE THE PRINTED OUTPUT TO A DISK FILE
C                NAMED: VOR1OUT LISTING A1 .
C            C.  PROGRAM WILL NOW RUN SENDING OUTPUT TO YOUR DESIGNATED
C                DEVICES.
C-----------------------------------------------------------------
C
C     ADDITIONAL PROGRAM NOTES:
C
```

```
C 1) THIS PROGRAM COMPUTES DENSITY AND VORTICITY IN A (M-2 X N-2) GRID
C     BY SOLVING THE BOUYANTLY SCALED FORM OF THE NAVIER-STOKES
C     EQUATIONS VIA AN "UPWIND DIFFERENCING" FINITE DIFERENCE METHOD.
C    -
C 2) THE VELOCITY FIELD IS COMPUTED USING A FORM OF THE BIOT-SAVAT
C     LAW AT EACH NODAL POINT INCLUDING THE CONTRIBUTION OF THE
C     "IMAGE VORTICIES " ADDED TO INCLUDE THE FREE SURFACE EFFECT.
C
C 3)  THIS VERSION OF THE PROGRAM INCLUDES A DISSPLA ROUTINE
C      TO PLOT THE DENSITY PERTUBATIONS ,CONSTANT DENSITY,
C      VORTICITY, AND VELOCITY FIELD AT EACH SELECTED TIME STEP.
C      THESE SELECTIONS FOR PLOTTING ARE INDICATED BY ENTRIES
C      IN THE ARRAY NSTEP. MAXIMUM NUMBER OF TIME STEPS IS INDICATED
C      BY AN ENTRY IN THE ARRAY MAXSTEP.
C
C
C 4)  THE COMPUTATIONAL GRID  (M-2)X(N-2)  IS USED FOR ALL COMPUTATIONS
C      EXCEPT FOR VELOCITY CALLS TO THE BIOT-SAVAT SUBROUTINES.
C      TWO ADDITIONAL GRIDS, ONE FOR U AND ONE FOR V, ARE SHIFTED H/2
C      UNITS IN THE X AND Y DIRECTION RESPECTIVELY. THE SUBROUTINES
C      COMPUTE U AND V VELOCITIES ON THESE GRIDS USING VORTICITY FROM
C      COMPUTATIONAL GRID. THE VELOCITIES ARE THEN AVERAGED ACROSS THE
C      COMPUTATIONAL GRID POINTS TO BE USED FOR THE FINITE DIFFERENCING.
C
C 5)  THIS VERSION OF THE PROGRAM IS  WRITTEN IN SINGLE PRECISION
C      AND IN AN OPTIMIZED FORM OF THE ORIGINAL CODE.
C
C 6)  THIS PROGRAM HAS THE OPTION OF SAVING THE RHO AND ZETA ARRAYS
C      AND OTHER PROGRAM CONSTANTS IN ORDER TO RESTART THIS SIMULATION
C      AT THE TIME A PREVIOUS RUN FINISHED AT. PROGRAM RSVOR1 IS
C      SPECIFICALLY WRITTEN TO INPUT THE DATAFILE WRITTEN BY THIS
C      PROGRAM AND RESTART THE SIMULATION WITH THE SAME PARAMETERS.
C
C      TO ACCESS THIS SAVE FEATURE SET VARIABLE ISAVE =1 . A FILEDEF
C      OF FORM ... FILEDEF 08 DISK <FN> <FT> <FM> ... MUST BE ISSUED
C      AT THE APPROPRIATE TIME IN EXECUTION.
C     (NOTE: TO DISABLE THIS SAVE FEATURE SET ISAVE =0 )
C
C*************************************************************************
C
C      MAJOR VARIABLES USED IN THIS PROGRAM;
C
C   REAL VARIABLES;
C   T      = NONDIMENSIONAL TIME
C   DT     = TIME STEP
C   H      = NONDIMENSIONAL GRID LENGTH PARAMETER= DX = DY
C   RO     = NONDIMENSIONAL VORTEX CORE RADIUS
C   XWIDTH= NONDIMENSIONAL WIDTH OF COMPUTATIONAL AREA
C   ZTMAX  = MAXIMUM VORTEX STRENGTH
C   SP     = NONDIMENSIONAL STRATIFICATION PARAMETER
C   FV     = NONDIMENSIONAL FROUDE NUMBER
C   BVND   = NONDIMENSIONAL BRUNT-VALSA FREQUENCY
C
C   INTEGER VARIABLES;
C   M      = NUMBER OF NODES IN X DIRECTION
```

```
C   M      = NUMBER OF NODES IN X DIRECTION
C   N      = NUMBER OF NODES IN Y DIRECTION
C   MP     = X NODAL POINT OFVORTEX START POSITION
C   NP     = Y NODAL POINT OF VORTEX START POSITION
C   MM     = X ARRAY DIMENSION
C   NN     = Y ARRAY DIMENSION
C   NFIG   = PLOT NUMBER
C   NSTEP  = ITERATION NUMBER
C
C   ARRAY VARIABLES;
C   RHO    = DENSITY PERTUBATIONS AT EACH NODE DUE TO DYNAMICS
C   RHOI   = INITAL VALUES OF DENSITY AT EACH NODE DUE TO GRADIENT
C   RHOT   = SUM OF BOTH DENSITY EFFECTS AT EACH NODE
C   RHNEW  = NEW VALUE OF RHO AT NEXT TIME STEP
C   ZETA   = VORTICITY AT EACH NODE
C   ZTNEW  = NEW VALUE OF VORTICITY AT NEXT TIME STEP
C   U      = X COMPONENT OF VELOCITY AT EACH NODAL POINT
C   V      = Y COMPONENT OF VELOCITY AT EACH NODAL POINT
C   U2     = U VELOCITYS COMPUTED AT BIOT-SAVAT NODAL POINTS
C   V2     = V VELOCITYS COMPUTED AT BIOT-SAVAT NODAL POINTS
C   X      = X COORDINATES AT EACH NODAL POINT
C   Y      = Y COORDINATES AT EACH NODAL POINT
C   XU     = X COORDINATE AT EACH U B. S. NODAL POINT
C   YU     = Y COORDINATE AT EACH U B. S. NODAL POINT
C   XV     = X COORDINATE AT EACH V B. S. NODAL POINT
C   YV     = Y COORDINATE AT EACH V B. S. NODAL POINT
C
C-----------------------------------------------------------------
C
C    SUBROUTINES USED IN THIS PROGRAM:
C
C      SUBROUTINE COUT  -  OUTPUTS NODE COORDINATES
C
C      SUBROUTINE OUTPT -  OUTPUTS VARIOUS PROGRAM ARRAYS WHEN CALLED
C
C      SUBROUTINE CPLOT -  CREATES ARRAY OF DENSITY AT EACH POINT
C                          AND CALLS DISSPLA CONTOURING ROUTINE TO PLOT.
C
C      SUBROUTINE ZPLOT -  CREATES ARRAY OF  VORTICITY AT EACH POINT AND
C                          CALLS DISSPLA COUTOURING ROUTINE TO PLOT.
C
C      SUBROUTINE DRPLOT-  CREATES ARRAY OF DENSITY PERTUBATIONS AT EACH
C                          POINT AND CALLS DISSPLA CONTOURING ROUTINE
C                          TO PLOT.
C
C      SUBROUTINE ZPL   -  OUTPUTS VORTICITY CONTOURS AS A PRINTER PLOT.
C
C      SUBROUTINE VPLOT - CREATES COMPLEX VELOCITY VECTORS AT EACH
C                         NODAL POINT AND THEN CALLS THE FOLLOWING
C                         SUBROUTINES TO PLOT THEM ON DISSPLA:
C                         A)     V2PLOT
C                         B)     AMIN
C                         C)     AMAX
C
C      SUBROUTINE CON  - CALLED BY ZPL TO CONTOUR VORTICITY ON PRINTER.
```

```
C
C
C  FUNCTIONS USED IN THIS PROGRAM:
C
C     _FUNCTION VBS - COMPUTES THE V COMPONENT OF VELOCITY USING
C                     THE BIOT-SAVART LAW.
C
C     FUNCTION UBS -  COMPUTES THE U COMPONENT OF VELOCITY USING
C                     THE BIOT- SAVART LAW.
C
C     FUNCTION PNEW - TAKES THE FINITE DIFFERENCE TO STEP THE
C                     EQUATIONS IN TIME.
C
C*********************************************************************
      DIMENSION RHOI(25,50),U(25,50),V(25,50),ZETA(25,50),RHO(25,50)
     * ,ZTNEW(25,50),RHNEW(25,50),NPLOT(8),X(25),Y(50)
     * ,XU(25),YU(50),XV(25),YV(50),U2(25,50),V2(25,50)
      CHARACTER*8 LABEL
      COMMON WK(15000)
      COMMON /PN/ DT,I,J,UF,UFA,UB,UBA,VF,VFA,VB,VBA,VPT,FV
      COMMON /PARM/ H,M,N,PI
      DATA MAXSTP/140/
      DATA NPLOT/1,20,40,60,80,100,120,140/
C
C -------( CALL GRAPHIC OUTPUT DEVICE )-------------
       CALL COMPRS
C      CALL TEK618
C-----------------------------------------------------
C
      MM= 25
      NN= 50
C
C -------- INPUT PROGRAM PARAMETERS --------------------------
C
      DT= 2.000E0
       T=0.0
      XWIDTH = 5.0
      RO= 0.09E0
      SP= 0.75
      FV=0.0182
      ZTMIN= 1.0E-8
      M= 24
      N= 44
      ISAVE= 0
C..... DESIGNATE NODAL POINTS TO PLACE INITAL VORTEX AT (MP,NP)
      MP=4
      NP=34
C------ COMPUTE ADDITIONAL PARAMETERS---------------------------------
C
C..... DENSITY GRADIENT IN Y DIRECTION INITALLY = DRHO
      DRHOI=-SP*SP*FV*FV
C..... NONDIMENSIONAL B. V. FREQUENCY = BVND
      BVND= SP*SP*FV*FV
C..... MAXIMUM VORTICITY AT ANY POINT = ZTMAX
      ZTMAX=-(FV/(RO*RO))
```

```
C..... GEOMETRIC CONSTANT PI
      PI= 4.0E0*ATAN(1.0E0)
C..... GRID LENGTH PARAMETER = H
      H= XWIDTH/(M-4)
C
C..... COMPUTE MISC M AND N PARAMETERS
        MM1= M-1
        MP1= M+1
        MM2= M-2
        NP1=N+1
        NM1=N-1
        NM2= N-2
C
C-----INITALIZE COORDINATE SYSTEM ORIGINS --------------------------
C
      X(1)= -H
      Y(1)=  H
      XU(1)= -1.5E0*H
      YU(1)=  H
      XV(1)= -H
      YV(1)=  1.5E0*H
C
C -------- COMPUTE COORDINATES ------------------
C  ( NOTE: COMPUTATIONAL GRID IS IN 4TH QUADRANT +X -Y )
C
      DO 10 I= 2,MP1
         DO 10 J= 2,NP1
         XU(I)= XU(I-1)+H
         YU(J)= YU(J-1)-H
         XV(I)= XV(I-1)+H
         YV(J)= YV(J-1)-H
         X(I)= X(I-1)+H
 10      Y(J)= Y(J-1)-H
      YHT = ABS(Y(N-2))
C..... OUTPUT INITAL PARAMETERS OF THIS RUN OF PROGRAM.............
C
      WRITE(6,1275)
      WRITE(6,1500)
      WRITE(6,1535) DT,H
      WRITE(6,1540) XWIDTH,YHT
      WRITE(6,1550) SP,FV
      WRITE(6,1560) M,N
      WRITE(6,1570) BVND
C
C......... OUTPUT COORDINATES OF NODES.......................
         WRITE(6,1580) X(MP),Y(NP)
         WRITE(6,1590)
         CALL COUT(X,Y,MM,NN)
C
C ------- SPECIFY INITAL VORTICITY AND DENSITY FIELDS ---------
C
C   ( FOR GRID SYSTEM X,Y (COMPUTATIONAL GRID) IN THE 4TH QUADRANT )
C    ( TERMS ARG1 - ARG4 ARE IN QUADRANTS 1 - 4 )
C
       ARGMN= 30.0
```

```
      XCENT= X(MP)
      YCENT= Y(NP)
      DEN= 2.0E0*RO*RO
      ZETA(MP,NP) = ZTMAX
      DO 30 J=1,N
        DO 30 I=1,M
      TRM1=0.0E0
      TRM2=0.0E0
      TRM3=0.0E0
      TRM4=0.0E0
        ARG1= ((X(I)-XCENT)**2 + (Y(J)+YCENT)**2)/DEN
              IF (ARG1 .GT. ARGMN) GO TO 12
        TRM1= EXP(-ARG1)
 12     ARG2= ((X(I)+XCENT)**2 + (Y(J)+YCENT)**2)/DEN
              IF(ARG2 .GT. ARGMN) GO TO 14
        TRM2= EXP(-ARG2)
 14     ARG3= ((X(I)+XCENT)**2 + (Y(J)-YCENT)**2)/DEN
              IF(ARG3 .GT. ARGMN) GO TO 16
        TRM3= EXP(-ARG3)
 16     ARG4= ((X(I)-XCENT)**2 + (Y(J)-YCENT)**2)/DEN
              IF(ARG4 .GT. ARGMN) GO TO 18
        TRM4= EXP(-ARG4)
 18     IF((J.EQ.NP) .AND. .(I .EQ.MP)) GO TO 20
      ZETA(I,J)=ZTMAX*(-TRM1 +TRM2 -TRM3 +TRM4)
        IF(ABS(ZETA(I,J)) .LT. ZTMIN)  ZETA(I,J)=0.0E0
 20     RHOI(I,J)=  DRHOI*Y(J)
        RHO(I,J)= 0.0E0
 30     CONTINUE
      WRITE(6,1250)
C     CALL OUTPT(ZETA,'ZTA(I,J)',MM,NN,0)
C     CALL OUTPT(RHOI,'ROI(I,J)',MM,NN,0)
C
C..... INITALIZE TIME STEP COUNTERS.....
      NFIG=0
      NSTEP=0
C
C                    ENTRY POINT OF TIME LOOP^                    ^
 60     CONTINUE
C
C.......... COMPUTE U VELOCITY FOR ALL NODES IN U VELOCITY GRID.....
C
      DO 70 I= 1,MP1
        DO 70 J= 1,N
 70     U2(I,J)= UBS(XU(I),YU(J),MM,NN,X,Y,ZETA)
C
C.......... COMPUTE V VELOCITY FOR ALL NODES IN V VELOCITY GRID.....
C
      DO 100 I= 1,M
        DO 100 J= 1,NP1
100     V2(I,J)= VBS(XV(I),YV(J),MM,NN,X,Y,ZETA)
C
C.......... INTERPOLATE VELOCITIES FROM VELOCITY GRIDS TO NODAL
C                                        POINTS ON COMPUTATIONAL GRID.
      VMIN= 1.0E-08
      DO 120 I= 1,M
```

```
        DO 120 J= 1,N
        U(I,J)= (U2(I,J) + U2(I+1,J))/2.0E0
        V(I,J)= (V2(I,J)+  V2(I,J+1))/2.0E0
        IF (ABS(U(I,J)) .LT. VMIN)  U(I,J)= 0.0E0
        IF (ABS(V(I,J)) .LT. VMIN)  V(I,J)= 0.0E0
 120    CONTINUE
C     IF (NSTEP .EQ. 0)  CALL OUTPT(V,'V(I,J)   ',MM,NN,1)
C     IF (NSTEP .EQ. 0)  CALL OUTPT(U,'U(I,J)   ',MM,NN,1)
C
C
C .....................................................................
C                    INCREASE TIME COUNTER BY ONE.
C    CHECK ITERATION COUNTER AND TERMINATE IF NSTEP IS MORE THAN MAX
C   COMPUTE VORTICITY AND DENSITY AT ALL INTERIOR POINTS
C         ( STORED AS ELEMENTS OF ZTNEW AND RHNEW )
C.....................................................................
C
      NSTEP=NSTEP+1
      IF (NSTEP .GT. MAXSTP) GO TO 1700
      T= T+DT
      DO 600 I=2,MM1
           DO 600 J=2,NM1
           VPT= V(I,J)
           UF= (U(I+1,J)+U(I,J))/2.0E0
           UFA=ABS(UF)
           UB= (U(I-1,J)+U(I,J))/2.0E0
           UBA=ABS(UB)
           VF= (V(I,J-1)+V(I,J))/2.0E0
           VFA=ABS(VF)
           VB= (V(I,J+1)+V(I,J))/2.0E0
           VBA=ABS(VB)
           ZTNEW(I,J)= PNEW(ZETA,RHO,MM,NN,-1.0E0,0.0E0,0.0E0)
 600       RHNEW(I,J)= PNEW(RHO,RHO,MM,NN,0.0E0,0.0E0,BVND)
C
C
C -------- APPLY BOUNDRY CONDITIONS TO RHO AND ZETA ---------------
C
C..... ASSIGN NEW VALUES OF RHO AND ZETA TO RHO AND ZETA ARRAYS ...
C
        DO  700 I= 2,MM1
           DO 700 J= 2, NM1
           ZETA(I,J)= ZTNEW(I,J)
 700       RHO(I,J)=RHNEW(I,J)
C..... CALCULATE RHO AND ZETA VALUES AT I=M-2 AND J=N-2 BOUNDRIES ...
C
      DO 800 I= 2,MM2
         DO 800 J= 2,NM2
         ZETA(MM2,J)= (ZETA(MM1,J)+ ZETA(M-3,J))/2.0E0
         ZETA(I,NM2)= (ZETA(I,NM1)+ ZETA(I,N-3))/2.0E0
         RHO(MM2,J)= (RHO(MM1,J)+ RHO(M-3,J))/2.0E0
         RHO(I,NM2)= (RHO(I,NM1)+ RHO(I,N-3))/2.0E0
           IF(ABS(ZETA(I,J)).LT. ZTMIN)  ZETA(I,J)=0.0E0
           IF(ABS(RHO(I,J)).LT. ZTMIN)  RHO(I,J)= 0.0E0
 800     CONTINUE
C
```

```
C.....
C     PLOT FLOW PATTERN WHEN NSTEP = VALUE SPECIFIED IN NPLOT
C
C     THEN RESTART ALGORITHM AT LINE 6 FOR A NEW TIME STEP
C.....
      DO 1100 K= 1,8
      IF (NSTEP-NPLOT(K))  1100,  1200,  1100
 1100 CONTINUE
      GO TO 60
 1200 NFIG=NFIG+1
      TM= T*FV
      IF (NSTEP .EQ. MAXSTP ) CALL OUTPT(ZETA,'ZTA(I,J)',MM,NN,NSTEP)
      IF (NSTEP .EQ. MAXSTP) CALL OUTPT (RHO, 'RHO(I,J)',MM,NN,NSTEP)
      WRITE(6,1300)NSTEP,T,TM
      CALL CPLOT(RHO,RHOI,MM,NN,NSTEP)
      CALL VPLOT(U,V,X,Y,MM,NN)
      CALL DRPLOT(RHO,MM,NN,NSTEP)
      CALL  ZPL(ZETA,MM,NN,XWIDTH,YHT,ITER)
      CALL ZPLOT(ZETA,MM,NN)
 1250 FORMAT(// 10X,'INITAL ZETA AND RHO VALUES : ')
 1275 FORMAT('1')
 1300 FORMAT(/10X,'ITERATION NUM:',I6,4X,'TIME=',F9.3,4X,'T* =',F10.6)
 1400 WRITE(6,1500)
 1500 FORMAT( ///)
 1530 FORMAT(' ',5X,'INITAL PROGRAM PARAMETERS:' )
 1535 FORMAT('0',5X,'TIME STEP= ',F8.4,5X,'GRID SPACING H = ',F8.4)
 1540 FORMAT('0',5X,'NON DIMENSIONAL CELL DIMENSIONS : XDIRECTION =',
     * F8.4,5X,'YDIRECTION =',F8.4)
 1550 FORMAT('0',5X,'STRATIFICATION PARAMETER =',F8.4,5X,
     * 'FROUDE NUMBER =',F8.4)
 1560 FORMAT('0',5X,'NUMBER OF NODES IN X DIRECTION =',I4,5X,
     *  'IN Y DIRECTION =',I4)
 1570 FORMAT('0',5X,'NONDIMENSIONAL B. V. FREQUENCY =',F15.9)
 1580 FORMAT('0',5X,'X COORDINATE OF VORTEX START POSITION =',F8.4,5X,
     *  'Y COORDINATE =',F8.4)
 1590 FORMAT('0',5X,'OUTPUT COORDINATES OF ALL OTHER NODES:')
C
C        LOOP BACK TO STARTING POINT OF ITERATION
      GO TO 60
 1700 CALL DONEPL
C1700 CONTINUE
C
C----- SAVE ARRAYS AND TIME DATA TO RESTART PROGRAM LATER ------
C
      IF (ISAVE .EQ. 0 ) GO TO 1900
      WRITE(8,*) SP,FV,DT,T
      WRITE(8,*) M,N,MP,NP
      WRITE(8,*) BVND,H,ZTMAX
      DO 1800 I= 1,M
         DO 1800 J= 1,N
 1800    WRITE(8,*) ZETA(I,J), RHO(I,J)
 1900  STOP
      END
C
C ++++++++++++++++++++++++++++++++++++++++++++++++++++++++++++++++++++++++
```

```
C
C            SUBROUTINES:
C
C ===================================================================
C
C-------------------------------------------------------------------
      REAL FUNCTION  PNEW(P,Q,MM,NN,A,B,C)
C
C  THIS FUNCTION INTEGRATES THIS EQUATION WITH RESPECT TO TIME
C $$$  DP/DT= (-D(UP)/DX -D(VP)/DY + A*DQ/DX + B*DEL(P) +C*V )     $$$
C     UTILIZING AN UPWIND DIFFERENCING SCHEME
C
      DIMENSION P(MM,NN),Q(MM,NN)
      COMMON /PN/ DT,I,J,UF,UFA,UB,UBA,VF,VFA,VB,VBA,VPT,FV
      COMMON /PARM/ H,M,N,PI
      P1= (UF-UFA)*P(I+1,J)  +(UF+UFA-UB+UBA)*P(I,J)  -(UB+UBA)*P(I-1,J)
      P2= (VF-VFA)*P(I,J-1)  +(VF+VFA-VB+VBA)*P(I,J)  -(VB+VBA)*P(I,J+1)
      P3= Q(I+1,J)  -Q(I-1,J)
      P4= P(I+1,J)  +P(I-1,J)+P(I,J-1)+P(I,J+1)-4.0E0*P(I,J)
      P5= 2.0E0*H*VPT
      PNEW=P(I,J)+(DT/(2.0E0*H))*(-P1-P2 +A*P3+(2.0E0/H)*B*P4+C*P5)
      RETURN
      END
C
C-------------------------------------------------------------------
C
      REAL FUNCTION UBS(XU,YU,MM,NN,X,Y,ZETA)
C
C     THIS SUBROUTINE FINDS BOUNDRY VALUES OF VELOCITY  U
C             UTILIZING THE BIOT-SAVAT LAW
C
C  (NOTE: TERMS IN EQUATION ARE EVALUATED CONSECUTIVELY IN EACH
C         QUADRANT FROM ONE TO FOUR  )
C-------------------------------------------------------------------
      DIMENSION X(MM),Y(NN),ZETA(MM,NN)
      COMMON /PARM/ H,M,N,PI
C
      UMIN= 1.0E-08
      U1= 0.0E0
      U2= 0.0E0
      U3= 0.0E0
      U4= 0.0E0
C
      SIGN=-1.0E0
      DA= H*H
C
C ------ COMPUTE U COMPONENT OF VELOCITY USING THE B-S LAW----
C   -- QUADRANT ONE --
      DO 5 I= 1,M
         DO 5 J= 1,N
         RSQ1=((XU-X(I))**2 + (YU+Y(J))**2)
  5      U1= U1+ ((-Y(J)-YU)/(2.0E0*PI*RSQ1))*SIGN*ZETA(I,J)*DA
C   -- QUADRANT TWO --
      SIGN=  1.0E0
      DO 10 I= 1,M
```

```
          DO 10 J= 1,N
          RSQ2= ((XU+X(I))**2 +(YU+Y(J))**2)
   10     U2= U2+ ((-Y(J)-YU)/(2.0E0*PI*RSQ2))*SIGN*ZETA(I,J)*DA
C    -- QUADRANT THREE --
       SIGN=-1.0E0
       DO 15 I= 1,M
          DO 15 J= 1,N
          RSQ3= ((XU+X(I))**2 +(YU-Y(J))**2)
   15     U3= U3+((Y(J)-YU)/(2.0E0*PI*RSQ3))*SIGN*ZETA(I,J)*DA
C    -- QUADRANT FOUR --
       SIGN= 1.0E0
       DO 20 I= 1,M
         DO 20 J= 1,N
          RSQ4= ((XU-X(I))**2 + (YU-Y(J))**2)
   20     U4 = U4 + ((Y(J)-YU)/(2.0E0*PI*RSQ4))*SIGN*ZETA(I,J)*DA
       UTEMP= U1+U2 +U3+ U4
       IF (ABS(UTEMP).LT.UMIN) UTEMP=0.0E0
       UBS= UTEMP
       RETURN
       END
C
C
C=======================================================================
C
       REAL FUNCTION VBS(XV,YV,MM,NN,X,Y,ZETA)
C
C      THIS SUBROUTINE FINDS BOUNDRY VALUES OF VELOCITY  V
C              UTILIZING THE BIOT-SAVAT LAW
C
C (NOTE : TERMS IN THE EQUATION ARE EVALUATED CONSECUTIVELY IN EACH
C           QUADRANT FROM ONE TO FOUR)
C-----------------------------------------------------------------------
       DIMENSION X(MM),Y(NN),ZETA(MM,NN)
       COMMON/PARM/ H,M,N,PI
C
       VMIN= 1.0E-08
       V1= 0.0E0
       V2= 0.0E0
       V3= 0.0E0
       V4= 0.0E0
C
       SIGN=-1.0E0
       DA= H*H
C
C ------ COMPUTE V COMPONENT OF VELOCITY USING THE B-S LAW----
C    -- QUADRANT ONE --
       DO 5 I= 1,M
          DO 5 J= 1,N
          RSQ1=((XV-X(I))**2 + (YV+Y(J))**2)
    5     V1= V1+ ((XV-X(I))/(2.E0*PI*RSQ1))*SIGN*ZETA(I,J)*DA
C    -- QUADRANT TWO --
       SIGN= 1.0E0
       DO 10 I= 1,M
          DO 10 J= 1,N
          RSQ2= ((XV+X(I))**2 +(YV+Y(J))**2)
```

```
   10      V2= V2+ ((XV+X(I))/(2.0E0*PI*RSQ2))*SIGN*ZETA(I,J)*DA
C    -- QUADRANT THREE --
       SIGN=-1.0E0
       DO 15 I= 1,M
          DO 15 J= 1,N
          RSQ3= ((XV+X(I))**2 +(YV-Y(J))**2)
   15     V3= V3+((XV+X(I))/(2.0E0*PI*RSQ3))*SIGN*ZETA(I,J)*DA
C    -- QUADRANT FOUR --
       SIGN= 1.0E0
       DO 20 I= 1,M
         DO 20 J= 1,N
          RSQ4= ((XV-X(I))**2 + (YV-Y(J))**2)
   20     V4 = V4 + ((XV-X(I))/(2.0E0*PI*RSQ4))*SIGN*ZETA(I,J)*DA
       VTEMP = V1+V2 +V3+ V4
       IF(ABS(VTEMP).LT.VMIN)  VTEMP=0.0E0
       VBS= VTEMP
       RETURN
       END
C
C
C-----------------------------------------------------------------------
C
       SUBROUTINE COUT(X,Y,MM,NN)
C
C
C-----------------------------------------------------------------------
       REAL X(MM),Y(NN),H,PI
       COMMON/PARM/H,M,N,PI
       WRITE(6,50)
       WRITE(6,*) '          ARRAY X'
       WRITE(6,*)
       WRITE(6,*) (X(I), I=1,M)
       WRITE(6,*)
       WRITE(6,*)
       WRITE(6,*) '          ARRAY Y     '
       WRITE (6,*)
       WRITE(6,*) (Y(J), J=1,N)
       WRITE(6,*)
       WRITE(6,*)
   50   FORMAT(///)
       RETURN
       END
C=======================================================================
       SUBROUTINE OUTPT(A,LBL,MM,NN,KAL)
C
C     THIS SUBROUTINE PRINTS OUT AN (NXM) ARRAY WITH A LABEL
C          IN A RECTANGULAR ( 2,M-2)X(2,N-2) GRID
C
       DIMENSION A(MM,NN)
       COMMON/PARM/ H,M,N,PI
       CHARACTER*8  LBL
       NM2= N-2
       MM2= M-2
       WRITE(6,50)
       WRITE(6,*)
```

```
      WRITE(6,*) '      OUTPUT OF ARRAY:    ',LBL,'    ITER NUM:',KAL
      WRITE(6,*)
      DO 10 J= 2,MM2
      WRITE(6,*)
      WRITE(6,*) (A(I,J), I=2,MM2)
   10 CONTINUE
   50 FORMAT('1')
      RETURN
      END
C
C-----------------------------------------------------------------------
C
      SUBROUTINE CPLOT(RHO,RHOI,MM,NN,NSTEP)
      COMMON WK(15000)
      COMMON /PARM/ H,M,N,PI
      REAL W(41,41)
      REAL RHO(MM,NN),RHOI(MM,NN),H,PI,RHOT(25,50)
      DATA ISCALE/4HSCAL/
C
C...CREATE ARRAY OF DENSITY CHANGES AT  EACH NODE (DRHO) .......
C
      MM2= M-2
      NM2= N-2
      MW= 41
      NW= 41
      DO 10 I= 2,MM2
         DO 10 J= 2,NM2
         JJ= (NM2+1)-J
         II= I+19
         RHOT(I,J)=RHO(I,J)+RHOI(I,J)
         W(II,JJ)= RHOT(I,J)
   10    CONTINUE
         DO 20 I= 3,MM2
         II= 23-I
           DO 20 J= 2,NM2
           JJ= (NM2+1) -J
   20      W(II,JJ)= RHOT(I,J)
C
C        CALL OUTPT(RHOT,'RHT(I,J)',MM,NN,NSTEP)
C..... CALL SUBROUTINE CONTR TO PLOT THESE PERTUBATIONS.....
C
      CALL RESET (3HALL)
      CALL PAGE(8.7,11.2)
      CALL PHYSOR(2.0,3.00)
      CALL AREA2D (5.0,6.0)
      CALL HEIGHT(.2 )
      CALL INTAXS
      CALL XNAME ('X/BO',4)
      CALL YNAME ('Y/BO',4)
      CALL XTICKS(2)
      CALL YTICKS(2)
      CALL GRAF (-5.0,1.,5.,10.,1.,0.)
      CALL FRAME
      CALL BCOMON (15000)
      CALL CONMIN(2.0)
```

```
      CALL CONANG (20.)
      CALL CONMAK (W,MW,NW, ISCALE)
      CALL HEIGHT(.08)
      CALL CONLIN (0,5HSOLID,'LABELS',2,5)
      CALL CONLIN (1,4HDASH,8HNOLABELS,1,3)
      CALL RASPLN(0.25)
      CALL CONTUR (2,6HLABELS,4HDRAW)
      CALL HEIGHT(.2)
      CALL COMPLX
      CALL RESET('HEIGHT')
      CALL RESET('COMPLX')
      CALL ENDPL (0)
      RETURN
      END
C
C-----------------------------------------------------------------------
C
      SUBROUTINE ZPLOT(ZETA,MM,NN)
      REAL ZETA(MM,NN),H,PI
      COMMON WK(1500)
      COMMON /PARM/ H,M,N,PI
      DIMENSION W(41,41)
      DATA ISCALE/4HSCAL/
C
C...CREATE ARRAY FOR PLOTTING OF ZETA IN ACTUAL COMPUTATIONAL AREA..
C
      MW= 41
      NW= 41
      MM2= M-2
      NM2=N-2
      DO 10 I= 2,MM2
         II= I+19
         DO 10 J= 2,NM2
         JJ= (NM2+1)-J
 10      W(II,JJ)=ZETA(I,J)
         DO 20 I= 3,MM2
         II= 23-I
           DO 20 J= 2,NM2
           JJ= (NM2+1) - J
 20        W(II,JJ) = -ZETA(I,J)
C
C..... CALL SUBROUTINE CONTR TO PLOT VORTICITY.....................
C
C
      CALL RESET (3HALL)
      CALL PAGE(8.7,11.2)
      CALL PHYSOR(2.0,3.00)
      CALL AREA2D (5.0,6.0)
      CALL HEIGHT(.2 )
      CALL INTAXS
      CALL XNAME ('X/BO',4)
      CALL YNAME ('Y/BO',4)
      CALL XTICKS(2)
      CALL YTICKS(2)
      CALL GRAF (-5.0,1.,5.,10.,1.,0.)
```

```
      CALL FRAME
      CALL BCOMON (15000)
      CALL CONANG (60.)
      CALL CONMIN(2.0)
      CALL CONMAK (W,MW,NW,ISCALE)
      CALL HEIGHT(.08)
      CALL CONLIN (0,5HSOLID,'LABELS',2,5)
      CALL CONLIN (1,4HDASH,'LABELS',1,3)
      CALL RASPLN(0.25)
      CALL CONTUR (2,6HLABELS,4HDRAW)
      CALL HEIGHT(.2)
      CALL COMPLX
      CALL RESET('HEIGHT')
      CALL RESET('COMPLX')
      CALL ENDPL (0)
      RETURN
      END
C
C
C-----------------------------------------------------------------------
C
      SUBROUTINE DRPLOT(RHO,MM,NN,NSTEP)
      COMMON WK(15000)
      COMMON /PARM/ H,M,N,PI
      REAL W(41,41)
      REAL RHO(MM,NN),H,PI
      DATA ISCALE/4HSCAL/
C
C...CREATE ARRAY OF DENSITY CHANGES AT  EACH NODE (DRHO) .......
C
      MM2= M-2
      NM2= N-2
      MW= 41
      NW= 41
      DO 10 I= 2,MM2
         DO 10 J= 2,NM2
         JJ= (NM2+1)-J
         II= I+19
         W(II,JJ)= RHO(I,J)
 10      CONTINUE
         DO 20 I= 3,MM2
         II= 23-I
           DO 20 J= 2,NM2
           JJ= (NM2+1) -J
 20        W(II,JJ)= RHO(I,J)
C
C..... CALL SUBROUTINE CONTR TO PLOT THESE PERTUBATIONS.........
C
      CALL RESET (3HALL)
      CALL PAGE(8.7,11.2)
      CALL PHYSOR(2.0,3.00)
      CALL AREA2D (5.0,6.0)
      CALL HEIGHT(.2 )
      CALL INTAXS
      CALL XNAME ('X/B0',4)
```

```
      CALL YNAME ('Y/BO',4)
      CALL XTICKS(2)
      CALL YTICKS(2)
      CALL GRAF (-5.0,1.,5.,10.,1.,0.)
      CALL FRAME
      CALL BCOMON (15000)
      CALL CONMIN(2.0)
      CALL CONANG (20.)
      CALL CONMAK (W,MW,NW,ISCALE)
      CALL HEIGHT(.08)
      CALL CONLIN (0,5HSOLID,'LABELS',2,5)
      CALL CONLIN (1,4HDASH,8HNOLABELS,1,3)
      CALL RASPLN(0.25)
      CALL CONTUR (2,6HLABELS,4HDRAW)
      CALL HEIGHT(.2)
      CALL COMPLX
      CALL RESET('HEIGHT')
      CALL RESET('COMPLX')
      CALL ENDPL (0)
      RETURN
      END
C
C=======================================================================
C
      SUBROUTINE CON(Z2,XRANGE,YRANGE,NX,H,MM,NN,ZMAX,ZMIN)
C
C     THIS SUBROUTINE GENERATES A CONTOUR PLOT OF ZETA IN A RECTANGULAR
C     DOMAIN OF SIZE:  YRANGE * XRANGE ON THE PRINTER.
C
      CHARACTER*1 SYMBOL(8),GRAPH(100)
      REAL LX,LY
      DIMENSION Z2(MM,NN),VALUE(7)
      DATA SYMBOL / 'X','A', '-',' ',' ', '+','1',' '/
      VALUE(1)= ZMIN
      VALUE(2)= ZMIN*.75
      VALUE(3)= ZMIN*.5
      VALUE(4)= 0.0
      VALUE(6)= ZMAX*.75
      VALUE(7)= ZMAX
      VALUE(5)=ZMAX*.45
      NY= 0.8*NX*YRANGE/XRANGE
      DELX= XRANGE/NX
      DELY= YRANGE/NY
      WRITE(6,50)
      WRITE(6,*) 'NX=',NX, 'NY=',NY,'XRANGE=',XRANGE,
     *           'YRANGE=',YRANGE
      WRITE(6,*)
        DO 11 I= 1,NX
 11     GRAPH(I)= 'T'
        WRITE(6,6) (GRAPH(I), I= 1,NX)
        DO 5 JSYMBL = 1,NY
        Y= (JSYMBL-0.5)*DELY
        J= 1+Y/H
        LY= Y-(J-1)*H
       HMLY= H-LY
```

```
          DO 4 ISYMBL = 1,NX
          X= (ISYMBL-0.5)*DELX
          I=1+X/H
          LX= X-(I-1)*H
      _   HMLX= H- LX
          A1= HMLX*HMLY
          A2= HMLX*LY
          A3= LX*LY
          A4= LX*HMLY
          Z2C= (A1*Z2(I,J) +A2*Z2(I,J+1) +A3*Z2(I+1,J+1)
     *          +A4*Z2(I+1,J))/H**2
C
C... DETERMINE THE VALUE OF NRANGE BASED ON Z2C.....................
C
C.... PRINT OUT  CHARACTERS IN ARRAY GRAPH BY ROW ..................
C
              DO 2 K= 1,7
              IF (Z2C-VALUE(K)) 1, 1, 2
   1          NRANGE = K
              GO TO 3
   2          CONTINUE
          NRANGE= 8
   3      GRAPH( ISYMBL)= SYMBOL(NRANGE)
   4     CONTINUE
   5     WRITE(6,6) (GRAPH(I), I=1,NX)
   6     FORMAT(' ',10X,100A1 )
 50      FORMAT('1')
         DO 60 I= 1,NX
 60      GRAPH(I)= 'B'
       WRITE(6,6) (GRAPH(I) ,I=1,NX)
       WRITE(6,*)
       WRITE(6,*) 'MAXIMUM VALUE OF NEGATINE VORTICITY = SYMBOL (X) = '
      *  ,ZMIN
       WRITE(6,*) ' 75% OF MAXIMUN NEGATIVE VORTICITY = SYMBOL (A) '
       WRITE(6,*) ' 50% OF MAXIMUM NEGATIVE VORTICITY = SYMBOL (-) '
       WRITE(6,*)
       WRITE(6,*) ' MAXIMUM VALUE OF POSITIVE VORTICITY = SYMBOL (1) ='
      * , ZMAX
       WRITE(6,*) ' 75% OF MAXIMUM POSITIVE VORTICITY = SYMBOL (+)'
       RETURN
       END
C-----------------------------------------------------------------------
C
       SUBROUTINE ZPL(ZETA,MM,NN,XWIDTH,YHT,ITER)
       COMMON /PARM/ H,M,N,PI
       DIMENSION Z2(25,50),ZETA(MM,NN)
C
C...CREATE ARRAY FOR PLOTTING OF ZETA IN ACTUAL COMPUTATIONAL AREA..
C
       MM3= M-3
       NM3=N-3
       DO 10 I= 1,MM3
          DO 10 J= 1,NM3
 10       Z2(I,J)= ZETA(I+1,J+1)
C..FIND THE MAXIMUM POSITIVE VORTICITY IN ARRAY Z2(MM,NN).....
```

```
C
      ZMIN= 0.0
      ZMAX= 0.0
      DO 20 I= 1,MM3
         DO 20 J= 1,NM3
         IF(Z2(I,J) .GT. ZMAX)  ZMAX=Z2(I,J)
  20     CONTINUE
C
C.. FIND THE MAXIMUM NEGATIVE VORTICITY IN ARRAY Z2(MM,NN).......
C
      DO 40 I= 1,MM3
         DO 40 J= 1,NM3
         IF( Z2(I,J) .LT. ZMIN)  ZMIN= Z2(I,J)
 40      CONTINUE
C
      IF (ZMAX .LT. 1.0E-4 ) ZMAX=1.0
C..... CALL SUBROUTINE CON TO PLOT VORTICITY.....................
C
      CALL CON(Z2,XWIDTH,YHT,100,H,MM,NN,ZMAX,ZMIN)
      RETURN
      END
C-----------------------------------------------------------------------
      SUBROUTINE VPLOT(U,V,X,Y,MM,NN)
      COMMON /PARM/ H,M,N,PI
      COMPLEX ZV(21,41), CV(21,41)
      DIMENSION U(MM,NN), V(MM,NN), X(MM), Y(NN)
      MM2= M-2
      NM2= N-2
C
C..... FORM COMPLEX U, V, AND Z ARRAYS FOR QUADRANTS 3 AND 4 ......
C
      DO 10 I= 2,MM2
         DO 10 J= 2,NM2
         II= I-1
         JJ= (NM2+1) -J
         ZV(II,JJ)= CMPLX(X(I),Y(J))
 10      CV(II,JJ)= CMPLX(U(I,J),V(I,J))
C
C
C....... PLOT VECTORS USING SUBROUTINE V2PLOT ..................
      CALL V2PLOT(ZV,CV,21,41)
C
      RETURN
      END
C
C-----------------------------------------------------------------------
C
      SUBROUTINE V2PLOT(Z,C,M,N)
C
C  ***************************************************************
C  *  SUBROUTINE V2PLOT TO PLOT MXN COMPLX VELOCIT FIELD C(M,N)  *
C  *  OVER A COMPLX DOMAIN Z(M,N)                                *
C  *                                                             *
C  ***************************************************************
         COMPLEX Z(21,41),C(21,41),CMAX
```

```
      REAL X(50),Y(50),YX(50),YN(50),XX(50),XN(50),X2(50),Y2(50)
      INTEGER PMAX,PMIN
      EXTERNAL AMAX
      EXTERNAL AMIN
C
      DO 20 J =1,N
         DO 10 I =1,M
            X(I) =ABS(REAL(C(I,J)))
            Y(I) =ABS(AIMAG(C(I,J)))
10       CONTINUE
         CALL AMAX(Y,M,YMAX,PMAX)
         CALL AMAX(X,M,XMAX,PMAX)
         YX(J) = YMAX
         XX(J) = XMAX
         CALL AMIN(Y,M,YMIN,PMIN)
         CALL AMIN(X,M,XMIN,PMIN)
         YN(J) =YMIN
         XN(J) =XMIN
20    CONTINUE
      CALL AMAX(YX,N,YMAX,PMAX)
C     CALL AMIN(YN,N,YMIN,PMIN)
      CALL AMAX(XX,N,XMAX,PMAX)
C     CALL AMIN(XN,N,XMIN,PMIN)
C
      CMAX = CMPLX(XMAX,YMAX)
      UMAX =SQRT((XMAX)**2+(YMAX)**2)
      DO 24 I =1,M
        DO 22 J=1,N
          C(I,J) = C(I,J)/UMAX
22      CONTINUE
24    CONTINUE
C
      DO 40 J =1,N
         DO 30 I =1,M
            X(I) =REAL(Z(I,J))
            Y(I) =AIMAG(Z(I,J))
30       CONTINUE
         CALL AMAX(Y,M,YMAX,PMAX)
         CALL AMAX(X,M,XMAX,PMAX)
         YX(J) = YMAX
         XX(J) = XMAX
         CALL AMIN(Y,M,YMIN,PMIN)
         CALL AMIN(X,M,XMIN,PMIN)
         YN(J) =YMIN
         XN(J) =XMIN
40    CONTINUE
      CALL AMAX(YX,N,YMAX,PMAX)
      CALL AMIN(YN,N,YMIN,PMIN)
      CALL AMAX(XX,N,XMAX,PMAX)
      CALL AMIN(XN,N,XMIN,PMIN)
C
      CALL RESET(3HALL)
      CALL PAGE(8.7,11.2)
      CALL PHYSOR(2.0,3.0)
      CALL AREA2D(5.,6.)
```

```
      CALL HEIGHT(.2)
      CALL INTAXS
      CALL XNAME('X/BO',4)
      CALL YNAME('Y/BO',4)
      CALL XTICKS(2)
      CALL YTICKS(2)
      CALL GRAF(0.0,0.5,5.0,-10.0,1.0,0.0)
C
         DO 60 J=1,N
            DO 50 I=1,M
               X(I) = REAL(Z(I,J))
               X2(I) = X(I)+REAL(C(I,J))
               Y(I)= AIMAG(Z(I,J))
               Y2(I) = Y(I)+AIMAG(C(I,J))
 50         CONTINUE
               CALL MARKER (3)
               CALL SCLPIC(.001)
               CALL CURVE(X,Y,M,-1)
            DO 54 I =1,M
               X11=X(I)
               X12=X2(I)
               Y11=Y(I)
               Y12=Y2(I)
               IF(X12.EQ.0..AND.Y12.EQ.0) GO TO 54
               CALL RLVEC (X11,Y11,X12,Y12,1121)
 54         CONTINUE
 60      CONTINUE
         CALL RESET('HEIGHT')
         CALL ENDPL(0)
      RETURN
      END
C
C
      SUBROUTINE AMAX(Y,N,YMAX,PMAX)
C
C        ***********************************************
C        *  SUBROUTINE TO COMPUTE THE LARGE ELELEMENT
C        *  IN A GIVEN ROW OR COLUMN IN ARRAY 'A'.
C        ***********************************************
C
C        *** VARIABLE DECLARATION ***
C        REAL AMAX
         INTEGER PMAX
         DIMENSION Y(N)
C
         YMAX=Y(1)
         DO 5100 I=2,N
            IF(Y(I).LE.YMAX) GO TO 5000
              YMAX=Y(I)
              PMAX=I
5000        CONTINUE
5100     CONTINUE
C        MAXROW=POS
      RETURN
      END
```

```
C
C
C
      SUBROUTINE AMIN(Y,N,YMIN,PMIN)
C     -
C        ***********************************************
C        *  SUBROUTINE TO COMPUTE THE SMALL ELEMENT
C        *  IN A GIVEN ROW OR COLUMN IN ARRAY 'A'.
C        ***********************************************
C
C        *** VARIABLE DECLARATION ***
C        REAL AMIN
         INTEGER PMIN
         DIMENSION Y(N)
C
         YMIN=Y(1)
         DO 6100 I=2,N
             IF(Y(I).GE.YMIN) GO TO 6000
               YMIN=Y(I)
               PMIN=I
6000         CONTINUE
6100     CONTINUE
      RETURN
      END
EOF:
```

INITIAL DISTRIBUTION LIST

Director DARPA (Attn: Dr. David C. Lewis) 1400 Wilson Blvd. Arlington, VA 22209	20
Chief of Naval Operations OP-95T, Room 5D616 The Pentagon Washington, DC 20350	
Attn: Dr. Jack Breedlove	1
Attn: Dr. A. Andreassen	1
Commander Department of the Navy Strategic Systems Project Office Washington, DC 20376	
Attn: Dr. Philip Selwyn (SP2023)	1
Chief of Naval Operations OP-021, Room 4D544 The Pentagon Washington, DC 20350	
Attn: Dr. Ed Harper	1
Dr. Irwin E. Alber Arete Associates P.O. Box 350 Encino, CA 91316	1
Dr. Steve Crow Poseidon Research 1299 Ocean Avenue Suite 821 Santa Monica, CA 90401	1
Dr. Wasyl Wasylkiwskyj Physical Dynamics, Inc. Suite 1620 1300 N. 17th Street Arlington, VA 22209	1
Dr. Richard Hoglund ORI, Inc. 1400 Spring Street Silver Spring, MD 70910	1

Dr. Denny Ko . . . 1
Dynamics Technology, Inc.
22939 Hawthorne Blvd.
Suite 200
Torrance, CA 90505

Dr. C. D. Donaldson 1
Aeronautical Research Associates of Princeton, Inc.
1800 Old Meadow Road
Suite 114
McLean, VA 22102

Applied Physics Laboratory
The John Hopkins University
Johns Hopkins Road
Laurel, MD 20810
Attn: Dr. L. Crawford 1
Attn: Dr. H. Gilreath 1
Attn: Dr. G. Merritt 1
Attn: Dr. Gary Smith 1
Attn: Dr. Tom Taylor 1
Attn: Dr. D. Wenstrand 1

Dr. Dennis Holliday 1
R&D Associates
4640 Admiralty Way
Marina del Rey, CA 90291

Dr. Don LeVine 1
JASON Program Office
The MITRE Corporation
1820 Dolley Madison Blvd.
McLean, VA 22102

Flow Research
21414 68th Ave. South
Kent, WA 98031
Attn: Peter Liu 1

Continuum Dynamics
P. O. Box 3073
32 Nassau St.
Princeton, NJ 08540
Attn: Alan Bilanin 1

Defense Technical Information Center 2
Attn: DTK-DDA-2
Building 5
Cameron Station
Alexandria, VA 22314

Dr. Thomas Taylor
Applied Physics Laboratory
The John Hopkins University
Johns Hopkins Road
Laurel, MD 20810 — 1

Dr. Bruce Lake
TRW Space & Technology Group
R-1/1008
1 Space Park
Redondo Beach, CA 90278 — 1

Dr. Robert Shuchman
Environmental Research Institute
of Michigan
P. O. Box 8618
Ann Arbor, Michigan 48107 — 1

Dr. T. Sarpkaya
Code 69SL
Mechanical Engineering
Naval Postgraduate School
Monterey, CA 93943 — 20

Office of Research Administration
Code 012A
Naval Postgraduate School
Monterey, CA 93943 — 1

Library, Code 0142
Naval Postgraduate School
Monterey, CA 93943 — 4

Chairman, Mechanical Engineering
Code 69
Naval Postgraduate School
Monterey, CA 93943 — 1

DUDLEY KNOX LIBRARY
3 2768 00335470 5